

DISSERTATION

Titel der Dissertation

Investigation of phase equilibria and structural
analysis in the systems Al-Cu, Cu-Si, Al-Cu-Si
and Al-Mo-Si

Verfasser

Mag.rer.nat. Norbert Ponweiser

angestrebter akademischer Grad

Doktor der Naturwissenschaften (Dr.rer.nat.)

Wien, September 2011

Studienkennzahl lt. Studienblatt: A 791 419

Dissertationsgebiet lt. Studienblatt: Chemie

Betreuerin / Betreuer: Ao. Univ.-Prof. Mag. Dr. Klaus Richter

Acknowledgment

The present work was accomplished in the period from July 2006 to September 2011 under the supervision of Ao. Univ.-Prof. Mag. Dr. Klaus Richter at the Department of Inorganic Chemistry / Materials Chemistry at the University of Vienna.

I would like to thank Prof. Richter for his support during this study. His experience in phase diagram evaluation and structural analysis of compounds always was of great help for me.

I want to thank O. Univ.-Prof. Dr. Herbert Ipser for welcoming me at the Institute and supporting me in organizational and personal matters.

Furthermore, I would like to thank Ao. Univ.-Prof. Dr. Christian Lengauer, Ao. Univ.-Prof. Dr. Theodoros Ntaflos, Mag. Dr. Stephan Puchegger and Franz Kiraly for their support in sample investigation.

I want to thank my colleagues at the Department of Inorganic Chemistry / Materials Chemistry for providing an excellent working atmosphere and for their help in scientific and personal matters. Special thanks appertain to Dr. Bea Huber, who was a highly valued advisor in various matters and became an especially close friend.

Particular thanks go to my friends and my parents, who always have been there for me.

Preface

This work covers a small selection of binary and ternary phase diagrams and contributes to knowledge on the systems investigated.

In the ternary phase diagram Al-Cu-Si previous authors performed a lot of work already. Since some of this work was not conclusive, an investigation of this system was the starting point of the present thesis. In course of this project, insufficiencies in the binary subsystems became obvious and proper investigations of the system Al-Cu and Cu-Si were worked out first.

The ternary phase diagram Al-Mo-Si has not been investigated over the whole range yet because of difficulties in the Al-rich part of the phase diagram, which will be pointed out in course of this work. The present work is an attempt to overcome this insufficiency.

A remark to avoid misunderstandings: since this work covers already published papers, each with its respective bibliography, this display format was kept for the entire work. Each main section, the Introduction, the Experimental part and every sub-chapter of the Results and Discussion part therefore concludes with its particular bibliography.

Table of contents

1	Introduction	- 1 -
1.1	The system Al-Cu.....	- 4 -
1.2	The system Cu-Si	- 8 -
1.3	The system Al-Cu-Si	- 11 -
1.4	The system Al-Mo-Si	- 13 -
2	Experimental	- 24 -
2.1	Light Optical Microscopy (LOM)	- 24 -
2.2	Powder X-Ray Diffraction (XRD)	- 25 -
2.3	Electron Probe Micro Analysis (EPMA) and Scanning Electron Microscopy (SEM)	- 26 -
2.4	Differential thermal analysis (DTA)	- 27 -
2.5	Structure determination from powder XRD data using Simulated Annealing	- 34 -
3	Results and discussion.....	- 40 -
3.1	Re-investigation of phase equilibria in the system Al-Cu and structural analysis of the high-temperature phase η_1 -Al ₁₋₈ Cu	- 40 -
3.2	Experimental investigation of the Cu-Si phase diagram at $x(\text{Cu}) > 0.72$	- 76 -
3.3	New investigation of phase equilibria in the system Al-Cu-Si	- 117 -
3.4	Phase equilibria in the Al-Mo-Si system.....	- 159 -
4	Summary	- 198 -
5	Zusammenfassung	- 200 -
	Appendix A: Supplementary material	- 202 -
	Appendix B: Permissions for prints	- 209 -
	Appendix C: <i>Curriculum vitae</i>	- 212 -

1 Introduction

Modern technology requires more than ever advanced materials for manifold purposes, e.g. for weight saving in transport industry, new materials in combustion engineering or for materials for high-temperature applications, e.g. in gas turbines.

Whenever the performance of a pure material is not sufficient for a specific purpose, alloying is an option to improve desired properties. The principle of alloying is known for thousands of years, starting with alloying of Cu with Zn in the Bronze Age for producing hardwearing tools and weapons. Nowadays, a huge number of alloys is used for countless applications.

A large group of important alloys are the aluminum-based ones. Pure aluminum offers many desirable properties for different purposes, e.g. a low density ($2698 \text{ kg}\cdot\text{m}^{-3}$ [1]), a high formability, corrosion resistance and electrical conductivity. Therefore, pure aluminum is used, for example, as foil and strip for packaging, chemical equipment, tank cars or truck bodies [2]. Alloying of aluminum increases the applicability of the material dramatically.

Alloying with Si, for example, reduces the thermal expansion coefficient, increases the corrosion and wear resistance, and improves the casting and machining characteristics of aluminum [3]. Usually, the alloys used are very aluminum-rich. During cooling, pure aluminum solidifies until the composition of the remaining liquid reaches the eutectic point at 12.2 at.% Si [4], where the eutectic Al-Si phase solidifies. At room temperature, the hypereutectic alloy consists of the soft and ductile primary aluminum and the hard and brittle eutectic silicon phase [3]. Al-Si alloys usually contain other elements like manganese, zinc or iron for improving their properties. Due to the high strength-to-weight ratio of the resulting alloys and their good processability properties (heat treatable, good flow characteristics [2]), they are predestined for utilization in automotive industry [5], e.g. for engine blocks [3].

Another important class of Al-based alloys are Al-Cu alloys. They are heat treatable and show high strength at room and elevated temperatures and, in special cases, good weldability [2]. Usually, these alloys are not resistant to atmospheric corrosion and need to be protected [2]. Like in the Al-Si alloys, most of the Al-Cu alloys used are Al-rich and contain additional elements to improve their properties. Al-Cu alloys are used, for example, for fatigue-critical applications in airframes [6].

For high-temperature applications in oxidizing environment Al-based alloys are not suitable. Several silicides, however, provide properties like excellent high-temperature oxidation resistance. Among a huge variety of silicides, molybdenum silicides are interesting compounds for high temperature applications. The most important alloys in this system are MoSi_2 and Mo_5Si_3 . Although pure Mo_5Si_3 does not show high oxidation resistance at high temperature, this alloy is still of interest for high-temperature applications due to its high creep resistance at elevated temperature. Alloying with a few percent Boron, however, increases its oxidation resistance dramatically [7]. The compound MoSi_2 has a congruent melting point of 2020 °C [8] and an excellent high-temperature oxidation resistance [9]. Unfortunately, the material has several drawbacks, too. It exhibits pest oxidation behaviour at intermediate temperatures in the range of 500 °C, a brittle-to-ductile transition around 1000 °C [9] and a high creep-rate at elevated temperature, for example. To overcome at least some of the disadvantages of the material, alloying with e.g. aluminum is advisable. The addition of Al leads to a new compound $\text{Mo}(\text{Al},\text{Si})_2$, which does not show pest oxidation behaviour and therefore allows a broad field of application. Molybdenum disilicides are used in high temperature applications like turbocharger rotors, industrial gas burners, high-temperature heat exchanger, glass processing and as coating material for refractory metals and carbon materials [9, 10].

Fundamental knowledge of phase equilibria and structures in the respective alloy systems is crucial for understanding alloy properties and further

improvement of alloy systems. In many cases, literature data are not consistent and/or incomplete which requires additional experimental investigations.

For describing phase equilibria, phase diagrams are used. Phase diagrams are graphical representations of the state of a material as a function of composition, temperature and pressure. In case of a single compound system, the state of a matter usually is shown in a diagram pressure vs. temperature, where one figure provides all information required. In binary phase diagrams, the pressure usually is kept constant; in a graphical representation, the temperature is drawn versus the composition.

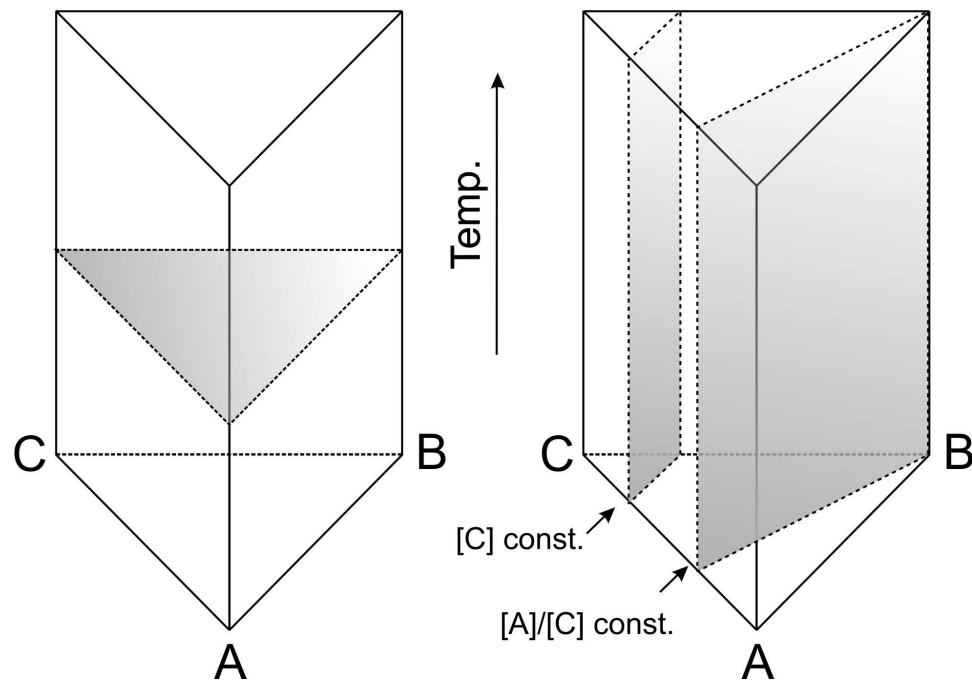


Fig. 1.1: Isothermal section (left) and vertical sections (isopleths, right) in a ternary phase diagram A-B-C

The graphical representation of three component systems is more complicated even if the pressure is kept constant. Since the graphical representation of all the binary systems combined versus temperature gets rather complicated for complex systems, different tools for illustration are used. These tools are the isothermal section (the temperature is kept constant; see Fig. 1.1), the vertical section (also

known as isopleth; the fraction of one constituent or the ratio between two constituents is kept constant; see Fig. 1.1) and the liquidus surface projection. Additionally, a ternary reaction scheme, the so-called Scheil-diagram is used to describe the invariant reaction in the ternary system.

In the current work the systems Al-Cu, Cu-Si, Al-Cu-Si and Al-Mo-Si were chosen as research foci. In some cases literature data do not provide conclusive, up-to-date information about the systems (Al-Cu, Cu-Si, Al-Cu-Si) or a full description of the system has not been published yet (Al-Mo-Si). In either case, new experiments were necessary to overcome those insufficiencies.

The following section will give a brief overview about the relevant literature data pointing out the scientific challenges in the respective fields.

Due to the cumulative character of the present dissertation, the following introduction is based on the papers [11-14] present in the *Results and Discussion* section and might therefore cover redundant information presented in the latter section anyway. Formal requirements, however, demand for a distinct *Introduction* section in this dissertation.

1.1 The system Al-Cu

The Al-Cu system was investigated intensively in the past decades. Due to the importance of Al-based alloys in transport industry, most investigations in the system were dealing with the Al-rich part of the phase diagram. Literature data is available in the Cu-poor part of the phase diagram as well but there are still some inconsistencies left.

The major assessment including the commonly accepted phase diagram of the system was published by Murray [15]. The phase diagram includes 12 intermetallic compounds; seven of them are stable at elevated temperatures only (see Fig. 1.2). Since this phase diagram was published in 1985, it does not represent the current level of knowledge of the system. Liu et al. published an

improved version of the Cu-rich part in 1998 [16], Riani et al. merged the work of Liu et al. and Murray [17]. A thermodynamic assessment is given by Saunders [18]. A detailed overview of the system is given by Ponweiser et al. [11, 13].

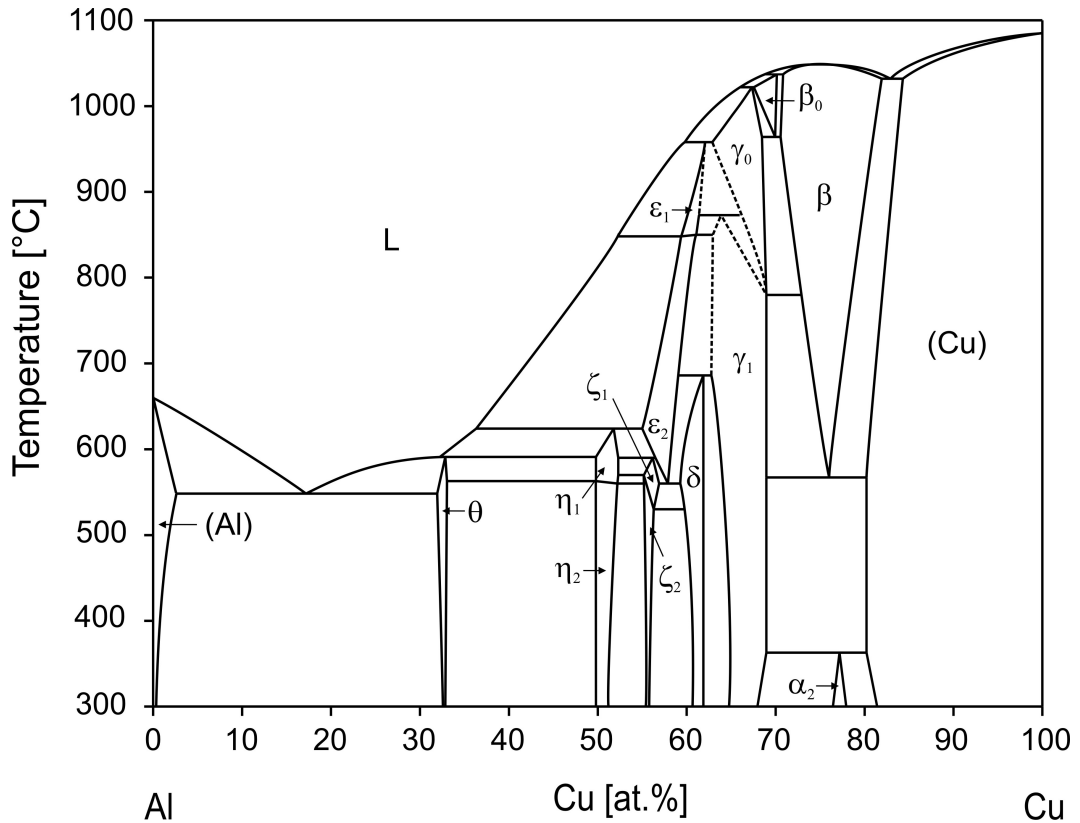


Fig. 1.2: The Al-Cu phase diagram according to Murray [15]

The structure of the phase θ -Al₂Cu was found by Friauf [19] in the 1920ies. The thermal stability up to 591 °C and its solubility range has been investigated intensively [15, 20].

The phase with the composition AlCu (designated η) has been under investigation for a long time, too. An orthorhombic structure was found in samples quenched from 602 °C [21] but analysis of slowly cooled samples by Bradley [22] showed some basic differences to the orthorhombic structure. The

author therefore suggested an allotropic transformation $\eta_1 \rightarrow \eta_2$ [22] and proposed an orthorhombic or a monoclinic structure for the low-temperature phase. El-Boragy et al. revealed the structure of the low-temperature phase to be monoclinic [23]. The structure of the high-temperature phase is still unknown. Preston suggested an orthorhombic structure [21], Lukas and Lebrun proposed an orthorhombic cell with the parameters $a = 4.087 \text{ \AA}$, $b = 12.00 \text{ \AA}$, $c = 8.635 \text{ \AA}$ and 32 atoms per unit cell [24]. According to the phase diagram in Fig 1.2 [15] the transition between the high- and the low-temperature phase is a higher order transition.

The phases ε_1 and ε_2 are both stable at elevated temperatures only and show a higher order transition (see Fig. 1.2). The structure of ε_2 was solved by El-Boragy who found a NiAs-type structure with partial occupation of interstitial positions by applying high temperature powder X-Ray diffraction [23]. The structure of ε_1 is still unknown.

The region near the approximate compound Al_3Cu_4 (ζ_1/ζ_2 -region in Fig. 1.2) was described by Preston [21] and Bradley [22] and it was soon discovered that a high- and a low-temperature phase are present. The work of Murray suggests a transition temperature between 530 and 570 °C dependent on the composition. Additionally, thermal effects between 373 and 450 °C are mentioned, too [15]. In more recent investigations, Dong et al. found a mixture of an orthorhombic face-centered structure, an orthorhombic body-centered structure and small amounts of $\gamma\text{-Al}_4\text{Cu}_9$ in as cast sample with the composition Al_3Cu_4 [25, 26]. After annealing at 500 °C the face-centered structure became the major phase and the authors suggested a transition $\gamma\text{-Al}_4\text{Cu}_9 + "oI" = "oF"$. The structures of the two phases ζ_1 and ζ_2 were finally solved by Gulay and Harbrecht. A sample with the composition $\text{Al}_{42.5}\text{Cu}_{57.5}$ shows a face-centered structure ($Fmm2$, Al_3Cu_4 -type) designated as ζ_1 [27]. ζ_2 ($Imm2$, $\text{Al}_3\text{Cu}_{4-\delta}$ -type) was found in a sample with the nominal composition $\text{Al}_{43.2}\text{Cu}_{56.8}$ [28]. This contradicts the findings of Dong who allocated the face-centered symmetry to the structure with the lower Cu content. The findings of Gulay and Harbrecht are not in agreement with the phase diagram

of Murray, too, since he suggested a low temperature phase ζ_2 and a high temperature phase ζ_1 with a slightly higher Cu-content [15]. Gulay and Harbrecht found the Cu-rich phase ζ_1 stable at 400 °C and the Cu-poor phase ζ_2 stable at 530 °C [27, 28]. The latter did not resist thermal treatment at 400 °C. The authors state that entropy may provide an essential contribution to the stabilization of the ζ_2 phase.

In the range from 60 to 70 at.% Cu, Bradley found three different phases: a cubic (γ), a monoclinic and a rhombohedral phase [29]. Westman discovered that the rhombohedral phase crystallizes in the space group $R3m$ and confirmed the existence of a third phase in this region [30]. Seshadri and Downie did not confirm the existence of a third phase in this region, they only distinguished between $\gamma_{(1)}$ and the cubic phase δ [31]. Murray did not include a third phase in this region (see Fig. 1.2), mostly because very slow cooling experiments of van Sande et. al [32] show $\gamma_{(1)}$ and δ in equilibrium. The distinction of the phases $\gamma_{(1)}$ and δ is very difficult due to very similar XRD pattern, but it is supported by a abrupt change in expansion coefficients from $\gamma_{(1)}$ to δ [31].

The existence of the high temperature phase γ_0 was confirmed by thermal analysis but the two phases γ_0 and γ_1 can not be distinguished metallographically [15]. The Cu-rich region of the phase diagram was investigated by Liu et al. using differential scanning calorimetry and high temperature X-Ray powder diffraction [16]. The authors state that the high temperature phase γ_1 crystallizes cubic (Cu₅Zn₈-type) and that no two phase field between the high- and the low-temperature phase was found thus indicating a higher order transition.

According to Murray, a high temperature phase β_0 is formed peritectically from liquid and β [15]. The phase β_0 was found by Dawson [33] metallographically and by dilatometry, but was never confirmed. Nevertheless, Murray included it in his phase diagram (see Fig. 1.2). Investigations by Liu et al. do not indicate a single phase region β_0 . A measured thermal effect at 1019 °C is interpreted to be related to the solidification of β than to the formation of β_0 [16].

The phase fields between γ_1 and (Cu) were investigated intensively and Murray gives a detailed overview on the results in this region [15]. The region is dominated by the binary phase β and its decomposition to γ_1 and (Cu). The decomposition temperature was found to be between 560 and 575 °C. This rather huge spread can be explained by the sluggishness of the reaction.

The low-temperature phase α_2 was found by West et al after long term annealing experiments [34]. According to Murray, it shows a fcc structure with a long period superlattice based on Cu_3Au and Al_3Ti [15].

The important task in this system is to re-investigate the discrepancies between the phase diagram published by Murray (see Fig. 1.2) and the findings of Liu et al. The resulting phase diagram has to include the current state of knowledge on compounds ζ_1 and ζ_2 as well. Additionally, investigations on unknown structures of high temperature phases have to be performed.

1.2 The system Cu-Si

The latest critical assessment of the system was done by Olesinski and Abbaschian [35] who gave the currently accepted phase diagram (see Fig. 1.3). More recently a thermodynamic description of the system was given by Yan and Chang [36]. An additional overview on the system is given by Sufryd et al. [12] as well as by Ponweiser et al. [13].

The system contains several binary compounds, located in the Cu-rich part of the phase diagram, starting with phases showing the nominal composition Cu_3Si . There exist three different compounds with this composition. At high temperature, the phase is denoted η , the compounds at intermediate and low temperatures are designated η' and η'' , respectively. Unfortunately, this nomenclature is not consistent in literature but used in the phase diagram given by Olesinski and

Abbaschian (see Fig. 1.3). The high temperature phase η melts congruently at 859 °C. The transition temperatures of the different Cu_3Si phases vary extremely with composition and are reported to be higher at higher Cu-content. The transition temperature of $\eta \rightarrow \eta'$ differs between 558 and 620 °C, the transition temperature of $\eta' \rightarrow \eta''$ varies between 467 and 570 °C [35], dependent on the composition. According to the work of Olesinski, the phases η and η' show rhombohedral structures ($R-3m$ and $R-3$).

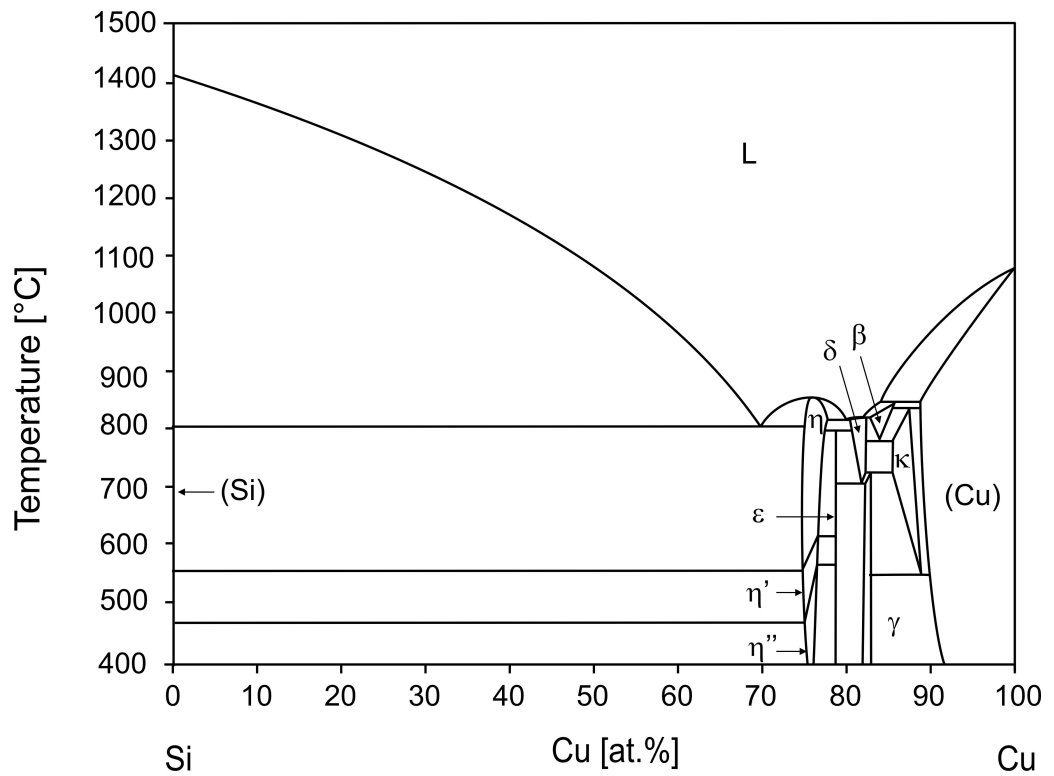


Fig. 1.3: The Al-Cu phase diagram according to Olesinski et al. [35]

The low temperature phase η'' is supposed to be orthorhombic [37] or tetragonal [38]. More recently, transmission electron microscopy investigations indicate $P-3m1$ and $R-3$ as the correct space groups for η and η' [39].

The existence of the phase ϵ -Cu₁₅Si₄ is discussed intensively in literature. The phase was first described by Arrhenius and Westgren [40]; a possible but yet not confirmed transition was described by Mukherjee et al. [38]. On the one hand, some diffusion couple experiments do not show any intermetallic compounds apart from Cu₃Si [41, 42] in the binary system Cu-Si. On the other hand, diffusion couple experiments prepared by sputter deposition show all three expected intermetallic phases (Cu₃Si, ϵ , and γ) [43, 44]. In other experiments, rapid quenching did suppress the formation of ϵ , but subsequent annealing at 500 °C facilitated its formation [45]. Riani et al. claimed that ϵ is stabilized by impurities and it is not stable if sample preparation was carried out using very pure basic materials [46].

The last intermetallic compound in the system stable at ambient temperatures is γ -Cu₅Si. It crystallizes cubic in the Mn-type structure and is formed peritectically at 729 °C (see Fig. 1.3). Like ϵ , this phase does not occur in some diffusion couple experiments [41, 42] but nevertheless it is considered a stable intermetallic compound.

At elevated temperatures two phases are considered stable in the Cu-Si system: β and δ (see Fig. 1.3). The compound β crystallizes cubic a W-type structure and forms peritectically from liquid and (Cu) at 852 °C. The structure of the compound δ was described as tetragonal [38] but recent splat cooling experiments by Mattern et al. lead to a hexagonal symmetry [45].

The main uncertainty in the system is whether ϵ -Cu₁₅Si₄ is a stable phase or not. Detailed experimental analysis needs to be performed to answer this question. Additionally, it is not certain if the hexagonal symmetry of δ obtained by splat cooling [45] experiments represents the equilibrium structure of the phase. High temperature X-ray powder analysis can help to answer this question.

1.3 The system Al-Cu-Si

A critical assessment of the system is given by Lukas and Lebrun [24]. The comprehensive work gives an overview about the limiting binary systems as well as information on the invariant ternary phase equilibria; the liquidus surface projection is given, too. The authors state that no ternary phase is present. Based on the work of Hisatsune [47], an isothermal section at 400 °C is given by Lukas and Lebrun [24]. A tentative reaction scheme (Scheil diagram) is given, too, but the authors do not include the high-temperature – low-temperature transition reactions of the respective phases in the Al-Cu and Cu-Si system for reasons of clarity. An overview on the Al-Cu-Si system also is given by Ponweiser et al. [13].

Since there is no ternary compound reported and the binary phases in the Cu-Si region are located in the Cu-rich part, the isothermal section at 400 °C is dominated by three phase fields of (Si) and binary Al-Cu compounds [24]. The binary phases δ -Al₄Cu₉, γ -Cu₅Si, ε -Cu₁₅Si₄ and η'' -Cu₃Si show significant solubility of Si or Al, respectively. The highest solubility range is shown by γ_1 -Al₄Cu₉, which is stable up to the composition Al₁₇Cu₇₂Si₁₁. The phase κ -(Cu,Si), only stable above 552 °C in the binary Cu-Si, is stabilized by the addition of Al to lower temperature and is present in the isothermal section at 400 °C. There is no information given on the solubility of Si in ζ_1/ζ_2 -Al₃Cu₄, η_2 -AlCu and θ -Al₂Cu because the isothermal section given in [24] only covers the Cu-rich corner of the ternary system.

Calculated isothermal sections at 500 and 600 °C are given by He et al. [48]. The most significant difference between these two calculated isothermal sections is the presence of β -AlCu₄ in the isothermal section at 600 °C. The solubilities of the binary compounds change slightly, e.g. the phase γ_1 -Al₄Cu₉ is stable up to the composition Al₁₅Cu₇₄Si₁₁ at 600 °C. Due to the thermal stability of β -AlCu₄ at 600 °C, the three phase field [(Cu) + β -AlCu₄ + γ_1 -Al₄Cu₉] is present.

He et al. present several vertical sections and a ternary reaction scheme, too [48]. The reaction scheme given by the authors differs from the reaction scheme given by Lukas and Lebrun [24] concerning the reaction temperatures as well as the type of reactions.

More recently, Riani et al. investigated the ternary system [46]. The extensive work gives detailed information on the ternary phase equilibria and the solubility ranges of the binary phases at 500 °C (see Fig. 1.4). A significant part of this work deals with the stability of ϵ -Cu₁₅Si₄. Riani et al. state that the phase is not stable in the binary system but is stabilized by addition of Al [46]. A more detailed investigation on the stability of ϵ -Cu₁₅Si₄ in the binary Cu-Si system is given by Sufryd et al. [12].

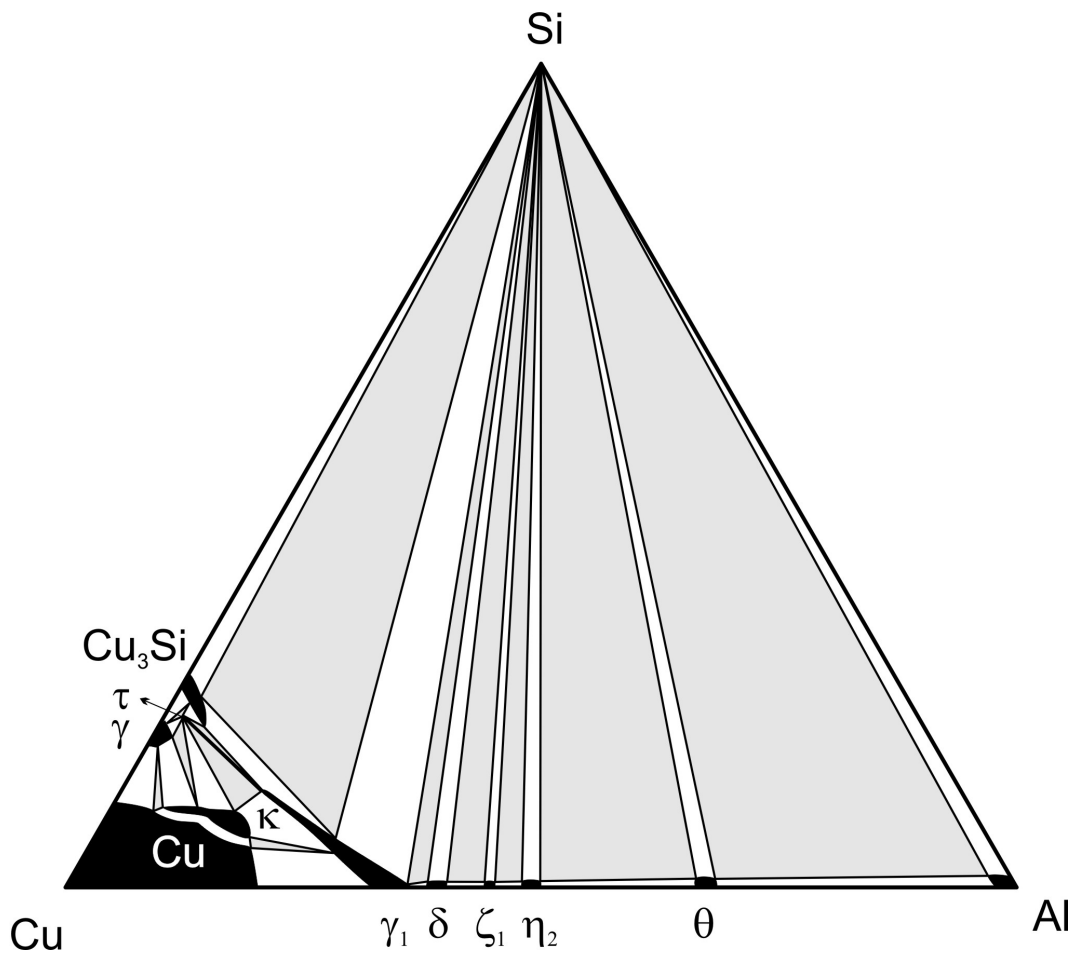


Fig. 1.4: The isothermal section of the Al-Cu-Si phase diagram at 500 °C according to Riani et al. [46]

Since there is no consensus in literature on the ternary reaction scheme in the system, the main task of further investigations should be to obtain additional information that can provide a ternary reaction scheme including the latest finding in the limiting binary systems. Additional investigations of isothermal sections higher than the ones mentioned above might be helpful.

1.4 The system Al-Mo-Si

The phase diagram of Al-Mo-Si is of high technological importance due to the high-temperature characteristics of several compounds in this system. A detailed review about molybdenum disilicide, its alloys and their properties, is given by Vasudevan and Petrovic [49]. An overview on the Al-Mo-Si system is also given by Ponweiser et al. [14].

The binary system Mo-Si was assessed by Gokhale and Abbaschian [8]. The system contains three intermetallic compounds, each with a very high melting point (see Fig. 1.5). The cubic phase Mo_3Si ($Pm-3m$, Cr_3Si -type) decomposes peritectically at 2025 °C. The compounds Mo_5Si_3 ($I4/mcm$, W_5Si_3 -type) and MoSi_2 ($I4/mmm$, MoSi_2 -type, Strukturbericht designation: C11_b) show tetragonal symmetry and melt congruently at 2180 and 2020 °C, respectively. According to Gokhale and Abbaschian, MoSi_2 undergoes a transition to a hexagonal high temperature form (designated as $\beta\text{-MoSi}_2$) at 1900 °C [8]. The authors state that only one author, Svechnikov [50], reported a phase transition [8]. Nevertheless, the transition was included in the phase diagram [8]. Due to its importance in high temperature applications, MoSi_2 is the most intensively studied phase in the system. Besides this phase, Mo_5Si_3 shows interesting properties, like a better creep resistance than MoSi_2 [51]. Unfortunately, Mo_5Si_3 exhibits poor oxidation resistance at high temperature, which can be improved by 5 orders of magnitude by adding 1-2 wt.% Boron [7].

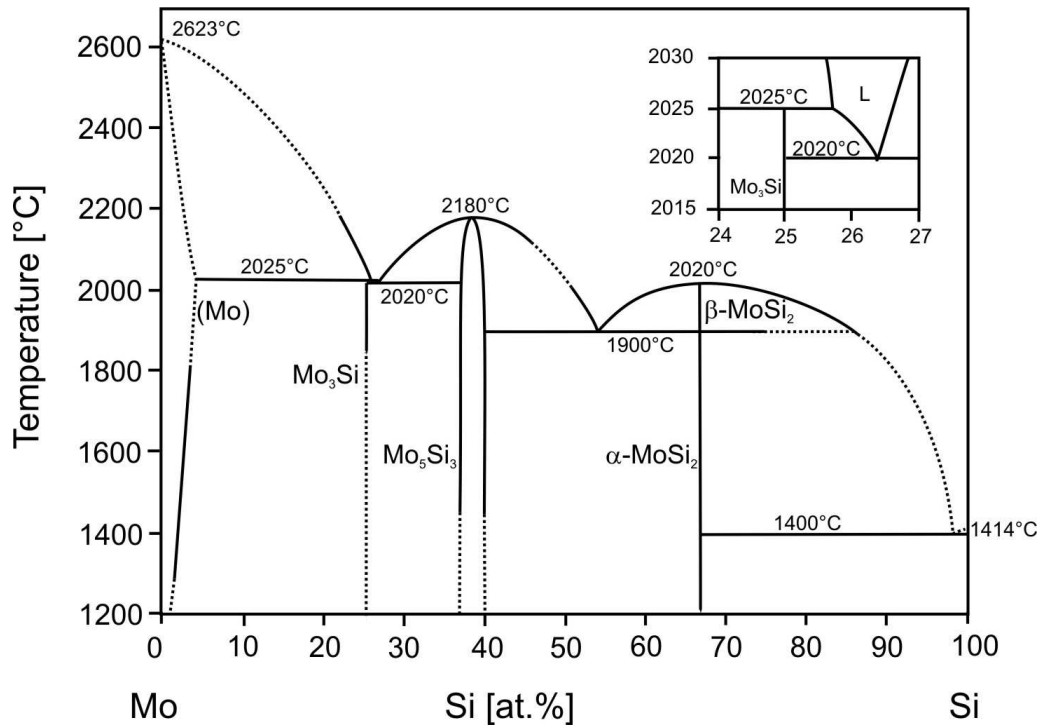


Fig. 1.5: The Mo-Si phase diagram according to Gokhale and Abbaschian [8]

The binary system Al-Mo was assessed by Saunders [52] in 1997 (see Fig. 1.6). According to the author, the system contains 7 intermetallic compounds; two of them are only stable at elevated temperatures. The phases stable down to low temperatures are AlMo_3 ($Pm-3n$, CrSi-type), Al_8Mo_3 ($C2/m$, Al_8Mo_3 -type), Al_4Mo (Cm , Al_4W -type), Al_5Mo ($P6_3$, Al_5W -type), and Al_{12}Mo ($Im-3$, Al_{12}W -type) [52]. The phase AlMo ($Im-3m$, W-type) is stable between 1470 and 1720 °C, the phase $\text{Al}_{63}\text{Mo}_{37}$ is stable between 1490 and 1570 °C [52-54]. The eutectoid decomposition of $\text{Al}_{63}\text{Mo}_{37}$ could not be inhibited by quenching, thus its structure is still unknown. Rexer [53] suggested congruent melting of the phase AlMo , but Saunders replaced the congruent melting of the phase by a peritectic decomposition reaction [52]. The authors states that the structure of AlMo is bcc ($cI2$) and therefore it is considered as an extension of the Mo-rich bcc solid

solution into the Al-richer part of the phase diagram, which makes the congruent melting of the phase thermodynamically unlikely [52].

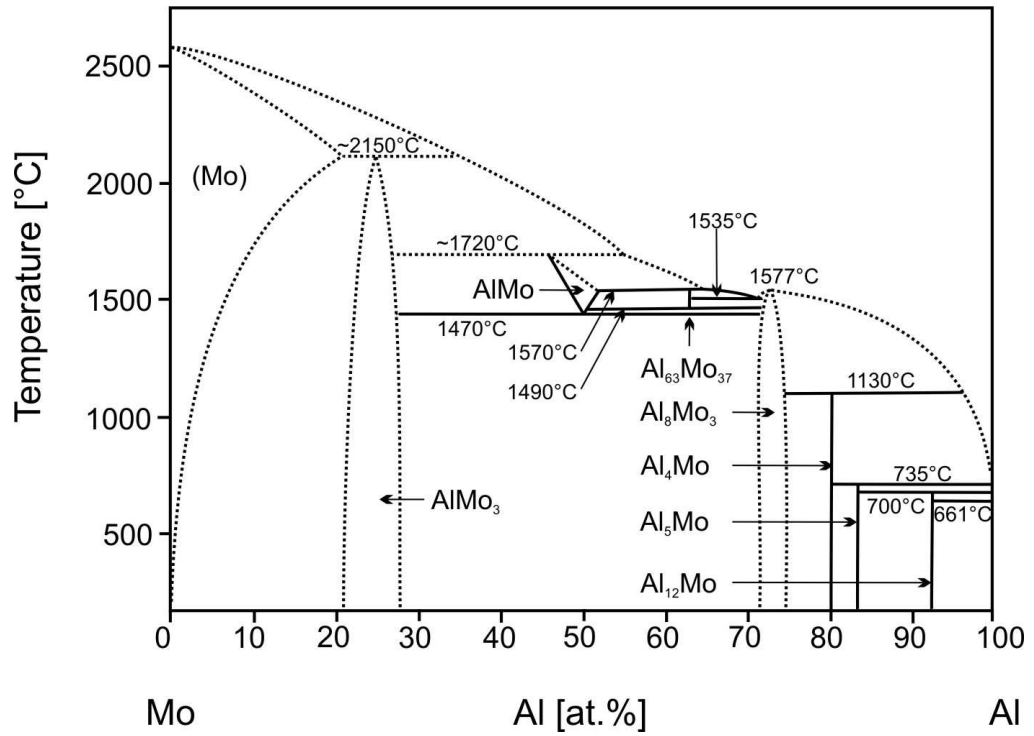


Fig. 1.6: The Al-Mo phase diagram according to Saunders et al. [52]

Contrary to this assumption, Cupid et al. [55] state that without assuming congruent melting of AlMo, it is impossible to calculate phase equilibria in the system Al-Mo-Ti in agreement with experimental data in this ternary system. Therefore Cupid et al. assume congruent melting of AlMo in their version of the binary Al-Mo system [55].

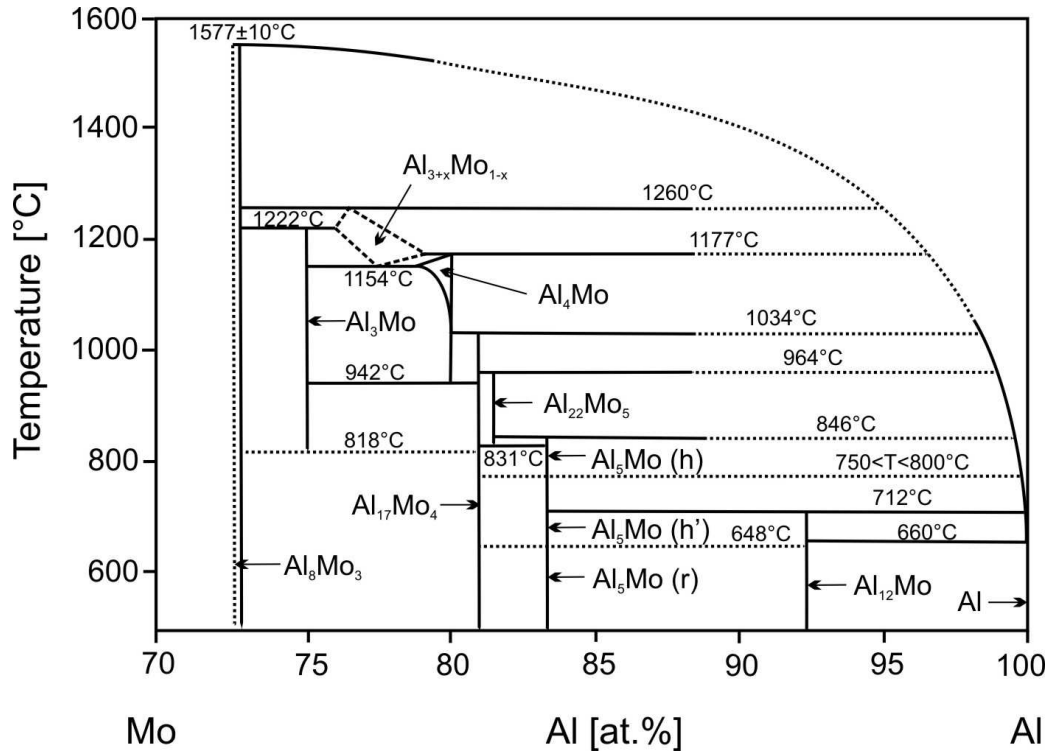


Fig. 1.7: The Al-Mo phase diagram according to Schuster et al. [56]

The Al-rich part of the phase diagram is dominated by a cascade of peritectic reactions. Even though a detailed investigation in this region has been performed by Schuster and Ipser [56] in 1991, their results did not find their way in Saunders' assessment [52]. Schuster and Ipser introduce four additional phases in the binary system (see Fig. 1.7): Al_3Mo (Cm , Al_3Mo -type), $Al_{17}Mo_4$ ($C2$, $Al_{17}Mo_4$ -type), $Al_{22}Mo_5$ ($Fdd2$, $Al_{22}Mo_5$ -type) and $Al_{(3+x)}Mo_{(1-x)}$ ($Pm-3n$, WO_3 -type). The latest investigation of the Al-rich part of the phase diagram was performed by Eumann et al. [57] who confirmed the existence of the additional binary compounds, except for $Al_{(3+x)}Mo_{(1-x)}$. Eumann et al. state that the phase $Al_{22}Mo_5$ is stable at least down to $600^\circ C$ [57], whereas Schuster and Ipser conclude that this phase is stable only at temperatures higher than $831^\circ C$. Okamoto [58] presents a phase diagram of the Al-Mo-system combining the results of Rexer [53], Saunders [52] and Eumann [57].

As mentioned above, the disadvantages of a high creep rate at elevated temperatures of the compound MoSi_2 have given rise to a wide field of research of Mo-Si-based ternary alloy systems, one of them being Al-Mo-Si. Since MoSi_2 is the most important alloy in the Mo-Si system, most research was done in the vicinity of this phase. Addition of Al to MoSi_2 leads to a new ternary compound $\text{Mo}(\text{Si},\text{Al})_2$ ($P6_222$, CrSi_2 -type, Strukturbericht designation: C40 [59]). Further addition of Al leads to the phase $\text{Mo}(\text{Si},\text{Al})_2$ which crystallizes orthorhombically ($Fddd$, TiSi_2 -type, Strukturbericht designation: C54 [60]). The most important compound of those three is $\text{Mo}(\text{Si},\text{Al})_2$ with the C40-structure (designated C40 from now on). In contrast to MoSi_2 (designated C11_b) it does not show pest oxidation at intermediate temperatures and therefore is considered to be a more promising material for oxidation resistance coatings at high service temperatures [61].

Isothermal sections of parts of the ternary system Al-Mo-Si sometimes were the byproduct of research on the C40 and C54 compounds. An isothermal at 1853 K is given by Yanagihara et al. [62]. This work does not include the phase C54 but assumes a wide solubility range for C40. An other isotherm including C54 was determined at 1400 °C by Eason et al. [63]. In this work, however, the compositions of the limiting single phase fields of the three-phase-field [C40 + C54 + Mo_5Si_3] were only estimated (see Fig. 1.8). Calculated isotherms between 1273 and 1873 °C were presented by Liu et al. [64]. The latter work includes a calculated liquidus surface projection, too. The authors predict a series of invariant reaction in the ternary system but do not give information on the reaction temperatures.

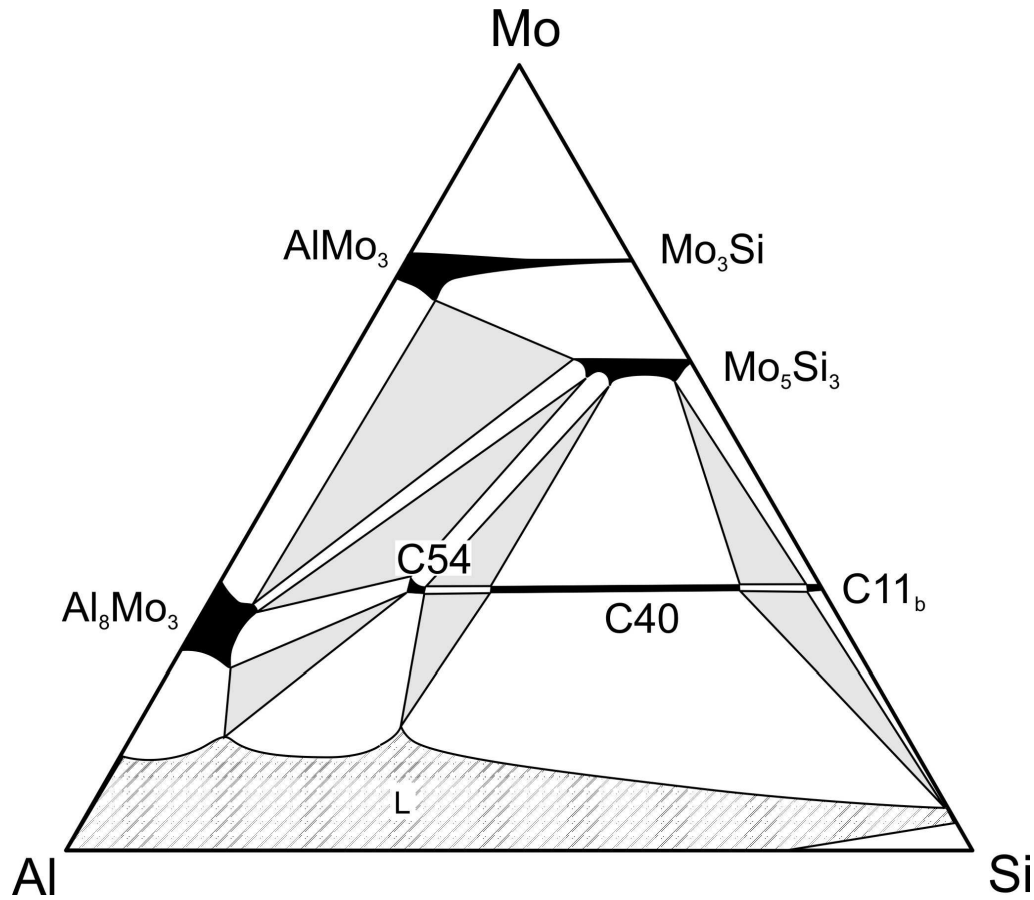


Fig. 1.8: The Al-Mo-Si isothermal section at 1400 °C according to Eason et al. [63]

Obviously a lot of work has been done in the system Al-Mo-Si but most of it is dealing with the Al-poor part. Since a lot of peritectic decomposition reactions of the Al-rich binary Al-Mo-phases appear and the technical applicability of alloys in this region is very limited, most researchers skip this part of the phase diagram. Nevertheless, a complete description of the phase diagram and a liquidus surface projection is necessary to understand the system.

References

- [1] J. Emsley, The Elements, in, Clarendon Press, Oxford, 1989.
- [2] I. The Aluminum Association, Aluminum Alloy: Selection and Application, in, The Aluminum Association, Inc. , Washington, D.C., 1998.
- [3] H. Ye, An overview of the development of Al-Si-alloy based material for engine applications, J. Mater. Eng. Perform., 12 (2003) 288-297.
- [4] J.L. Murray, A.J. McAlister, The Al-Si (aluminum-silicon) system, Bull. Alloy Phase Diagr., 5 (1984) 74-84, 89-90.
- [5] Y.S. Choi, J.S. Lee, W.T. Kim, H.Y. Ra, Solidification behavior of Al-Si-Fe alloys and phase transformation of metastable intermetallic compound by heat treatment, J. Mater. Sci., 34 (1999) 2163-2168.
- [6] J.B. Borradaile, Future Aluminium Technologies and their Application in Aircraft Structures, RTO Meeting Proc., 25 (1999) 4-1 - 4-4.
- [7] M.K. Meyer, M. Akinc, Oxidation behavior of boron modified Mo_5Si_3 at 800-1300°C, J. Am. Ceram. Soc. , 79 (1996) 7.
- [8] A.B. Gokhale, G.J. Abbaschian, The Mo-Si (molybdenum-silicon) system, J. Phase Equilib., 12 (1991) 493-498.
- [9] J.J. Petrovic, Molybdenum disilicide-based high-temperature structural silicides, MRS Bull., 18 (1993) 35-40.
- [10] Z. Yao, J. Stiglich, T.S. Sudarshan, Molybdenum silicide based materials and their properties, J. Mater. Eng. Perform., 8 (1999) 291-304.
- [11] N. Ponweiser, C.L. Lengauer, K.W. Richter, Re-investigation of phase equilibria in the system Al-Cu and structural analysis of the high-temperature phase Al(1-\delta)Cu , Intermetallics, 19 (2011) 1737-1746.
- [12] K. Sufryd, N. Ponweiser, P. Riani, K.W. Richter, G. Cacciamani, Experimental investigation of the Cu-Si phase diagram at $x(\text{Cu}) > 0.72$, Intermetallics, 19 (2011) 1479-1488.
- [13] N. Ponweiser, K.W. Richter, Investigation of phase equilibria in the system Al-Cu-Si, Intermetallics, submitted (2011).

- [14] N. Ponweiser, W. Paschinger, A. Ritscher, J.C. Schuster, K.W. Richter, Phase equilibria in the Al-Mo-Si system, *Intermetallics*, 19 (2011) 409-418.
- [15] J.L. Murray, The aluminium-copper system, *Int. Met. Rev.*, 30 (1985) 211-233.
- [16] X.J. Liu, I. Ohnuma, R. Kainuma, K. Ishida, Phase equilibria in the Cu-rich portion of the Cu-Al binary system, *J. Alloys Compd.*, 264 (1998) 201-208.
- [17] P. Riani, L. Arrighi, R. Marazza, D. Mazzone, G. Zanicchi, R. Ferro, Ternary rare-earth aluminum systems with copper: A review and a contribution to their assessment, *J. Phase Equilib. Diffus.*, 25 (2004) 22-52.
- [18] N. Saunders, System Al-Cu, in: I. Ansara, A.T. Dinsdale, M.H. Rand (Eds.) *COST 507 - Thermochemical Database for Light Element Alloys vol. 2*, 1998, pp. 28-33.
- [19] J.B. Friauf, The crystal structure of two intermetallic compounds, *J. Am. Chem. Soc.*, 49 (1927) 3107-3114.
- [20] T. Goedecke, F. Sommer, Solidification behavior of the Al₂Cu phase, *Z. Metallk.*, 87 (1996) 581-586.
- [21] G.D. Preston, An x-ray investigation of some copper-aluminum alloys, *Philos. Mag.*, 12 (1931) 980-993.
- [22] A.J. Bradley, H.J. Goldschmidt, H. Lipson, The intermediate phases in the aluminium-copper system after slow cooling, *J. Inst. Met.*, 63 (1938) 149-162.
- [23] M. El-Boragy, R. Szepan, K. Schubert, Crystal structure of Cu₃Al₂+(h) and CuAl(r), *J. Less-Common Met.*, 29 (1972) 133-140.
- [24] H.L. Lukas, N. Lebrun, Al-Cu-Si (Aluminium-Copper-Silicon), in: G. Effenberg, S. Ilyenko (Eds.) *SpringerMaterials - The Landolt-Börnstein Database*, 2005, pp. 135-147.
- [25] C. Dong, Q.H. Zhang, D.H. Wang, Y.M. Wang, Al-Cu approximants and associated B2 chemical-twinning modes, *Micron*, 31 (2000) 507-514.
- [26] C. Dong, Q.H. Zhang, D.H. Wang, Y.M. Wang, Al-Cu approximants in the Al₃Cu₄ alloy, *Eur. Phys. J. B*, 6 (1998) 25-32.
- [27] L.D. Gulay, B. Harbrecht, The crystal structure of zeta(1)-Al₃Cu₄, *J. Alloys Compd.*, 367 (2004) 103-108.
-

- [28] L.D. Gulay, B. Harbrecht, The crystal structure of $\zeta(2)$ -Al₃Cu₄-delta, *Z. Anorg. Allg. Chem.*, 629 (2003) 463-466.
 - [29] A.J. Bradley, Structure of Cu₃₂Al₁₉, *Nature (London, U. K.)*, 168 (1951) 661.
 - [30] S. Westman, Phase Analysis at 660°C of the Gamma Region of the Copper-Aluminium System, *Acta Chem. Scand.*, 19 (1965) 2369-2372.
 - [31] S.K. Seshadri, D.B. Downie, High-temperature lattice parameters of copper-aluminum alloys, *Met. Sci.*, 13 (1979) 696-698.
 - [32] M. Van Sande, J. Van Landuyt, M. Avalos-Borja, G.T. Villaseñor, S. Amelinckx, A reinvestigation of the γ phase in copper-aluminum alloys: a new long-period superstructure, *Mater. Sci. Eng.*, 46 (1980) 167-173.
 - [33] A.G. Dawson, *J. Inst. Met.*, 61 (1937) 197-204.
 - [34] D.R.F. West, D.L. Thomas, Some observations on constitutional changes in copper-aluminum alloys at temperatures below that of the β \rightarrow $\alpha + \gamma_2$ eutectoid, *J. Inst. Met.*, 83 (1955) 505-507.
 - [35] R.W. Olesinski, G.J. Abbaschian, The copper-silicon system, *Bull. Alloy Phase Diagr.*, 7 (1986) 170-178, 193-176.
 - [36] X.Y. Yan, Y.A. Chang, A thermodynamic analysis of the Cu-Si system, *J. Alloys Compd.*, 308 (2000) 221-229.
 - [37] J.K. Solberg, Crystal-Structure of η -Cu₃Si Precipitates in Silicon, *Acta Crystallogr., Sect. A: Found. Crystallogr.*, 34 (1978) 684-698.
 - [38] K.P. Mukherje, J.P. Bandyopadhyaya, K.P. Gupta, Phase Relationship and Crystal Structure of Intermediate Phases in Cu-Si System in Composition Range of 17 at Pct Si to 25 at Pct Si, *Trans. Metall. Soc. AIME*, 245 (1969) 2335-2338.
 - [39] C.-Y. Wen, F. Spaepen, In situ electron microscopy of the phases of Cu₃Si, *Philos. Mag.*, 87 (2007) 5581-5599.
 - [40] S. Arrhenius, A. Westgren, X-radiation analysis of copper-silicon alloys, *Z. Phys. Chem.*, 14 (1931) 66-79.
 - [41] F.A. Veer, W.G. Burgers, W.G. Burgers, Diffusion in the Cu₃Si phase of the copper-silicon system, *Trans. Am. Inst. Min. Metall. Pet. Eng.*, 242 (1968) 669-673.
-

- [42] W.J. Ward, K.M. Carroll, Diffusion of copper in the copper-silicon system., J. Electrochem. Soc., 129 (1982) 227-229.
- [43] R.R. Chromik, W.K. Neils, E.J. Cotts, Thermodynamic and kinetic study of solid state reactions in the Cu-Si system, J. Appl. Phys., 86 (1999) 4273-4281.
- [44] R.R. Chromik, W.K. Neils, E.J. Cotts, Erratum: "Thermodynamic and kinetic study of solid state reactions in the Cu-Si system" [J. Appl. Phys. 86, 4273 (1999)], J. Appl. Phys., 87 (2000) U3-U3.
- [45] N. Mattern, R. Seyrich, L. Wilde, C. Baetz, M. Knapp, J. Acker, Phase formation of rapidly quenched Cu-Si alloys, J. Alloys Compd., 429 (2007) 211-215.
- [46] P. Riani, K. Sufryd, G. Cacciamani, About the Al-Cu-Si isothermal section at 500 DegC and the stability of the epsilon.-Cu₁₅Si₄ phase, Intermetallics, 17 (2009) 154-164.
- [47] C. Hisatsune, Constitution Diagram of the Copper-Silicon-Aluminium System, Memb. Coll. Eng. Kyoto Imp. Univ., 9 (1936) 18-47.
- [48] C.-Y. He, Y. Du, H.-L. Chen, H. Xu, Experimental investigation and thermodynamic modeling of the Al-Cu-Si system, CALPHAD, 33 (2009) 200-210.
- [49] A.K. Vasudevan, J.J. Petrovic, A comparative overview of molybdenum disilicide composites, Mater. Sci. Eng., A, A155 (1992) 1-17.
- [50] V.N. Svechnikov, Y.A. Kocherzhinskii, L.M. Yupko, Phase diagram of the molybdenum-silicon system, Diagrammy Sostoyaniya Metal. Sist., Mater. Vses. Soveshch., 4th, (1971) 116-119.
- [51] D.L. Anton, D.M. Shah, High-temperature properties of refractory intermetallics, Mater. Res. Soc. Symp. Proc., 213 (1991) 733-738.
- [52] N. Saunders, The Al-Mo system (aluminum-molybdenum), J. Phase Equilib., 18 (1997) 370-378.
- [53] J. Rexer, Phase Equilibria in Aluminium-Molybdenum System at Temperatures above 1400 Degrees C, Z. Metallkd., 62 (1971) 844-&.
- [54] G. Petzow, J. Rexer, Melting equilibriums of the U-UAl₂-Al₈Mo₃-Mo system, Z. Metallk., 60 (1969) 449-453.
-

- [55] D.M. Cupid, O. Fabrichnaya, F. Ebrahimi, H.J. Seifert, Thermodynamic assessment of the Al–Mo system and of the Ti–Al–Mo System from 0 to 20 at.% Ti, *Intermetallics*, 18 (2010) 17.
- [56] J.C. Schuster, H. Ipser, The Al–Al₈Mo₃ section of the binary system aluminum-molybdenum, *Metall. Trans. A*, 22A (1991) 1729-1736.
- [57] M. Eumann, G. Sauthoff, M. Palm, Re-evaluation of phase equilibria in the Al–Mo system, *Int. J. Mater. Res.*, 97 (2006) 1502-1511.
- [58] H. Okamoto, Al–Mo (Aluminum–Molybdenum), *J. Phase Equilib. Diffus.*, Online FirstTM (2010).
- [59] H. Nowotny, C. Brukl, Ternary system–Mo–Al–Si, *Monatsh. Chem.*, 91 (1960) 313-318.
- [60] C. Brukl, H. Nowotny, O. Schob, F. Benesovsky, Crystal structures of TiSi, Ti(Al,Si)₂, and Mo(Al,Si)₂, *Monatsh. Chem.*, 92 (1961) 781-788.
- [61] T. Tabaru, K. Shobu, M. Sakamoto, S. Hanada, Effects of substitution of Al for Si on the lattice variations and thermal expansion of Mo(Si,Al)₂, *Intermetallics*, 12 (2004) 33-41.
- [62] K. Yanagihara, T. Maruyama, K. Nagata, Isothermal and cyclic oxidation of Mo(Si_{1-x}, Al_x) up to 2048 K, *Mater. Trans., JIM*, 34 (1993) 1200-1206.
- [63] P.D. Eason, K.L. Jolly, M.J. Kaufman, Reassessment of the Mo–Si–Al ternary isotherm at 1400 °C, *Ceram. Eng. Sci. Proc.*, 19 (1998) 437-444.
- [64] Y. Liu, G. Shao, P. Tsakirooulos, Thermodynamic reassessment of the Mo–Si and Al–Mo–Si systems, *Intermetallics*, 8 (2000) 953-962.

2 Experimental

For the determination of isothermal and vertical sections (see Fig. 1.1), equilibrated alloy samples are used. To achieve equilibrated samples, the constituents have to be homogenized and the sample then has to be annealed at a certain temperature for a sufficient period of time to reach equilibrium. To preserve the equilibrated state of the sample for further analysis at room temperature, the sample has to be quenched, i.e. cooled very quickly. Unfortunately, quenching of a sample does not always work. If phase equilibria at high temperatures can not be quenched, there is the possibility of using high-temperature analysis methods like high temperature powder X-Ray diffraction (see section 3.1). In case of quenchable phase equilibria, different analysis tools are available for determining a phase diagram.

2.1 Light Optical Microscopy (LOM)

This method is very useful to check quickly if a respective sample is well homogenized and qualified for further investigations. Therefore it is usually the first analysis method applied. Additionally, this method also indicates the number of present phases and gives first information on the melting behaviour of the alloy.

A representative part of a sample is cut, ground and polished to obtain an ideally scratch-free surface and then investigated with the microscope. In the current work a Zeiss Axiotech 100 microscope was used operating in four different modes. In the bright field (BF) mode some phases are distinguishable due to their different reflectance. This mode usually provides less information than the other modes available on a proper light optical microscope. In the dark field (DF) mode, the directly reflected light from the sample surface does not

reach the eye. Instead, the light scattered on scratches, holes and edges appears bright to the observer. This mode provides information on the quality of the polishing process and it can show the different grains due to little edges at the grain boundaries. In the polarized imaging (PI) mode, the incident light beam is polarized and the sample modifies the plane of polarization according to its optical properties. Different phases appear in different colours in this mode. Grains of the same phase with different orientations appear in different colours, too, but show the same sequence of colours if the plane of the sample is rotated. Usually, samples with low symmetry affect the polarized light more than samples showing high symmetry. The last mode used is the difference interference contrast (DIC) mode. The incident light beam is split in two beams. If the sample shows a height profile, the two light beams have to cover different path lengths and interfere according to this difference in path lengths. The possible height profile in the sample originates in different hardness of the phases in the sample and subsequent different wastage rates during grinding and polishing.

2.2 Powder X-Ray Diffraction (XRD)

This analysis method uses structural information obtained by diffraction of X-Rays to identify phases.

In the current work, the Rietveld Method [1, 2] was applied for structural refinement of phases using the software TOPAS [3]. The Rietveld Method is a refinement technique using the least square approach to adapt a theoretical line profile to the measured line profile.

The measured line profile was obtained using a Bruker AXS D8 Advance Diffractometer which follows the Bragg-Brentano geometry. The standard setting uses Cu-K α radiation and a Lynxeye silicon strip detector. Structural information on phases present in a sample is obtained from literature, e.g. *Pearson's Handbook of Crystallographic Data* [4]. The diffraction pattern is calculated

using the software TOPAS. The calculated diffraction pattern then is tried to fit to the measured pattern by refinement of structural parameters chosen by the user.

The most important structural parameters to be refined are the lattice parameters, crystal size, atomic positions, occupation factors and the atomic displacement factors. Additionally, a preferred orientation of the crystals during the measurement can be taken into account, e.g. when a phase tends to form needles. Parameters not related to the sample can be refined as well, e.g. the sample displacement or the function describing the background.

The peak shape can be described by different mathematical models. Ideally, a peak is a single line, but in reality peak broadening occurs. The reason for peak broadening is on the one hand the sample itself which does not show perfect crystals only and, on the other hand, the instrument setup. In the current work, the *fundamental parameter Ansatz* [5-7] was used to describe the peak broadening caused by the instrument setup. This method uses instrumental parameters to describe the peak broadening instead of experimental parameters without any physical meaning.

Careful adjustment and refinement of the parameters mentioned above leads to a final structure with different structural properties compared to the initial structure model. If different phases are present in a sample, additionally the amount of the respective phase can be estimated by comparing the area of the peaks of the respective phases.

2.3 Electron Probe Micro Analysis (EPMA) and Scanning Electron Microscopy (SEM)

The methods applied for precise measurement of the composition of phases are EPMA and SEM in combination with EDS analysis. Both methods use the characteristic spectrum of X-Rays emitted by specific atoms when excited by high-energy electrons to deduce the concentration of different elements in a phase.

In EPMA, wavelength dispersive spectroscopy (WDS) is used for quantitative measurement. Scanning Electron Microscopy uses energy dispersive spectroscopy (EDS). Both methods require proper calibration. In EPMA, calibration is done by measuring pure elements or compounds with definite composition. In SEM calibration can be done like in EPMA, too, or an internal standard is used. Both, EPMA and SEM, use backscattered electron (BSE) imaging to find a proper spot for the measurement on the sample surface. In BSE mode, phases with distinct compositions are distinguishable because of their difference in the average atomic number. Elements with a high atomic number scatter electrons have a higher backscatter coefficient than light atoms and therefore appear brighter.

In the current work, EPMA measurements were carried out using a Cameca SX 100 Electron Probe Micro Analyzer (Cameca, Courbevoie, France). Conventional ZAF matrix correction was used to determine the composition from the measured X-Ray intensities. Calibration was done using the pure elements of Al, Cu, Si and Mo. SEM measurements were performed using a Zeiss Supra 55 VP Scanning Electron Microscope and the internal standard was used for the quantitative analysis with EDS.

2.4 Differential thermal analysis (DTA)

Differential Thermal analysis (DTA) is a dynamic standard technique used in combination with the methods discussed before. Since it is still of high importance for the determination of phase reactions, it will be discussed in more detail in the following section. Special focus will be set on proper interpretation of DTA measurements, because this is still a confusing topic for some researchers.

2.4.1 Basic principle and instrumental setup

DTA is a thermal analysis method. The heat flow to and from a sample is derived from the temperature difference between the sample and an inert reference while passing through a temperature program.

The basic setup of a DTA involves a sample holder, two crucibles, a furnace, a cooling system, a temperature controller and a recording device. Usually, the analysis chamber containing the sample and the reference is flushed with an inert gas to avoid oxidation. Ti or Mo sometimes is used as additional getter material. The analysis chamber is constructed symmetrically which means that the surrounding of the sample and the reference geometrically is the same. There are a lot of different configurations of the reaction chambers which will not be discussed in detail here. For further information see *B. Wunderlich: Thermal Analysis* [8].

The sample holder is equipped with two thermocouples, one measuring the temperature of the crucible containing the sample, the other for measuring the temperature of the reference crucible. The crucibles are made from an inert material, such as Alumina, Graphite or Tungsten. The material used for an investigation is dependent on the nature of the sample and the investigated temperature range. The reference has to be a substance which does not undergo any transition in the temperature range of interest; in most cases an empty crucible is sufficient as reference material.

Calibration of a DTA setup is achieved using the measurements of melting points of pure metals, such as Sn, Al, Ag, Au, Ni and Pt. The temperature range of thermal effects of interest in a sample should be within the melting points of the metals used for calibration. Additionally, the mass of the standard metals should be in the same range as the sample mass, usually between 10 and 80 mg, depending on the instrument.

To check the reversibility of reactions often a second heating/cooling cycle is recorded. Sometimes thermal effects are more intense than because of better thermal conductivity of the re-solidified sample with the crucible. But the experimenter always has to keep in mind that the sample sometimes is not in

thermodynamic equilibrium any more and if the first and the second heating cycle show different effects, usually the first one is more trustworthy.

In the current work, two different instruments were used, a Netzsch DTA 404 PC and a Setaram Setsys Evolution 2400.

The Netzsch instrument can be operated between room temperature and 1550 °C. The sample crucibles are made from Alumina and the sample mass used in analysis is between 15 and 25 mg. A dynamic Argon flow of 50 ml·min⁻¹ is applied and a Pt/Pt-10%Rh thermocouple is used (Type S) for temperature measurement.

The Setaram instrument is a combination of thermogravimetry and DTA, but the thermogravimetry mode has not been used in the current work. In the standard setup, the instrument can be used to temperatures up to around 1500 °C. Contrary to the Netzsch instrument, several thermocouples (“Type S”) are connected in series for the sample and the reference, respectively. This allows more sensitive temperature measurements and thus the use of smaller sample masses, between 5 and 20 mg.

A high temperature setup allows using the instrument for measurements up to 2400 °C. Therefore the alumina furnace tube is replaced by a graphite tube; the applied sample holder is made of tungsten and a W-5%Re/W-26%Re thermocouple (“W5-Type”) is used. Measurements at very high temperatures are always difficult to achieve. Problems start with the correct choice of the crucible. Alumina can not be used up to 2400 °C, Tungsten or Graphite can react with the sample. This has to be considered in doing high temperature measurements.

2.4.2 Evaluation of DTA data

The DTA signal is derived from the temperature difference between the sample and the reference. Since the reference material does not undergo any transition in the investigated temperature interval and the sample chamber setup is

symmetrically, the difference in temperature between the sample and the reference is derived from transitions in the sample. When a phase transition takes place during heating of the sample, the heat put into the sample is used to promote the phase transition and not to rise the temperature. Therefore the temperature of the sample is lower than the temperature of the reference material. The difference between the two temperature signals is recorded versus time by the instrument. After transition to a temperature-dependent diagram the effects can be evaluated. It has to be considered that different thermal effects result in different shapes of the respective signal (see below).

In Fig. 2.1 an example of a rather complicated binary phase diagram is shown on the bottom. The top shows the projection of the respective DTA curves taken on heating.

In the binary phase diagram shown in Fig. 2.1, the single phase fields are indicated by the Roman numeral I, two phase fields are indicated using the Roman numeral II. Point 1 and 2 indicate eutectic points, a peritectic point is indicated by point 7. Compound formation can be seen at point 3. The points 4, 5 and 6 indicate single phase solid solutions.

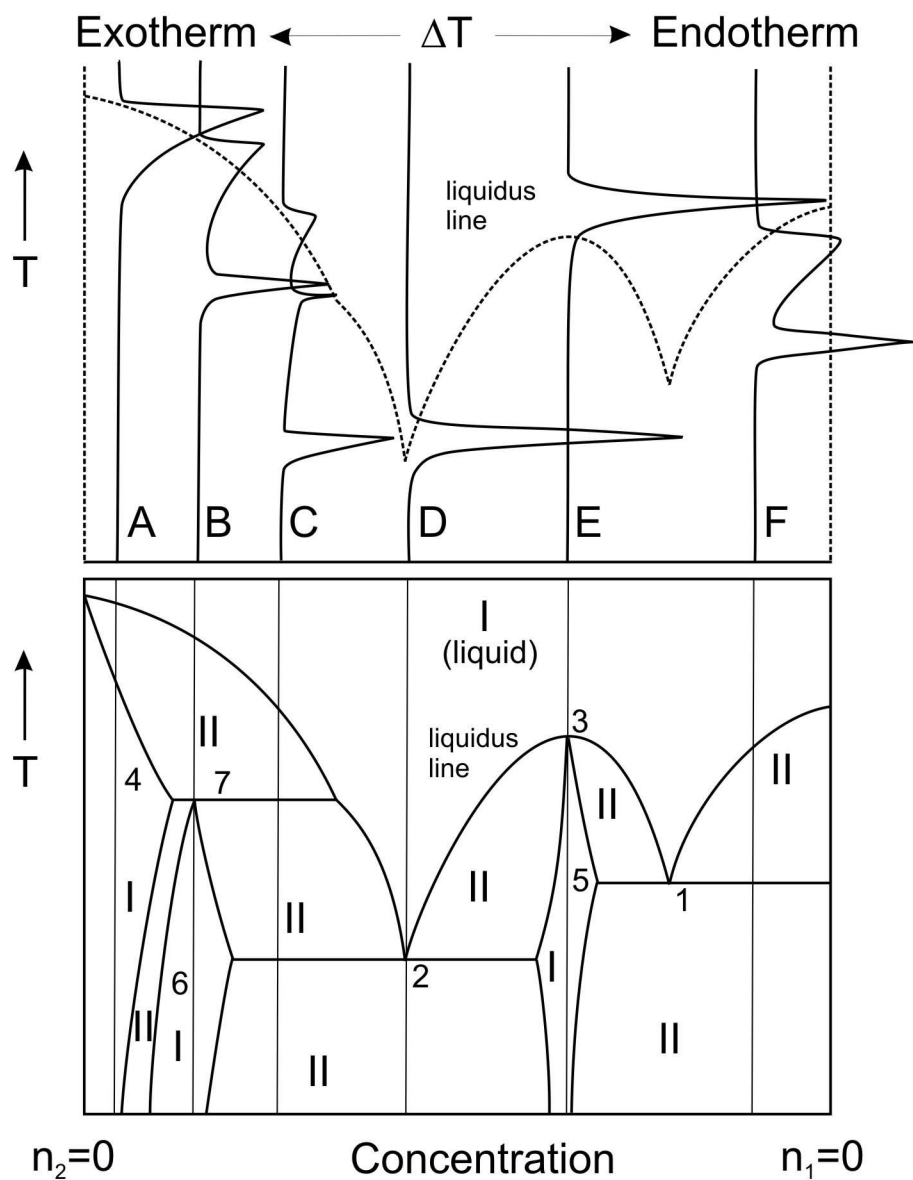


Fig. 2.1: Binary phase diagram (bottom) and the respective DTA curves at the concentrations A-F projected sideways (top)

reprinted from: *Thermal Analysis by Bernhard Wunderlich*, Copyright © 1990 by Academic Press Inc.[8]

The DTA curve on concentration F is shown in the upper diagram. In the first section, no thermal effect in the sample occurs and the temperature difference between the sample and the reference material is (ideally) zero. When the sample temperature reaches the eutectic temperature, a sharp melting peak appears. This originates from the melting of all of the solid solution 5 and an amount of pure n_2 , that the composition of the melt meets exactly the eutectic composition. During this process, the sample temperature stays (ideally) at the eutectic temperature resulting in a linear rise of the difference peak between the temperatures of the sample and the reference assuming the temperature program is linear. After the melting of the eutectic composition, the temperature in the sample rises again, resulting in lowering the difference signal. Rising temperature in the sample results in continuous melting of pure n_2 , leading in a broad melting peak as indicated in Fig. 2.1.

After melting of all the solid material in the sample, the difference signal returns to its base line. Recapitulatorily it can be said that the eutectic reaction starts at the beginning of the eutectic peak (onset) and the melting of the sample is finished, where the difference signal returns to the base line (in this case: peak maximum). Consequently, these two points are the ones to evaluate (see Fig. 2.2). It has to be mentioned that the liquidus peak can be a very small step in the DTA curve, depending on the amount of liquid in the sample. Usually the (exothermic) solidification peak during cooling of the sample is more intense. Due to undercooling, the onset of the solidification peak is always lower than the melting temperature on heating of the sample.

Curve E shows the melting peak of a congruently melting phase. The phase does not undergo any transition before melting and the melting peak as shown in Fig.2.2 should be very sharp. Peak broadening occurs only due to instrumentation lag.

The same type of curve is shown with curve D. The only difference is that in this case a eutectic mixture between 5 and 6 is melting. This should result in a

very sharp melting peak as well. In both cases, E and D, the onset of the respective peak is evaluated (see Fig. 2.2).

Curve C crosses the invariant reaction 2, resulting in a peak with a linear slope, before hitting the peritectic reaction 7, which results in an invariant effect, too. The melting peak of this sample looks similar to the melting peak in curve E and is evaluated similarly (see Fig. 2.2).

In curve B the peritectic decomposition of phase 6 results in an invariant effect followed by a broad melting peak due to the melting of phase 4.

Finally, curve A does not cross any invariant reactions. The beginning of the broad melting peak indicates the start of the melting of phase 4, the peak maximum represents the intersection between the concentration coordinate and the liquidus line. The correct evaluation is shown in Fig. 2.2.

It has to be mentioned, that thermal effects involving solids sometimes show very low intensity making it almost impossible to identify them. It is the same case for transition of a single phase field to a two phase field or vice versa if the limiting phase boundary is very steep.

In this case, it is up to the responsibility of the experimenter to interpret the data in accordance with thermodynamic requirements and experimental results of neighboring samples.

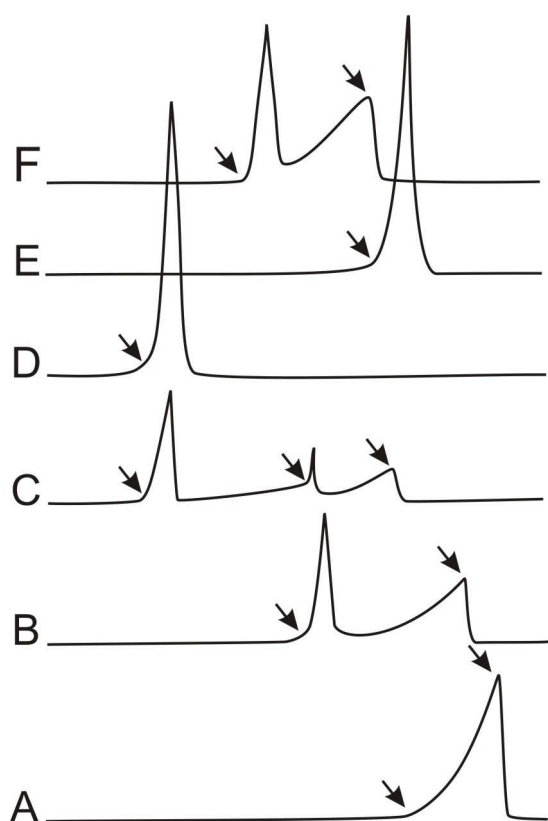


Fig. 2.2: *Correct evaluation of the DTA curves shown in Fig 2.2*

2.5 Structure determination from powder XRD data using Simulated Annealing

Whenever the structure of a new phase has to be determined, the experimenter aims to find a proper single crystal and tries to solve the structure by single crystal structure determination methods. In case of a proper crystal showing no twinning and which does not contain a large amount of very light atoms, this approach usually results in a proper structure refinement.

In some cases, single crystals are not accessible due to various reasons, e.g. the structure to investigate is not stable at room temperature and it is not possible to

quench it. In this case, structure determination using high temperature powder XRD is an option. In the following section the structure determination from powder XRD data using the software TOPAS [3] is described.

2.5.1 Steps in structure determination

A. Determining the space group

For determination of the correct space group it is very important to identify the first 15 to 25 peaks which belong to the phase. It is crucial not to miss peaks in this range which belongs to the structure of interest, because this can lead to a completely wrong space group making it very difficult to solve the structure at all. Peak shapes are described using the *fundamental parameter Ansatz* [5-7]. The entirety of peaks forms a *peak phase*. Refinement of the *peak phase* refining the position, the area and the crystallite size of the peaks, leads to precise positions of the peaks. In this step, the refined crystallite size can give a hint if the refined peaks belong to the same phase. If this is the case, the value for the crystallite size should be within the same order of magnitude. But this criterion has to be treated with extreme care, especially if the peak intensity is very different and the crystallite size of weak peaks is used by the software to fit the background. Additionally, fixing the crystal size of all peaks to an average value and subsequent refinement can give information on whether broad, overlapping peaks are covered by a sufficient number of peaks of the *peak phase*.

The position of the peaks in the peak phase is then imported in an indexing routine (*indexing range*). With this routine, it is possible to search for Bravais lattices, which fit the position of the peaks. The results are ordered according to their GOF (goodness of fit) and their cell volume. If none of the suggested solutions fits the position of the peaks satisfactorily, it is necessary to re-check the identified peaks whether peaks are missing or peaks are spuriously imputed to the unknown phase. For further investigation, the solution showing the highest

symmetry as well as the smallest volume is the right choice so far. Additionally, literature research about related compounds showing comparable cell parameters and compositions is indispensable to find a proper structural solution.

The Bravais lattice, found to be the most promising one, is now used to create a so-called *hkl-phase*. This phase now bears the information about the space group of the structure and the lattice parameters but does not contain any information about the distribution of the atoms across the unit cell. Refinement of the *hkl-phase* only shows if the measured powder XRD pattern can be explained by the discovered structure on basis of systematic extinction and peak positions according to the given lattice parameters. If the *hkl-phase* fits the pattern satisfactorily, the proposed structure is then used for the structure determination using *Simulated Annealing*.

B. Structure determination by Simulated Annealing

Simulated annealing (SA), in general, is a method used for optimization of a given function finding a global optimum or, at least, a good approximation to it.

Its name is based on the term *annealing* in metallurgy where metals undergo defined heating and cooling programs. During a slow cooling process, the atoms have a good chance to re-arrange properly and thus avoiding crystal defects. The structure reaches a minimum of internal energy.

This minimum of internal energy is comparable to the global optimum in SA. For reaching the global optimum, in each step of the SA process the optimized function is replaced by a function which is very “close” to the preceding one. The probability for this replacement is dependent on the difference of the corresponding function parameters and an additional value (*Temperature T*, also a reference to the annealing process in metallurgy). The T-factor is gradually reduced during the annealing process, making it more and more unlikely, that the preceding function is replaced which leads ideally to finding the global optimum. The strength of this method is that an optimized function is replaced by a random

function “nearby” which makes it possible to escape a local minimum and reach a global one.

Structure determination by SA [9] is done in the Launch Kernel of TOPAS [3]. This approach needs an input-file with all the relevant data, including the measured diffractogram and instrumental parameters. This file can be created directly from the graphical mode of TOPAS.

According to the volume of the unit cell and the expected density of the material, a number of atoms are included in the input file, matching the expected composition of the phase. The number of atoms in the cell is estimated based on the assumption that every atom is located at a general position.

In the beginning, all the atoms are located near the origin and the atomic coordinates are set to be refined, as well as the scaling factor. An additional command (*occ_merge*) is necessary in the input file for subsequent identification of special positions and recognition of overlapping atoms. The indicating parameter is called *occupation*, which should not be mistaken for *site occupation* in Rietveld refinement. If the *occupation* of one position, for example, is close to 1/2 after a SA cycle, this means that the atom at this position is overlapping with itself indicating a special position.

Starting the program leads to an output file with a calculated structure which represents the minimum of the least square refinement. The output file shows refined lattice parameters, atom coordinates and the refined *occupation*. A graphical illustration of the final structure is shown, too, using the command *view_structure* in the input file. Usually, the shown structure is not the solution of the structural problem.

A close look at the atom coordinates is necessary. Special positions need to be identified by investigating the *occupation* values of the different positions in combination with structural information on the space group given by the *International Tables of Crystallography* [10]. If an atom tends to occupy a special position, its coordinates need to be set to the exact coordinates of the special

position given by the *International Tables of Crystallography* [10] and not refined furthermore. Furthermore, if two different atoms show the same value for the *occupation*, it is highly likely that they try to share the same position in the unit cell. Therefore one of these atoms has to be removed.

After removing overlapping atoms and setting atoms at special positions, the total number of atoms in the cell is reduced and has to be compensated for the next optimization step by adding atoms. The modified output file serves as the new input file for the next step. The optimization of an input file and modification of the output file is repeated until the resulting structure is reasonable with respect to atomic distribution and interatomic distances and explains the measured pattern satisfactorily. If this does not happen, it might be possible that the selected space group or the unit cell is wrong. Then it is necessary to go back to the determination of the space group and reconsider the former selection.

C. Structure refinement and standardization

The structure obtained by the procedure above has to be checked for additional symmetry, refined by Rietveld refinement and standardized. For standardization and checking for additional symmetry, the program package Structure Tidy [11, 12] was used in the current work. Rietveld refinement can be carried out using TOPAS [3].

References

- [1] H.M. Rietveld, Line profiles of neutron powder-diffraction peaks for structure refinement, *Acta Crystallogr.*, 22 (1967) 151-152.
- [2] H.M. Rietveld, Profile refinement method for nuclear and magnetic structures, *J. Appl. Crystallogr.*, 2 (1969) 65-71.
- [3] A.X.S. BRUKER, TOPAS V3: General profile and structure analysis software for powder diffraction data, in: *Users's Manual*, Bruker AXS, Karlsruhe, Germany, 2005.
- [4] P. Villars, L.D. Calvert, *Pearson's Handbook of Crystallographic Data for Intermetallic Phases*, 2nd ed., ASM International, 1991.
- [5] R.W. Cheary, A. Coelho, A fundamental parameters approach to x-ray line-profile fitting, *J. Appl. Crystallogr.*, 25 (1992) 109-121.
- [6] R.W. Cheary, A.A. Coelho, J.P. Cline, Fundamental Parameters Line Profile Fitting in Laboratory Diffractometers, *J. Res. Natl. Inst. Stan.*, 109 (2004) 1-25.
- [7] A. Kern, A.A. Coelho, R.W. Cheary, Convolution based profile fitting, *Diffraction Analysis of the Microstructure of Materials*, in: E.J. Mittemeijer, P. Scardi (Eds.) *Materials Science Springer*, 2004.
- [8] B. Wunderlich, *Thermal Analysis*, Academic Press, Inc., 1990.
- [9] A.A. Coelho, Whole-profile structure solution from powder diffraction data using simulated annealing, *J. Appl. Crystallogr.*, 33 (2000) 899-908.
- [10] *International Tables for Crystallography*, Kluwer Academic Publishers, 1996.
- [11] L.M. Gelato, E. Parthé, STRUCTURE TIDY - a computer program to standardize crystal structure data, *J. Appl. Crystallogr.*, 20 (1987) 139-143.
- [12] E. Parthe, L.M. Gelato, The standardization of inorganic crystal-structure data, *Acta Crystallogr., Sect. A: Found. Crystallogr.*, A40 (1984) 169-183.

3 Results and discussion

3.1 Re-investigation of phase equilibria in the system Al-Cu and structural analysis of the high-temperature phase η_1 -Al_{1- δ} Cu

Norbert Ponweiser^a, Christian L. Lengauer^b and Klaus W. Richter^{a*}

^aUniversity of Vienna, Department of Inorganic Chemistry/Materials Chemistry,
Währinger Straße 42, 1090 Wien, Austria

^bUniversity of Vienna, Institute for Mineralogy and Crystallography,
Althanstraße 14, 1090 Wien, Austria

* corresponding author

Email: klaus.richter@univie.ac.at

Accepted: *Intermetallics* (2011), doi:10.1016/j.intermet.2011.07.007

Contributions to this paper:

N.P.: sample preparation, analysis and most of the interpretation, wrote the paper

C.L.L.: high-temperature XRD measurements, advice in structure determination

K.W.R.: proofreading, general advice and helpful comments

Contribution of N. Ponweiser to the article: 80 %

Abstract

The phase equilibria and reaction temperatures in the system Al-Cu were re-investigated by a combination of optical microscopy, powder X-ray diffraction (XRD) at ambient and elevated temperature, differential thermal analysis (DTA) and scanning electron microscopy (SEM). A full description of the phase diagram is given. The phase equilibria and invariant reactions in the Cu-poor part of the phase diagram could be confirmed. The Cu-rich part shows some differences in phase equilibria and invariant reactions compared to the known phase diagram. A two phase field was found between the high temperature phase η_1 and the low temperature phase η_2 thus indicating a first order transition. In the ζ_1/ζ_2 region of the phase diagram recent findings on the thermal stability could be widely confirmed. Contrary to previous results, the two phase field between δ and γ_1 is very narrow. The results of the current work indicate the absence of the high temperature β_0 phase as well as the absence of a two phase field between γ_1 and γ_0 suggesting a higher order transition between γ_1 and γ_0 . The structure of γ_0 (*I*-43*m*, Cu₅Zn₈-type) was confirmed by means of high-temperature XRD. Powder XRD was also used to determine the structure of the high temperature phase η_1 -Al_{1- δ} Cu. The phase is orthorhombic (space group *Cmmm*) and the lattice parameters are $a = 4.1450(1)$ Å, $b = 12.3004(4)$ Å and $c = 8.720(1)$; atomic coordinates are given.

Introduction and literature review

The system Al-Cu has been investigated intensively during the last decades, mainly due to the importance of Al-based alloys, for example in aviation and transport industry. In view of this, the main focus of most studies in the system is the very Al-rich part. Although a lot of work was done in the Cu-rich part as well, there are still some uncertainties and inconsistencies in the phase diagram present.

The major assessment of the system was done in 1985 by Murray [1]. His extensive paper gives an equilibrium phase diagram as well as manifold information on metastable phase equilibria which are not part of the current investigation. According to [1], the equilibrium phase diagram contains 5 intermetallic compounds stable at ambient temperature and 7 additional compounds stable at elevated temperature (see Fig. 1). The phase diagram given by Murray does not represent the current level of knowledge about the system. A more recent phase diagram combining the assessment of Murray [1] with new data from Liu et al. [2] is given by Riani et al. [3]. Thermodynamic calculations in the system were performed by several authors concentrating on transition- and ordering phenomena [4-7], as well as on atomic mobility [8]. A thermodynamic assessment is given by Saunders [9]. An overview on the Al-Cu phases described by different authors [1, 10-21] is given in Table 1.

The structure of the θ -phase with the composition Al₂Cu was originally revealed by Friauf [22] and found to be tetragonal. According to Murray [1] the phase is stable up to 591 °C. Additional investigations in the region between 31 and 37.5 at.% Cu by Goedecke and Sommer [23] indicate a composition of 32.4 at.% Cu for θ at its formation temperature of 592 °C. The eutectic line of the reaction $L = (Al) + \theta$ ends at 32.05 at.% Cu. The widest solubility range of the phase is 0.55 at.% at 549 °C [23].

Structural investigations of the compound η -AlCu have already been performed by Preston [10] who found an orthorhombic structure in a sample quenched from 602 °C. Bradley et al. [20] investigated slowly cooled samples of the same

composition and proposed an allotropic transformation $\eta_1 \rightarrow \eta_2$ on basis of structural differences compared to the work of Preston. The authors suggested orthorhombic or monoclinic symmetry for the low temperature phase. El-Boragy et al. [11] were able to solve the structure of the low temperature phase which was found to be monoclinic. The high temperature structure is still unknown. Preston suggested the structure to be orthorhombic (*oP16* or *oC16*) [10], Lukas and Lebrun [12] mentioned in their assessment of the Al-Cu-Si system an orthorhombic cell with lattice parameters $a = 4.087 \text{ \AA}$, $b = 12.00 \text{ \AA}$, $c = 8.635 \text{ \AA}$ and 32 atoms per unit cell. Although the supposed type of transition reaction was not mentioned explicitly, the assessed phase diagram by Murray [1] and Riani et al. [3] obviously suggest a transition of higher order between η_2 and η_1 .

According to the assessment of Murray, the introduction of the high temperature phase ε_1 and ε_2 goes back to 1920. However, the structure of ε_2 was solved for the first time in 1972 by El-Boragy et al. [11], applying high temperature XRD. According to the authors, the structure of ε_2 -Cu₃Al_{2+x} is of the NiAs-type with partial occupation of the additional interstitial position. The structure of the high temperature modification ε_1 is still unknown.

The compound with the proximate composition Al₃Cu₄ (ζ_1/ζ_2 – region) was also described by Preston [10] and Bradley [20] and was found to show a high and a low temperature modification. The work of Murray suggests a transition temperature between 530 and 570 °C but mentions other reported thermal effects between 373 and 450 °C as well [1]. Dong et al. [24, 25] investigated as-cast and annealed samples with the composition Al₃Cu₄. In the as-cast samples the authors find a mixture of an orthorhombic face-centered and an orthorhombic body-centered structure as well as a small amount of γ -Al₄Cu₉. After annealing at 500 °C for 10 hours the *oF* structure became the major phase thus the authors suggested a transition γ -Al₄Cu₉ + “*oI*” = “*oF*”. Electron Probe Micro Analysis (EPMA) measurements indicated compositions of Al_{43.2}Cu_{56.8}, Al_{41.3}Cu_{58.7} and Al_{39.6}Cu_{60.4} for “*oF*”, “*oI*” and γ -Al₄Cu₉, respectively. The crystal structures of ζ_1 (*Fmm2*, structure type Al₃Cu₄) and ζ_2 (*Imm2*, structure type Al₃Cu₄₋₈) were finally solved by Gulay and Harbrecht using powder XRD [13, 14]. The composition of

the samples for structure analysis of ζ_1 (Al_{42.5}Cu_{57.5}) and ζ_2 (Al_{43.2}Cu_{56.8}) contradicts the findings of Dong et. al. [24, 25] who allocated the face-centered symmetry to the phase with lower Cu content. Thermal analysis of samples by Gulay and Harbrecht [13, 14] reveals another contradiction. The assessment of Murray shows a low temperature phase ζ_2 and a high temperature phase ζ_1 with a slightly higher Cu-content; the transition temperature is supposed to be between 530 and 570 °C. Gulay and Harbrecht, however, found the Cu-richer phase ζ_1 (only phase in a sample with the composition Al_{42.5}Cu_{57.5}) to be stable at 400 °C [14]. The Cu-poorer phase ζ_2 (only phase in a sample with the composition Al_{43.2}Cu_{56.8}) was found to be stable at elevated temperatures (530 °C) and did not resist thermal treatment at 400 °C [13]. The authors claim that entropy provides an essential contribution to the stabilization of the ζ_2 phase.

The range from 60 to 70 at.% Cu was investigated intensively for many decades. Bradley [26] claimed that three different phases are present in this region: a cubic (γ), a monoclinic and a rhombohedral compound. Westman [27] found the latter to crystallize in space group $R3m$ and confirmed the existence of a third phase of unknown structure between the cubic and the rhombohedral compound. Seshadri and Downie [28] claimed that there are only five intermetallic phases stable in the temperature range between 25 and 500 °C, namely $\gamma_{(1)}$, δ (described by a cubic structure), ζ_2 , η_2 and θ . The separation of γ_1 and δ is supported by an abrupt change in expansion coefficient from γ_1 to δ . In the assessed phase diagram the third phase of unknown structure mentioned above is not included since there is no consensus about its existence. Murray pleads diffusion couple experiments of Funamizu et al. [29] which do not show any other phase between γ_1 and δ . More importantly, very slow cooling experiments performed by van Sande et al. [30] show γ_1 and δ in equilibrium, too. These two experiments support the non-existence of a third equilibrium phase in the indicated region. The existence of the high temperature phase γ_0 was demonstrated by thermal analysis but the transition γ_0 to γ_1 could not be confirmed metallographically [1]. Liu et al. [2] examined the Cu-rich part of the phase diagram by diffusion coupling, differential scanning calorimetry and high

temperature XRD. The authors state that γ_0 crystallizes in the Cu₅Zn₈-type and they do not find a two phase field between γ_0 and γ_1 , thus proposing a higher order transition between the two phases, in contradiction to Murray's assessment [1].

According to Murray [1], quoting Dawson [31] the high temperature phase β_0 is formed peritectically from β and liquid at 1037 °C. Dawson determined the composition and stability range of β_0 by metallography and dilatometry but the findings have never been reconfirmed and the structure of β_0 remains unknown [1]. Nevertheless, β_0 was included in the equilibrium phase diagram. In 1998 diffusion couple experiments performed by Liu et al. [2] showed a two phase region between β and γ_0 and no single phase β_0 was found. Additionally, the authors found only one peak in DSC measurements at 1019 °C which they interpreted to be the solidus of the β phase rather than the reaction temperature of the eutectoid transformation $\beta_0 = \beta + \gamma_0$. Hurtado et al. [32] investigated the region between 85 and 89 at.% Cu at temperatures from 450 to 850 °C, finding a square-like shaped phase which has, however, not been confirmed by other authors.

The β -phase and the two-phase region between β and (Cu) was frequently investigated and the assessment of Murray [1] gives a broad overview about the results of this research. It shows that the eutectoid temperature was found between 560 and 575 °C which can be explained by the sluggishness of the reaction. Reaction temperatures between 515 and 540 °C can be considered due to metastable eutectoid and peritectoid reactions.

The α_2 -phase was first described by West et al. [33] during long term annealing experiments. According to Murray, later studies confirmed the peritectoid decomposition temperature to be 363 °C at 77.25 at % Cu. According to Murray's assessment, α_2 has an ordered fcc structure with a long period superlattice based on Cu₃Au and Al₃Ti (Strukturbericht designations: L1₂ and D0₂₂, respectively) [1]. A more detailed description about investigations of the low temperature phase α_2 , including thermal analysis experiments in this region is given by Adorno et al. [34].

Experimental

The samples were prepared from Aluminum slug (99.999%), and Copper wire (99.95%), both supplied by Alfa Aesar, Karlsruhe, Germany. The Cu wire was reduced in a H₂-flow at 300 °C for 3 hours. The calculated amounts of Al and Cu were weighted to an accuracy of 0.05 mg; the sample weight usually was 1000 mg. Sample homogenization was done in an arc furnace MAM-1 by Edmund Buehler with a water-cooled copper plate and zirconium as the getter material. For homogenization of the sample, the resulting bead was turned and re-melted two times. The occurring mass loss during this procedure was found to be below 1 % and therefore considered not to affect the sample composition significantly. The resulting bead was wrapped in Molybdenum foil (99.97 %, Plansee SE, Reutte, Austria) and annealed at 500°C under vacuum in a quartz glass tube for 24 days. Subsequently the samples were quenched in cold water and prepared for further investigation. Representative sections of all annealed samples were investigated by means of optical microscopy using a Zeiss Axiotech 100 microscope. Selected samples were analyzed by means of Scanning Electron Microscopy (SEM). The quantitative chemical analyses were performed on a Zeiss Supra 55 VP in combination with energy dispersive spectroscopy (EDS) using the pure elements for calibration. Measurements of the phase composition were performed with a minimum of three different spots and the results were averaged.

X-ray powder diffraction analyses were performed using a Bruker D8 ADVANCE diffractometer operating in reflection mode (Cu K α_1 radiation, LynxEye silicon strip detector). For selected samples high temperature X-ray powder diffraction analysis was applied using an Anton Paar XRK900 reactor chamber with an automated alignment stage. The temperature resolved measurements were performed under evacuated conditions. For evaluation of the resulting diffractograms, both at ambient as well as at elevated temperature, the software TOPAS [35] was used.

The DTA measurements were performed on a Setaram Setsys Evolution 2400 (Setaram Instrumentation, Caluire, France) and a Netzsch DTA 404 PC (Netzsch,

Selb, Germany). The measurement devices used Pt / Pt-10%Rh thermocouples (Type S) which were calibrated using the melting points of pure Sn, Au and Ni. The samples with a weight of approximately 20 mg were placed in open alumina crucibles and measured under an argon flow of 50 ml·min⁻¹ for the Netzsch and 20 ml·min⁻¹ for the Setaram device. Applying a heating / cooling rate of 5 °C·min⁻¹, two consecutive curves were recorded for each sample. The possible mass loss during the DTA investigations was checked routinely and no relevant mass changes were observed.

Results and Discussion

Phase equilibria in the system Al-Cu

Combining results from both DTA and SEM measurements, it was possible to obtain the complete description of the Al-Cu system which is plotted in Fig. 2. It is, for the most part, in good agreement to the phase diagram of Liu et al. [2] and Riani et al. [3] but it shows significant differences to the phase diagram proposed by Murray [1]. The occurring invariant reactions together with the composition of the reacting phases and the reaction temperature are given in Table 2, selected SEM images taken in back-scattered electron (BSE) mode are shown in Fig. 3.

The Al-rich part of the phase diagram has not been investigated extensively in the current study. Concerning the reaction temperatures and the phase composition SEM and DTA measurements confirm the findings of previous authors. The solubility of Cu in Al was found to be 2.2(1) at.% at 500 °C. The lattice parameters of the phase θ (θ /12, Al₂Cu-type) vary from $a = 6.0718(1)$ and $c = 4.8802(1)$ Å at 32(1) at.% Cu to $a = 6.0613(1)$ and $c = 4.8724(1)$ Å at 33.6(2) at.% Cu. The phase boundaries of the binary phases in the Al-rich part of the phase diagram have been determined by means of SEM measurements and are indicated as black dots in Fig. 2.

In the region of a Cu-content of more than 50 at.%, the evaluation of phase equilibria was more challenging. The phases η_1 -AlCu and η_2 -AlCu are supposed to be stable around 50 at% Cu with a solubility range of 1 to 2 at.% Cu [1]. The results in the current investigations, however, reveal a shift of the composition towards the Cu-rich side. The solubility limits of the phase η_2 -AlCu at 500 °C were confirmed by SEM measurements. The Cu-poor and the Cu-rich composition limit were found at 51.9(5) at.% Cu and at 54.8(5) at%, respectively. XRD analysis of the samples with the nominal composition Al₄₉Cu₅₁ (showing θ and η_2 in equilibrium), Al_{47.5}Cu_{52.5} and Al_{46.5}Cu_{53.5} (showing single phase η_2) and Al₄₅Cu₅₅ (showing η_2 plus traces of ζ_1) indicate a Cu-rich solubility limit between 54 and 55 at.% Cu which supports the SEM measurements.

The lattice parameters for η_2 (*mC20*, AlCu-type) range from $a = 12.0925(1)$, $b = 4.1001(1)$, $c = 6.9085(1)$ Å, $\beta = 55.03(1)^\circ$ on the Cu-poor side to $a = 12.2012(1)$, $b = 4.0997(2)$, $c = 7.0047(3)$ Å and $\beta = 54.787(1)^\circ$ for the Cu-rich side of this compound.

The phase diagrams of Riani and Murry indicate a transition temperature from the high temperature η_1 -phase to the low temperature η_2 -phase at 563 °C at the Cu-poor side and 560 °C at the Cu-rich side [1, 3]. According to our measurements the transition temperatures are 574(3) °C for the Cu-poor side and 580(1) °C for the Cu-rich side. Consequently, we propose also different solid state reactions in this area: the eutectoid decomposition $\eta_1 = \eta_2 + \theta$ at 574(3) °C and the peritectoid reaction $\eta_1 + \zeta_2 = \eta_2$ at 581(1) °C. The peritectic decomposition temperature of the phase η_1 was found to be 625(2) °C which is in agreement with the phase diagrams mentioned above.

The region of Al₄Cu₉ with the supposed high temperature modification ζ_1 and the low temperature phase ζ_2 is also complex. Gulay and Harbrecht find the Cu-rich phase ζ_1 stable at 530 and 400 °C, but the Cu-poor phase ζ_2 stable at 530 °C and not stable at 400 °C [13, 14]. They discovered that after a heat treatment at 400 °C, ζ_2 is decomposed into ζ_1 and small amounts of η_2 . Additionally, Gulay and Harbrecht state that at 450 °C the phase ζ_2 segregates in a mixture of ζ_1 and ζ_2 . Therefore, the authors conclude that the temperature of the eutectoid decomposition of ζ_2 is between 400 and 450 °C. The present work shows a sample with the nominal composition of Al₄₅Cu₅₅ exhibiting η_2 as major phase with very small traces of a second phase. Comparison of systematic extinctions of ζ_1 and ζ_2 suggests that the second phase is ζ_1 . Due to the very low amount of ζ_1 in the respective sample, SEM analysis of this sample shows only one suitable measurement point at 56.3 at.% Cu which can be assigned to the Cu-poor solubility limit of ζ_1 . XRD analysis of a sample with the nominal composition Al_{42.5}Cu_{57.5} shows ζ_1 [14] and some unidentified peaks (see Tab. 3). These XRD results narrow the solubility limits of ζ_1 (*oF88*, Al₃Cu₄-type) between approx. 56 and 57.5 at.% Cu. In the present investigation, DTA analysis of the sample with the nominal composition of Al₄₅Cu₅₅ does not show any effects related to the

transition of ζ_1 to ζ_2 , caused by the fact that the amount of ζ_1 is very small in the sample. DTA analysis of the sample with the nominal composition Al_{42.5}Cu_{57.5} shows an invariant effect at 561(2) °C which is considered to be related to the reaction $\zeta_2 + \delta = \zeta_1$. These results do confirm the previous authors [13, 14] concerning the stability of the low temperature phase ζ_1 which is considered to be stable between ambient temperature and 561(2) °C. The phase ζ_2 is stable up to 596(1) °C where it decomposes peritectically. Since the XRD results of the sample Al₄₅Cu₅₅ show small traces of ζ_1 we suggest a transition temperature $\zeta_2 = \zeta_1 + \eta_2$ above 500 °C.

The solubility limit at the Cu-rich side of ζ_1/ζ_2 was not accessible due to low contrast and fine microstructure. However, δ was found as the only phase present in Al₄₀Cu₆₀, while Al_{42.5}Cu_{57.5} showed ζ_1 with traces of δ . Therefore, the situation of the two phase field can be specified quite accurately.

It was not possible to determine the phase boundaries between the two phases δ and γ_1 by SEM measurements due to the lack of contrast and possibly very fine microstructure. In XRD it was possible to distinguish the single phase region δ ($R3m$, $a = 12.285(1)$ Å, $c = 15.1486(1)$ Å [15]) from the single phase region γ_1 ($P43m$, $a = 8.7068(3)$ Å [16]) by peak splitting and selective peak broadening even though the patterns look very similar. Samples with the nominal composition Al₄₀Cu₆₀ to Al₃₇Cu₆₃ show δ as the only present phase. The sample Al₃₆Cu₆₄ shows a main pattern corresponding to δ plus some small extra peaks that could not be explained by δ or γ_1 . They may be caused by superstructure reflections, corresponding to the monoclinic structure proposed by Bradley [26] and Westman [27], which was omitted in the assessment of Murray [1]. We marked the respective area in Fig. 2 with a question mark. More detailed studies would be required to confirm the existence of an additional phase. The absence of invariant effects at 684(1) °C dedicated to the reaction $\varepsilon_2 + \gamma_1 = \delta$ in the sample Al₃₈Cu₆₂ and Al₃₇Cu₆₃ can be explained by a shift of the γ_1 phase field towards the Cu-poorer region at elevated temperatures and, therefore, a smaller amount of δ taking part in the reaction. This leads to a smaller endothermic effect and since the respective endothermic peaks in the samples Al₄₀Cu₆₀ and Al₃₉Cu₆₁ are already

small the resulting effect in the samples Al₃₈Cu₆₂ and Al₃₇Cu₆₃ might be insufficient to observe.

The region between γ_1 and (Cu) has been the subject of an intensive research in the past and the present work does not provide any contradictory information. The solubility of Al in (Cu) as well as the upper solubility limit of γ_1 was confirmed by SEM measurements. DTA analysis of samples in the respective area show very small thermal effects close to the solubility limit of (Cu) at 567 °C and thermal effects related to the formation of β at higher temperature, which are indicated as diamond shaped points in Fig. 2.

In general, solubility ranges and thermal stability of the high temperature compounds ε_1 and ε_2 could be confirmed in the present work by DTA observations. Slight changes concerning reaction temperatures and solubility ranges are shown in Table 2.

Since there is no consensus in literature concerning the transition of the high temperature phase γ_0 to the low temperature form γ_1 this area is of special interest. Analysis of thermal effects of samples in the respective field show very weak effects varying continuously with the composition. We did not observe any pointer for an invariant decomposition of γ_1 in any of the investigated samples. Therefore we conclude that the transition $\gamma_1 = \gamma_0$ is of higher order, in agreement with the previous obtained results by Liu et al. [2].

Structural analysis of a sample with the nominal composition Al₃₂Cu₆₈ confirm the structure given for γ_0 by Liu (*I*-43*m*, Cu₅Zn₈-type [2]), and reveals a lattice parameter of $a = 8.8692(1)$ Å at 900 °C. XRD data of the sample at selected temperatures are shown in Fig. 4.

According to Murray [1], the high temperature phase β_0 was included in the equilibrium phase diagram although its existence could not be confirmed. Liu et al. [2] did not find any evidence of its existence and consequently was not incorporated in the assessed phase diagram of Riani et al. [3]. Results of the present work confirm that there is no evidence of the existence of β_0 and all observed DTA effects in this composition area can be explained by the formation of the phases β and γ_0 .

Structural analysis of η_1

Up to now, the crystal structure of η_1 was not known. Preston [10] suggested the space groups *Cmmm* or *Pban* and orthorhombic lattice parameters were given by Lukas and Lebrun [12]. In the current study, we used high temperature powder XRD data to establish a structural model for η_1 . Measurements were carried out in a temperature range from 500 to 750 °C at intervals of 25°C using a sample with the nominal composition Al₅₀Cu₅₀. A selection of these diffractograms is shown in Fig. 5. The measurements up to 550 °C show the low-temperature η_2 -phase in equilibrium with traces of the θ -phase. At 575 °C a third pattern, η_1 , appears which is the only phase at 600 and 625 °C. Above 650 °C only ε_2 is present and significant peak broadening can be observed, indicating the partial melting of the powder. After cooling back the sample to 500 °C one again observes η_2 and θ , the diffraction lines, however, are significantly broadened. Some unidentified peaks of very low intensity may be attributed to oxide formation at the sample surface during the long stay in the non ambient device. Since the amount of possible oxide is very small, further investigation was not performed.

The pattern measured at 600 °C could be successfully indexed using the orthorhombic unit cell suggested by Lukas and Lebrun [12]. Cell refinement in space group *Cmmm* yielded the lattice parameters $a = 4.1450(1)$, $b = 12.3004(4)$ and $c = 8.720(1)$ Å. According to the phase diagram discussion at 600 °C the measured sample with the nominal composition Al₅₀Cu₅₀ is in equilibrium with a small amount of liquid phase. This affects the background of the XRD measurement, which was compensated by modeling an additional broad peak at 43.9(1) °2 θ . Further details of measurement and structure refinement of the η_1 phase including the calculated errors of the parameters are listed in Table 3. The refined pattern of η_1 is shown in Fig. 6.

The structural model for η_1 was established by a twofold approach. Given the similarities of the lattice parameters between the monoclinic phase η_2 and the orthorhombic η_1 , $a_{ortho} \approx b_{mono}$, $b_{ortho} \approx a_{mono}$ and $V_{ortho} \approx 1.5 \cdot V_{mono}$, we tried to develop the structural model by rearranging the atomic positions of the low

temperature phase in the orthorhombic high temperature cell using the space group *C222*. This approach was supported by simulated annealing calculations [36] using the TOPAS software [35, 36]. The atomic coordinates of this structural model were finally transformed to *Cmmm* and standardized by applying the program Structure Tidy [37, 38]. During the consecutive Rietveld refinement, unusually large differences at the individual isotropic displacement factors were observed, indicating a decrease of electron density at some atomic positions. Therefore, all occupation factors were refined independently. The occupations of Al2, Al3 and Cu2 were found to be significantly reduced while all other sites were found to be fully occupied within 3 esd's and were therefore fixed during the final refinements. The final structural model shows reasonable displacement factors and the refined overall composition Al_{14.1}Cu_{14.8} (equivalent to 51.2 at.% Cu) is in excellent agreement with the Al-rich phase boundary of η_1 (51.5(5) at.% Cu). The structural parameters of η_1 are listed in Table 4. More details on the crystal structure investigation can be obtained from the Fachinformationszentrum Karlsruhe, 76344 Eggenstein-Leopoldshafen, Germany, (Fax: +497247 808666; e-mail: crysdata@fiz.karlsruhe.de) on quoting the depository number CSD 423053.

The coordination polyhedra for the 7 independent positions of η_1 are shown in Fig. 7. Apart from the high-symmetry positions Cu3 and Cu4, the coordination figures are quite irregular with coordination numbers between CN = 10 and CN = 14. Interatomic distances in the first coordination sphere are given in Table 5.

A comparison of the atomic arrangements in the low temperature phase η_2 and the high temperature phase η_1 is shown in Fig. 8. The figure shows the layer in (001) of orthorhombic η_1 in comparison to the layer in (010) of the monoclinic η_2 , i.e. both structures are projected along their short axis. All atoms shown are situated within the mirror plane at $z = 0$ and $y = 0$, respectively. The corresponding second layer of each structure (situated at $z = 1/2$ and $y = 1/2$, respectively) shows the same atomic arrangement shifted by $1/2$ in [010] for η_1 and in [100] for η_2 according to space group symmetry.

Fig 8 shows that both structures have a common structural motif; i.e. a diamond shaped unit consisting of 5 Cu- and 4 Al-atoms. These motifs are arranged in a rectangular pattern and interconnected along their corners in case of the high temperature structure. In the monoclinic structure the motifs are re-arranged and interconnected diagonally along their edges. While only one atom, Al3, is not part of the diamond-shaped motif of η_2 , three of the seven sites in η_1 (Al1, Cu2 and Cu3) are not part of this motif.

Although the two structures are obviously related it should be pointed out that it is not possible to transform one structure into the other in a simple way and a second order transition between η_1 and η_2 can be definitely ruled out. This is consistent with our phase diagram investigation which clearly indicates an invariant reaction related to the transformation from η_2 to η_1 . As an example, the DTA curve for the sample with the nominal composition Al₅₀Cu₅₀ (used also for the high temperature XRD) is shown in Fig. 9. At onset 571 °C a sharp reaction peak corresponding to the eutectoid formation of η_1 occurs. This effect is followed by the peritectic decomposition of θ (590 °C) and η_1 (625 °C) and finally the liquidus effect at 804 °C.

Summary

The current work revealed significant improvements on the established phase diagram in the system Al-Cu by solving several inconsistencies in literature. The Al-rich part of the phase diagram could be confirmed. The phases η_1 and η_2 show a significant shift to the Cu-rich side of the phase diagram and exhibit, contrary to previously published phase diagrams [1-3], a first order transition reaction. The ζ_1/ζ_2 region was re-investigated and the recent findings of Gulay and Harbrecht [13, 14] were widely confirmed. The transition between γ_0 and γ_1 does not show a two phase field thus indicating a higher order transition and confirming the results of Liu et al. [2]. The absence of the high temperature phase β_0 was confirmed.

The structure of the high temperature phase η_1 was determined from powder diffraction data. The phase is orthorhombic (space group *Cmmm*) and the lattice parameters are $a = 4.1450(1) \text{ \AA}$, $b = 12.3004(4) \text{ \AA}$ and $c = 8.720(1)$. The structural relations to the low-temperature compound η_2 are discussed.

Supplementary Material

A table with experimental data from DTA, SEM and XRD is available as supplementary material

Acknowledgements

The authors thank the Austrian Science Found FWF for supporting this work under the project number P19305. Additionally the authors want to thank Markus Seidl and Mario Ecker for their help in sample preparation as well as Stephan Puchegger from the Department of Dynamic of Condensed Systems at the University of Vienna for his assistance with the SEM measurements.

Tables

Table 1

Structural information on the compounds in the system Al-Cu

Phase	Composition range [1]	Pearson symbol	space group	structure type	lattice parameters {Å}	reference
(Al)	0 – 2.48	<i>cF4</i>	<i>Fm-3m</i>	Cu	$a = 4.049750(15)$	[17]
θ	31.9 – 33.0	<i>tI12</i>	<i>I4/mcm</i>	Al ₂ Cu	$a = 6.063(3)$ $c = 4.872(3)$	[18]
η_1	49.8 – 52.4	<i>oP16</i> or <i>oC16</i>	<i>Pbam</i> or <i>Cmmm</i>	unknown	$a = 4.087$ $b = 12.00$ $c = 8.635$	[10] [12]
η_2	49.8 – 52.3	<i>mC20</i>	<i>C2/m</i>	AlCu	$a = 12.066$ $b = 4.105$ $c = 6.913$ $\beta = 55.04^\circ$	[11]
ζ_1	55.2 – 59.8	<i>hP42</i> <i>oF88</i>	<i>P6/mmm</i> <i>Fmm2</i>	Al ₃ Cu ₄	--- $a = 8.1267(3)$ $b = 14.4985(5)$ $c = 9.9928(3)$	[10] [14]

ζ_1	55.2 – 59.8	<i>hP42</i>	<i>P6/mmm</i>	---	[10]
		<i>oF88</i>	<i>Fmm2</i>	$a = 8.1267(3)$	[14]
				$b = 14.4985(5)$	
				$c = 9.9928(3)$	
ζ_2	55.2 – 56.3	<i>oI24-3.5</i>	<i>Imm2</i>	$a = 4.0972(1)$	[13]
				$b = 7.0313(2)$	
				$c = 9.9793(3)$	
ε_1	59.4 – 62.1	Cubic?	unknown		[20]
ε_2	55.0 – 61.1	<i>hP4</i>	<i>P6₃/mmc</i>	$a = 4.146(1)$	[11]
				$c = 5.063(3)$	
δ	59.3 – 61.9	<i>hR52</i>	<i>R3m</i>	$a = 8.7066(1)$	[15]
				$a = 89.74(1)^{o1)}$	
γ_0	59.8 – 69		<i>I-43m</i>	--- ²⁾	[2]
γ_1	52.5 – 59	<i>cP52</i>	<i>P-43m</i>	$a = 8.7068(3)$	[16]
β_0	67.6 – 70.2	unknown	unknown		
β	70.6 – 82.0	<i>cI2</i>	<i>Im-3m</i>	$a = 2.9504(2)$	[19]
α_2	76.5 – 78		long-period super structure based on Al ₃ Ti and		[1]

(Cu)	80.3 100	<i>cF4</i>	<i>Fm-3m</i>	Cu ₃ Au Cu	<i>a</i> = 3.61491	[21]
------	----------	------------	--------------	--------------------------	--------------------	------

¹⁾ Rhombohedral lattice parameters are given in non-standard setting for better comparison with cubic γ_0

²⁾ No lattice parameters given

Table 2

Invariant reactions in the system Al-Cu according to the present work (bold) compared to Murray [1]

Reaction	Composition			Temperature (°C)	Ref.
L = (Cu)	---	100	---	1084.87	[1]
L = (Cu) + β	83.0	84.4	82.0	1032	[1]
	83.0(5)	84.5(5)	82.0(5)	1035(5)	this work
β = (Cu) + γ_1	76.1	80.3	69	567	[1]
	76.0(5)	81.5(5)	70.0(5)	567(2)	this work
L + β = β_0	69.2	70.9	70.2	1037	[1]
	reaction not confirmed				this work
β_0 = β + γ_0	70.0	70.6	68.5	964	[1]
	reaction not confirmed				this work
γ_1 + (Cu) = α_2	69	80.3	77.25	363	[1]
L + β_0 = γ_0	66.1	67.6	67.4	1022	[1]
	reaction not confirmed				this work
L = β	---	75	---	1049	[1]
				1052(5)	this work
γ_0 = β + γ_1	~69	72.8	~69	780	[1]
	reaction not confirmed				this work
γ_0 = γ_1		69.0		~800	this work
		65.0		874(2)	this work
β + L = γ_0	69.0(5)	63.0(5)	65.0(1)	993(2)	this work
γ_0 + L = ε_1	62.9	59.8	62.1	958	[1]
	65.5(5)	60.0(5)	64.5(5)	960(2)	this work
γ_0 + ε_1 = γ_1	66.0	61.4	63.9	873	[1]
	reaction not confirmed				this work
γ_1 + ε_2 = δ	62.8	59.2	61.9	686	[1]
	63.0(5)	58.5(5)	61.5(5)	684(1)	this work

$\gamma_1 + \varepsilon_1 = \varepsilon_2$	62.5	~61.1	~61.1	850	[1]
	64.0(5)	62.5(5)	62.5(5)	847(1)	this work
$\varepsilon_1 = \varepsilon_2 + L$	~59.4	~59.4	52.2	848	[1]
	59.5(5)	59.5(5)	52.5(5)	847(1)	this work
$\varepsilon_2 + L = \eta_1$	55.0	36.3	51.8	624	[1]
	54.5(5)	38.5(5)	52.0(5)	625(2)	this work
$\eta_1 + L = \theta$	59.8	32.2	32.8	591	[1]
	51.5(5)	32.5(5)	33.5(5)	591(2)	this work
$\varepsilon_2 = \delta + \zeta_1$	57.9	59.3	56.9	560	[1]
	reaction not confirmed				this work
$\varepsilon_2 = \delta + \zeta_2$	57.5(5)	60.0(5)	56.0(5)	578(2)	this work
$\zeta_1 = \zeta_2 + \delta$	~59.8	56.3	~59.8	530	[1]
	reaction not confirmed				this work
$\delta + \zeta_2 = \zeta_1$	60.0(5)	56.5(5)	57.0(5)	561(2)	this work
$\zeta_1 + \eta_1 = \zeta_2$	55.2	52.3	55.2	570	[1]
	reaction not confirmed				this work
$L = \theta + (Al)$	17.1	31.9	2.48	548.2	[1]
	17(1)	32.0(5)	2.5(5)	550(2)	this work
$\eta_1 = \eta_2 + \theta$	49.8	49.8	33.0	563	[1]
	52.0(5)	52.5(5)	33.5(5)	574(3)	this work
$\varepsilon_2 + \eta_1 = \zeta_1$	56.5	52.4	56.2	590	[1]
	reaction not confirmed				this work
$\varepsilon_2 + \eta_1 = \zeta_2$	56.5(5)	53.0(4)	55.5(5)	597(1)	this work
$\zeta_2 + \eta_1 = \eta_2$	54.5(5)	52.5(5)	53.5(5)	580(1)	this work
$\eta_1 = \eta_2 + \zeta_1$	~52.3	~52.3	55.25	560	[1]
	reaction not confirmed				this work
$L = (Al)$	---	0	---	660.452	[1]

Table 3

Structure refinement of η_1 -Al_{1- δ} Cu

Compound	AlCu _{1-δ}
Number of formula units per unit cell	15
Space group	<i>Cmmm</i>
<i>a</i> {Å}	4.1450(1)
<i>b</i> {Å}	12.3004(4)
<i>c</i> {Å}	8.720(1)
Cell Volume {Å ³ }	444.53(3)
Number of atoms in the cell	30
Calculated density (g/cm ³)	4.93(1)
Diffractometer	Bruker AXS D8-Advance
Radiation, wavelength {Å}	Cu K α , 1.5406
Peak shape function	Fundamental parameter approach
Number of refined parameters	32
R _{wp} / GOF	3.88 / 1.34
Texture	Spherical harmonics, 4 th order

Table 4

Atomic coordinates, site occupancies and displacement factors for η_1 -AlCu_{1- δ}

Atom	Site	x/a	y/b	z/c	Occ.	$B_{eq}^{1)}$
	multiplicity					
	Wyckoff					
	letter					
Cu1	8n	0	0.1828(3)	0.1514(4)	1	1.0(1)
Cu2	4j	0	0.152(1)	1/2	0.70(1)	2.1(3)
Cu3	2c	1/2	0	1/2	1	1.1(2)
Cu4	2a	0	0	0	1	1.4(2)
Al1	8n	0	0.336(1)	0.338(1)	1	0.9(2)
Al2	4k	0	0	0.304(2)	0.68(2)	1.0(3)
Al3	4i	0	0.375(1)	0	0.84(2)	1.0(3)

¹⁾ *isotropic displacement factor as defined by Fischer and Tillmanns [39].*

Table 5

Relevant interatomic distances (Å) for η_1 -AlCu (3.6 Å coordination sphere)

Atoms		distance	coordination number
Cu1	1 Al1	2.4824	12
	2 Al3	2.5597	
	1 Al2	2.6134	
	2 Al1	2.6396	
	1 Al3	2.7132	
	1 Cu4	2.6073	
	1 Cu1	2.6404	
	2 Cu1	2.6512	
	1 Cu2	3.0626	
Cu2	4 Al1	2.5171	14
	2 Al2	2.5322	
	2 Al1	2.6698	
	2 Cu3	2.7916	
	2 Cu1	3.0626	
	2 Cu2	3.1785	
Cu3	4 Al1	2.4692	12
	4 Al2	2.6851	
	4 Cu2	2.7916	
Cu4	4 Al3	2.5770	10

	2 Al2	2.6523	
	4 Cu1	2.6073	
Al1	1 Cu3	2.4692	13
	1 Cu1	2.4824	
	2 Cu2	2.5171	
	2 Cu1	2.6396	
	1 Cu2	2.6698	
	1 Al1	2.8413	
	2 Al2	2.9080	
	2 Al1	2.9583	
	1 Al3	2.9790	
Al2	2 Cu2	2.5322	12
	2 Cu1	2.6134	
	1 Cu4	2.6523	
	2 Cu3	2.6851	
	4 Al1	2.9080	
	1 Al2	3.4143	
Al3	4 Cu1	2.5597	11
	2 Cu4	2.5770	
	2 Cu1	2.7132	
	2 Al1	2.9790	
	1 Al3	3.0631	

Figures

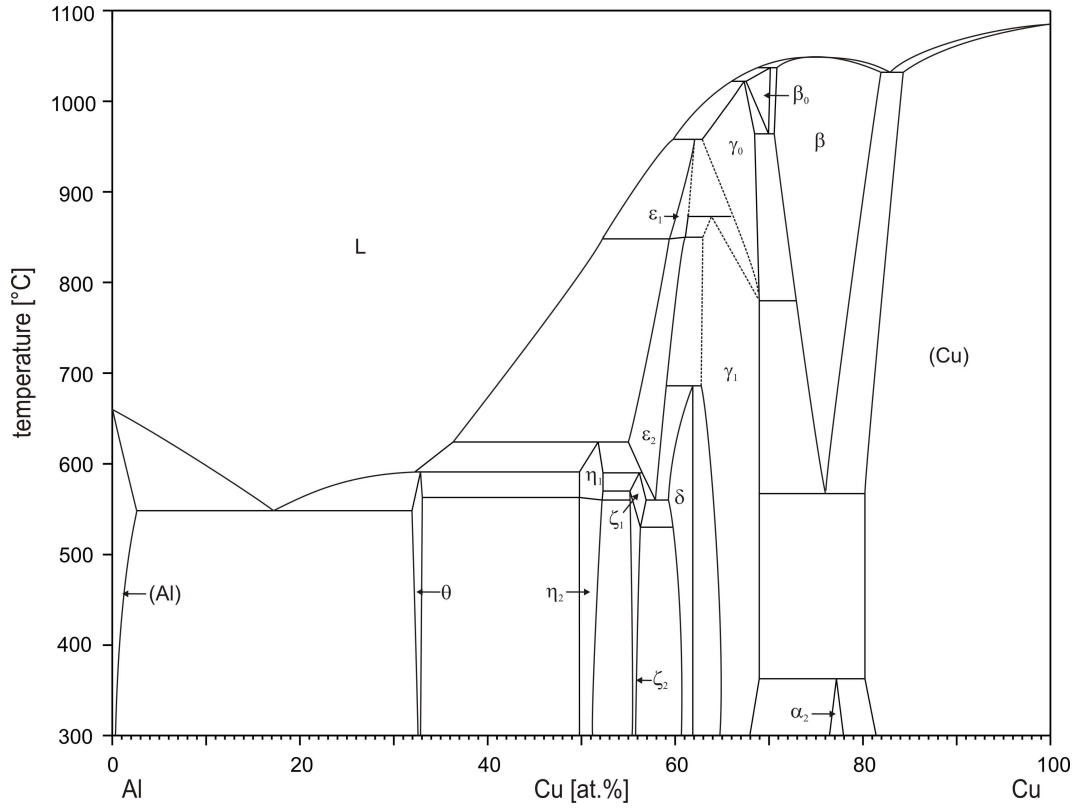


Fig. 1: The Al-Cu phase diagram according to Murray [1]

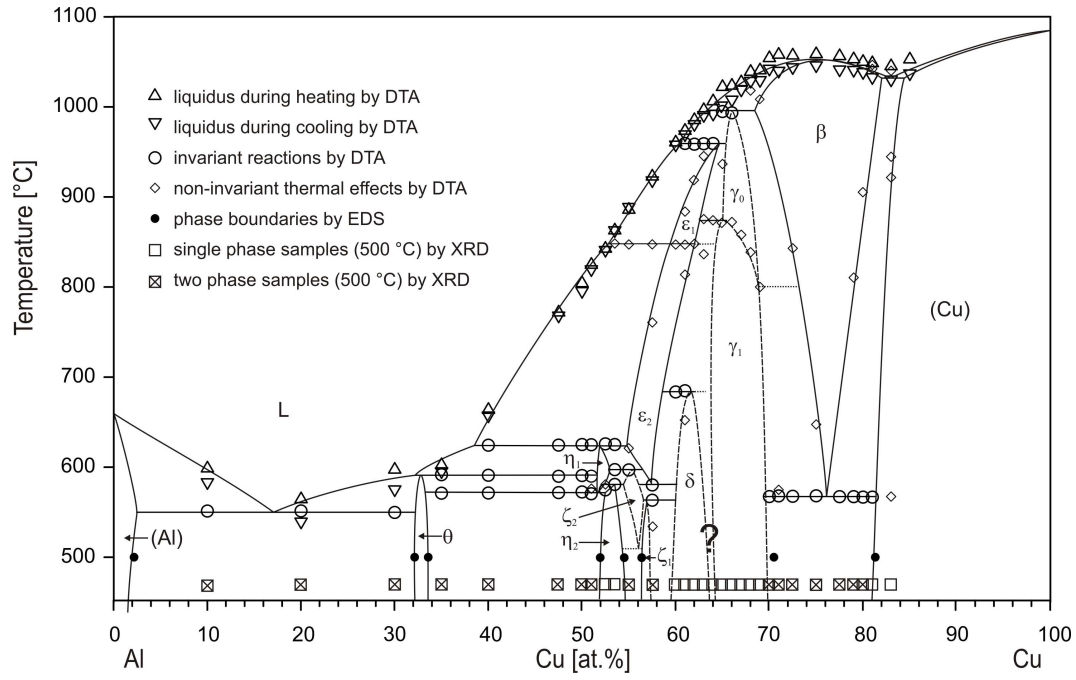


Fig. 2: The Al-Cu phase diagram determined in the present work with experimental data points.

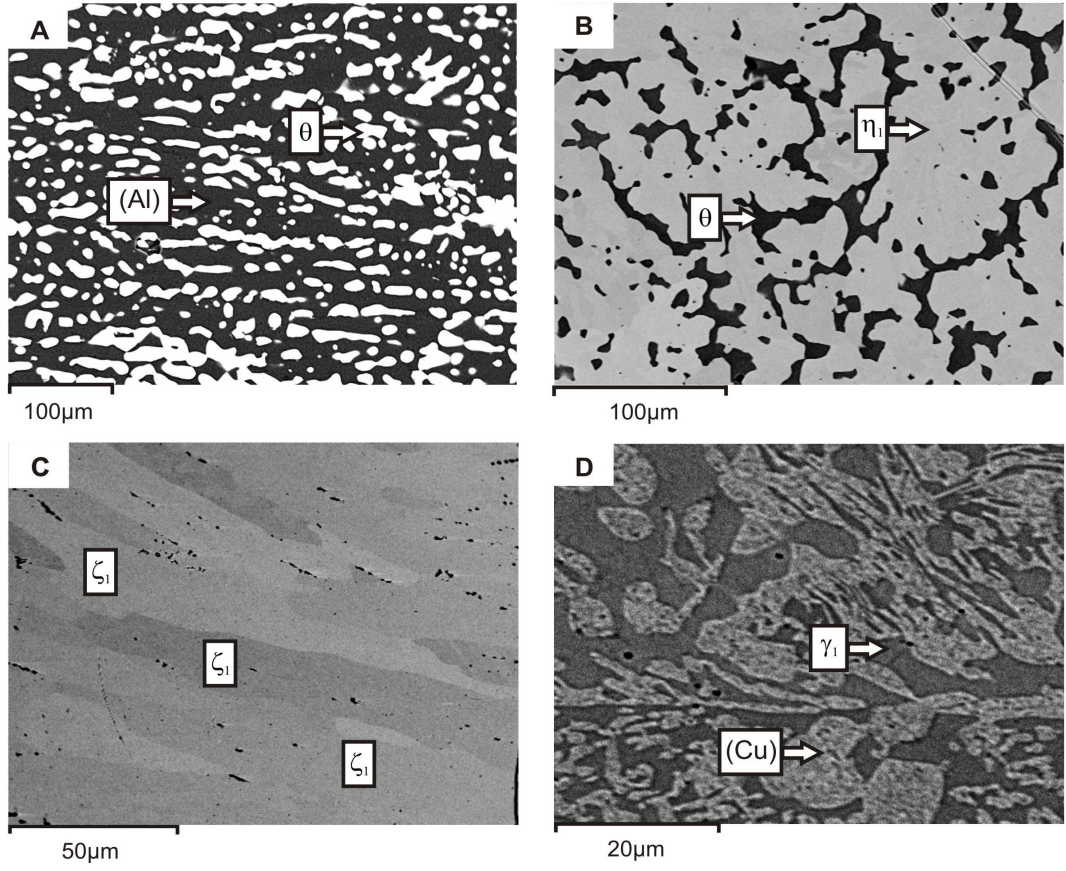


Fig. 3: BSE pictures of samples with the nominal composition A: Al₉₀Cu₁₀ [(Al) + θ], B: Al_{52.5}Cu_{47.5} [θ + η₂], C: Al_{42.5}Cu_{57.5} [ζ₁ + δ (traces)] and D: Al₂₅Cu₇₅ [γ₁ + (Cu)]

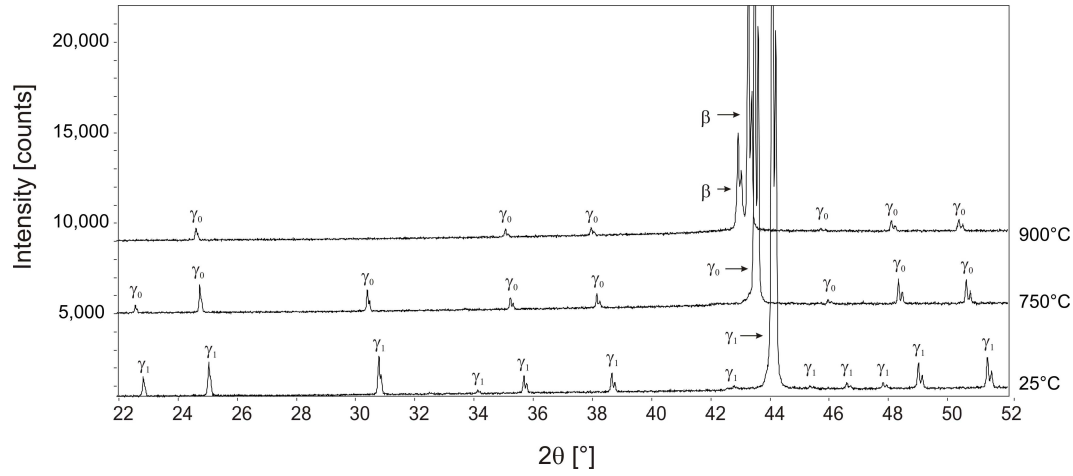


Fig. 4: High-temperature X-Ray powder diffraction of a sample with the nominal composition Al₃₂Cu₆₈. 25°C: γ_1 , 750°C: γ_1 , 900°C: γ_0 and traces of β

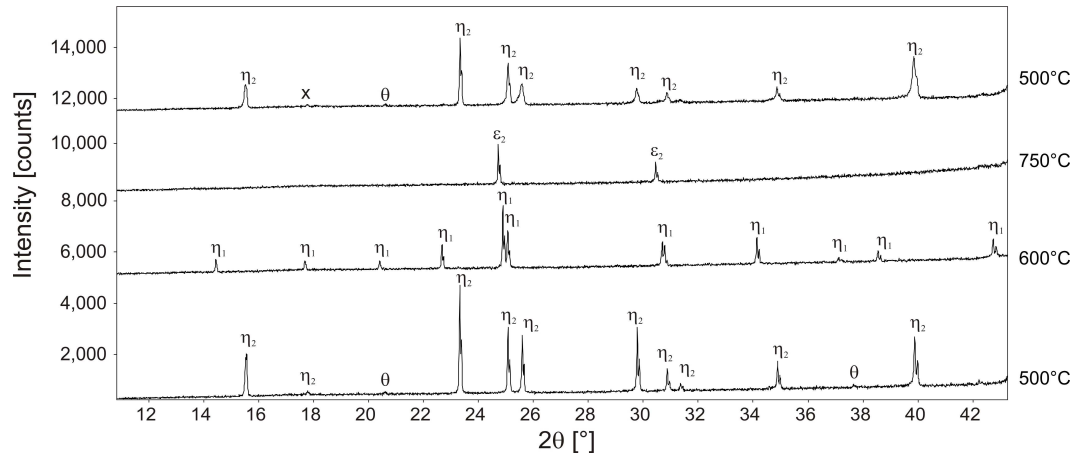


Fig. 5: High-temperature X-Ray powder diffraction of a sample with the nominal composition Al₅₀Cu₅₀. 500°C: η_1 and traces of θ , 600°C: η_1 , 750 °C ϵ_2 , 500°C: η_2 , traces of θ and an unidentified peak (x) maybe due to oxidation. Note that the diffractograms were recorded in the 2θ-range between 10 and 120°, but are only shown up to 44 °C for the sake of clarity of representation.

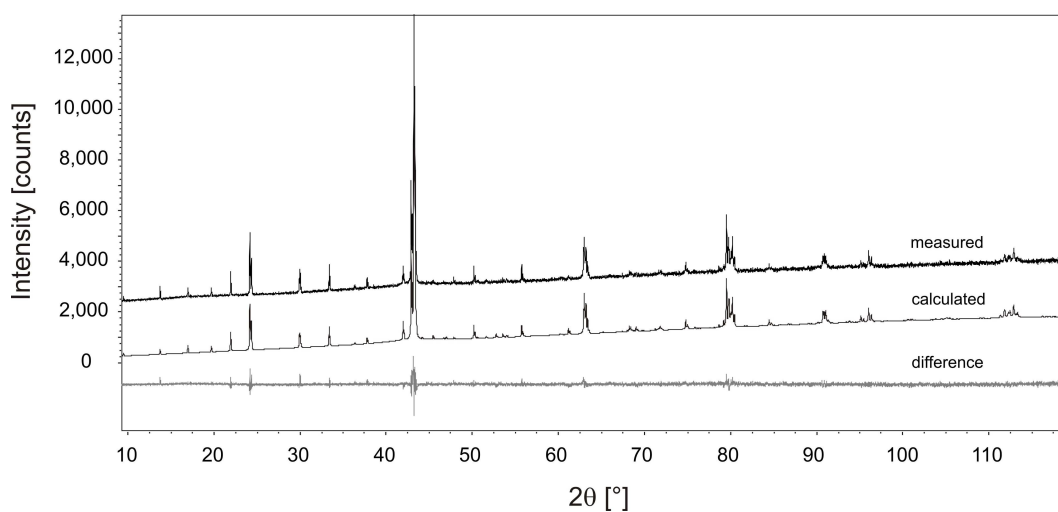


Fig. 6: Refined powder XRD pattern of a sample with the nominal composition Al₅₀Cu₅₀ at 600 °C showing single phase η_1 .

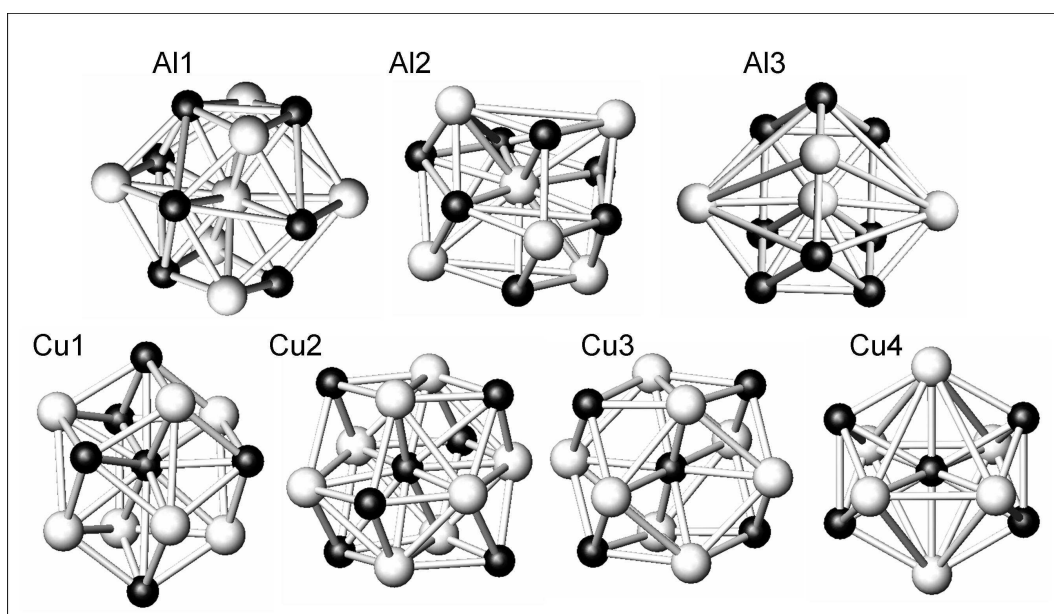


Fig. 7: The first coordination sphere of the different atom positions in η_1 . Black: Cu, White: Al

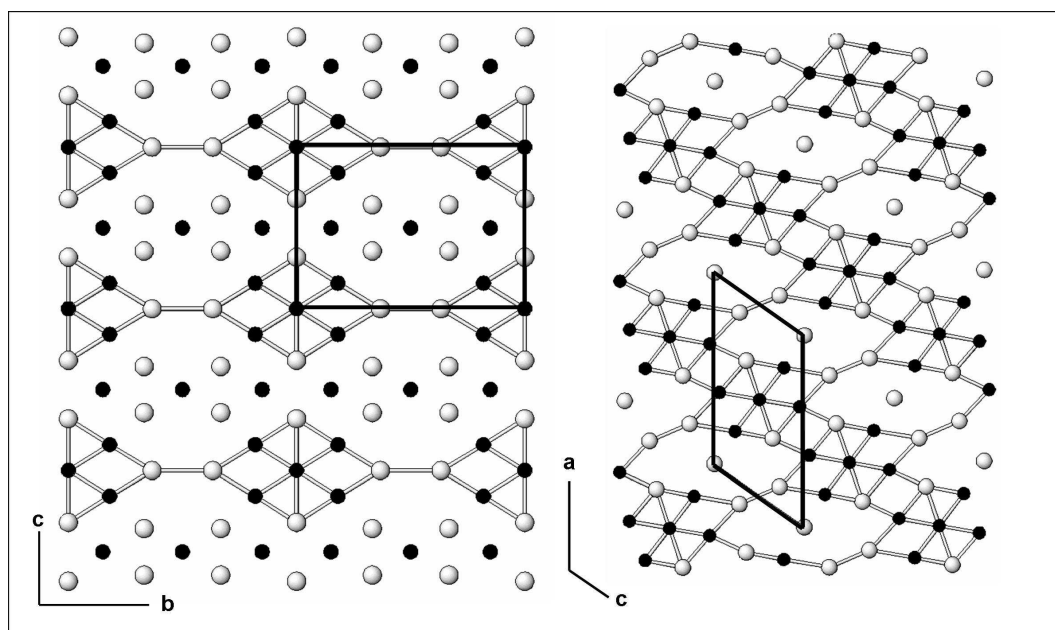


Fig. 8: Comparison of the (100)-plane of the high temperature phase η_1 and the (010)-plane of the low temperature phase η_2 . Black: Cu, White: Al

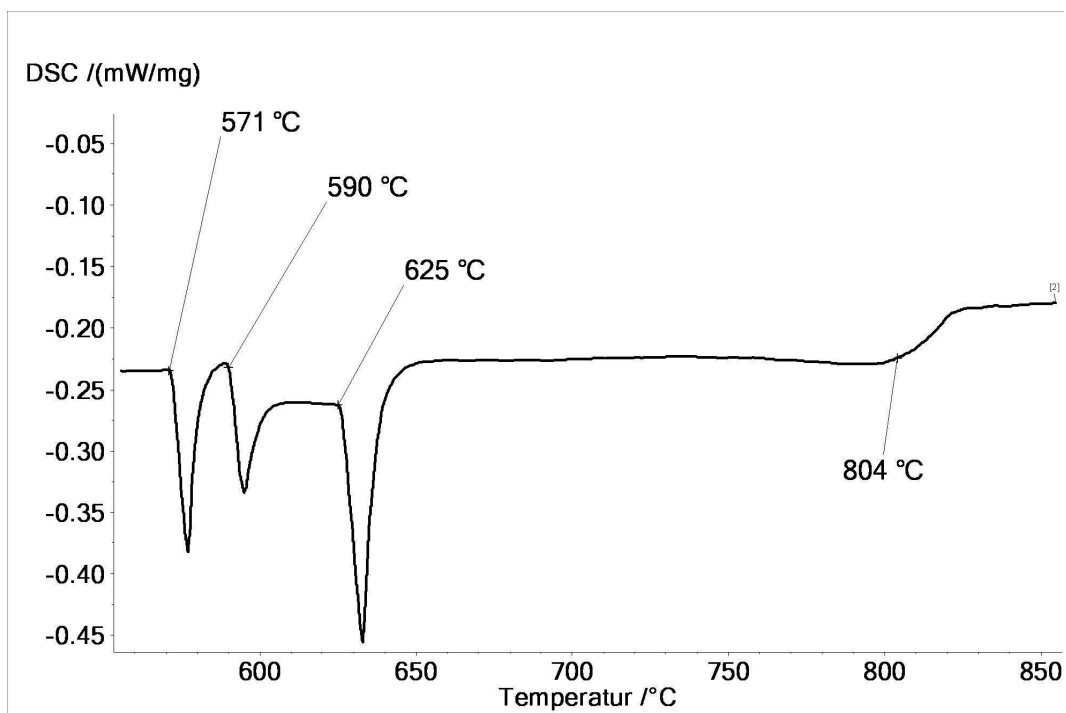


Fig. 9: DTA curve for the sample with the nominal composition Al₅₀Cu₅₀, showing thermal effects related to the η_1/η_2 -transition.

References:

- [1] J.L. Murray, The aluminium-copper system, *Int. Met. Rev.*, 30 (1985) 211-233.
- [2] X.J. Liu, I. Ohnuma, R. Kainuma, K. Ishida, Phase equilibria in the Cu-rich portion of the Cu-Al binary system, *J. Alloys Compd.*, 264 (1998) 201-208.
- [3] P. Riani, L. Arrighi, R. Marazza, D. Mazzone, G. Zanicchi, R. Ferro, Ternary rare-earth aluminum systems with copper: A review and a contribution to their assessment, *J. Phase Equilib. Diffus.*, 25 (2004) 22-52.
- [4] X.W. Zhou, T.Y. Hsu, Thermodynamics of the martensitic transformation in copper-aluminum alloys, *Acta Metall. Mater.*, 39 (1991) 1041-1044.
- [5] W. Liuding, Z. Liu, C. Chen, Statistical physics and thermodynamics of transformation in Cu-Al system, *Xibei Daxue Xuebao, Ziran Kexueban*, 24 (1994) 121-125.
- [6] X.Y. Yan, F.Y. Xie, M. Chu, Y.A. Chang, Microsegregation in Al-4.5Cu wt.% alloy: experimental investigation and numerical modeling, *Mater. Sci. Eng., A*, 302 (2001) 268-274.
- [7] F. De Geuser, B.M. Gable, B.C. Muddle, CALPHAD based kinetic Monte Carlo simulation of clustering in binary Al-Cu alloy, *Philos. Mag.*, 91 (2011) 327-348.
- [8] D. Liu, L. Zhang, Y. Du, H. Xu, S. Liu, L. Liu, Assessment of atomic mobilities of Al and Cu in fcc Al-Cu alloys, *CALPHAD*, 33 (2009) 761-768.
- [9] N. Saunders, System Al-Cu, in: I. Ansara, A.T. Dinsdale, M.H. Rand (Eds.) *COST 507 - Thermochemical Database for Light Element Alloys vol. 2*, 1998, pp. 28-33.
- [10] G.D. Preston, An x-ray investigation of some copper-aluminum alloys, *Philos. Mag.*, 12 (1931) 980-993.
- [11] M. El-Boragy, R. Szepan, K. Schubert, Crystal structure of Cu₃Al₂+(h) and CuAl(r), *J. less-common met.*, 29 (1972) 133-140.

- [12] H.L. Lukas, N. Lebrun, Al-Cu-Si (Aluminium-Copper-Silicon), in: G. Effenberg, S. Ilyenko (Eds.) SpringerMaterials - The Landolt-Börnstein Database, 2005, pp. 135-147.
- [13] L.D. Gulay, B. Harbrecht, The crystal structure of zeta(2)-Al₃Cu₄-delta, Z. Anorg. Allg. Chem., 629 (2003) 463-466.
- [14] L.D. Gulay, B. Harbrecht, The crystal structure of zeta(1)-Al₃Cu₄, J. Alloys Compd., 367 (2004) 103-108.
- [15] E.H. Kisi, J.D. Browne, Ordering and Structural Vacancies in Nonstoichiometric Cu-Al Gamma Brasses, Acta Crystallogr., Sect. B: Struct. Sci., 47 (1991) 835-843.
- [16] L. Arnberg, S. Westman, Crystal Perfection in a Non-Centrosymmetric Alloy - Refinement and Test of Twinning of Gamma-Cu₉Al₄ Structure, Acta Crystallogr., Sect. A: Found. Crystallogr., 34 (1978) 399-404.
- [17] A.S. Cooper, Precise lattice constants of germanium, aluminum, gallium arsenide, uranium, sulfur, quartz, and sapphire, Acta Crystallogr., 15 (1962) 578-583.
- [18] E.E. Havinga, Compounds and pseudobinary alloys with the CuAl₂ (C16)-type structure. II. Theoretical discussion of crystallographic parameters, J. less-common met., 27 (1972) 187-193.
- [19] K.W. Andrews, W. Hume-Rothery, The alpha -beta -brass type of equilibrium, Proc. R. Soc. London, Ser. A, 178 (1941) 464-473.
- [20] A.J. Bradley, H.J. Goldschmidt, H. Lipson, The intermediate phases in the aluminium-copper system after slow cooling, J. Inst. Met., 63 (1938) 149-162.
- [21] M.E. Straumanis, L.S. Yu, Lattice Parameters, Densities, Expansion Coefficients and Perfection of Structure of Cu and of Cu-in Alpha Phase, Acta Crystallogr., Sect. A: Cryst. Phys., A 25 (1969) 676-682.
- [22] J.B. Friauf, The crystal structure of two intermetallic compounds, J. Am. Chem. Soc., 49 (1927) 3107-3114.
- [23] T. Goedecke, F. Sommer, Solidification behavior of the Al₂Cu phase, Z. Metallk., 87 (1996) 581-586.

- [24] C. Dong, Q.H. Zhang, D.H. Wang, Y.M. Wang, Al-Cu approximants in the Al₃Cu₄ alloy, *Eur. Phys. J. B*, 6 (1998) 25-32.
- [25] C. Dong, Q.H. Zhang, D.H. Wang, Y.M. Wang, Al-Cu approximants and associated B2 chemical-twinning modes, *Micron*, 31 (2000) 507-514.
- [26] A.J. Bradley, Structure of Cu₃₂Al₁₉, *Nature* (London, U. K.), 168 (1951) 661.
- [27] S. Westman, Phase Analysis at 660°C of the Gamma Region of the Copper-Aluminium System, *Acta Chem. Scand.*, 19 (1965) 2369-2372.
- [28] S.K. Seshadri, D.B. Downie, High-temperature lattice parameters of copper-aluminum alloys, *Met. Sci.*, 13 (1979) 696-698.
- [29] Y. Funamizu, K. Watanabe, Interdiffusion in the aluminum-copper system, *Trans. Jpn. Inst. Met.*, 12 (1971) 147-152.
- [30] M. Van Sande, J. Van Landuyt, M. Avalos-Borja, G.T. Villaseñor, S. Amelinckx, A reinvestigation of the γ phase in copper-aluminum alloys: a new long-period superstructure, *Mater. Sci. Eng.*, 46 (1980) 167-173.
- [31] A.G. Dawson, *J. Inst. Met.*, 61 (1937) 197-204.
- [32] M.R.F. Hurtado, J. Portillo, Y. Maniette, A.T. Adorno, A.V. Benedetti, A complex structure in the (β + $\gamma(0)$) region of the Cu-Al alloys, *J. Alloys Compd.*, 280 (1998) 188-195.
- [33] D.R.F. West, D.L. Thomas, Some observations on constitutional changes in copper-aluminum alloys at temperatures below that of the β \rightarrow α + γ_2 eutectoid, *J. Inst. Met.*, 83 (1955) 505-507.
- [34] A.T. Adorno, M.R. Guerreiro, A.V. Benedetti, Thermal behavior of Cu-Al alloys near the α -Cu-Al solubility limit, *J. Therm. Anal. Calorim.*, 65 (2001) 221-229.
- [35] TOPAS, Version 3.0, Bruker AXS Inc., Karlsruhe, Germany, (1999).
- [36] A.A. Coelho, Whole-profile structure solution from powder diffraction data using simulated annealing, *J. Appl. Crystallogr.*, 33 (2000) 899-908.
- [37] E. Parthe, L.M. Gelato, The standardization of inorganic crystal-structure data, *Acta Crystallogr., Sect. A: Found. Crystallogr.*, A40 (1984) 169-183.

- [38] L.M. Gelato, E. Parthé, STRUCTURE TIDY - a computer program to standardize crystal structure data, J. Appl. Crystallogr., 20 (1987) 139-143.
- [39] R.X. Fischer, E. Tillmanns, The equivalent isotropic displacement factor, Acta Crystallogr., Sect. C: Cryst. Struct. Commun., 44 (1988) 775-776.

3.2 Experimental investigation of the Cu-Si phase diagram at $x(\text{Cu}) > 0.72$

Katarzyna Sufryd^a, Norbert Ponweiser^b, Paola Riani^a, Klaus W. Richter^b, Gabriele Cacciamani^{a*}

^aDipartimento di Chimica e Chimica Industriale, Università di Genova, Genova, Italy

^bDepartment of Inorganic Chemistry / Materials Chemistry, University of Vienna, Austria

* corresponding author

E-mail: cacciamani@chimica.unige.it

Published: *Intermetallics* (2011), 19(10), 1479-1488

Contributions to this paper:

N.P.: preparation, analysis and interpretation of samples for the phase diagram, preparation of about half the samples for determination of the stability of ϵ , DTA and XRD measurements of samples for determination of the stability of ϵ , wrote about half the paper

K.S., P.R. G.C.: preparation of half the samples for determination of the stability of ϵ , SEM measurements and interpretation, interpretation of the stability of ϵ , wrote about half the paper,

K.W.R.: proofreading, general advice and helpful comments, interpretation of the stability of ϵ

Contribution of N. Ponweiser to the article: 50 %

Abstract

Cu-Si phase equilibria have been investigated at compositions greater than 72 at% Cu by X-ray diffraction, optical and electronic microscopy, electron probe microanalysis and differential thermal analysis.

The general aspects of the phase equilibria already reported in literature have been substantially confirmed, but selected composition ranges and the nature of a few invariant equilibria have been modified. In particular stability ranges of the β , δ and η phases have been slightly modified as well as temperature and nature of the invariant equilibria related to the $\gamma \rightleftharpoons \delta$ transformation.

Stability of the ϵ -($\text{Cu}_{15}\text{Si}_4$) phase has been especially investigated concluding that it is thermodynamically stable but kinetically inhibited by nucleation difficulties which become especially effective when samples are synthesised in very high purity conditions.

Crystal structure and composition ranges of the high temperature β and δ phases, despite difficulties by the non-quenchability of these phases, have been investigated by different methods including high temperature XRD.

Introduction

Cu-Si is a key system for several applications: from traditional silicon bronzes to catalysis [1], microelectronics [2] and, more recently, Li-ion batteries [3, 4]. On the other hand, Cu-Si phase equilibria, though long investigated, are still known with insufficient detail and affected by some uncertainties, especially about the equilibria involving the β -(Cu,Si), δ -(Cu,Si) and ε -Cu₁₅Si₄ phases. For this reason a re-investigation of the Cu-rich part of the phase diagram has been performed.

A comprehensive critical assessment of the Cu-Si literature data up to 1982 was carried out by Olesinski and Abbaschian [5], who presented an assessed version of the phase diagram mainly based on experimental results by Rudolphi [6] and Smith [7, 8, 9]. Equilibria among (Cu), κ -(Cu,Si) and γ -(Cu,Si) were especially investigated by Andersen [10], Hibbard et al. [11] and Hopkins [12].

The Cu-Si intermediate phases are located in the Cu-rich part of the diagram, between 5 and 25 at% Si. The only congruent melting compound, Cu₃Si, is an intermediate solid solution with a small composition range (23-25 at% Si) and a melting point of 859°C. For this phase three allotropic modifications denoted as η -Cu₃Si at high temperature, η' -Cu₃Si at intermediate temperature, and η'' -Cu₃Si at low temperature have been reported in literature. However, there are uncertainties about the three crystal structures. Solberg [13] investigated the crystal structure of Cu₃Si precipitates on a Si surface by transmission electron microscopy (TEM) and came to the conclusion that these phases are electron compounds based on a trigonally deformed bcc lattice which probably contains a large number of vacancies. The structure was actually first identified as an hexagonal distortion of a bcc lattice [14, 15] and Solberg [13] confirmed that this may result when only strongest reflections are considered. Moreover he [13] concluded that η -(Cu,Si) has a disordered structure, while η' -(Cu,Si) and η'' -(Cu,Si) are ordered superstructures with η'' -(Cu,Si) being a two-dimensional long-period superlattice originating from periodic displacements in η' -(Cu,Si). Additionally, the η'' -(Cu,Si) superstructure is expected to vary with composition.

More recently Mattern et al. [16] refined the η -(Cu,Si) crystal structure on the basis of high temperature XRD measurements. The same authors observed, in samples annealed at 500°C, the appearance of superstructure reflections ascribed to the formation of the η'' -(Cu,Si) phase, but they were not able to solve the structure.

Three additional high temperature disordered solid solutions have been identified in the Cu-Si system: κ -(Cu,Si), Mg-type, reported at 552-842°C and 11-14.5 at% Si; β -(Cu,Si), W-type, reported in a small temperature (785-852°C) and composition (14-17 at% Si) range, and δ -(Cu,Si), reported at 710-824°C and 17.5-19.5 at% Si, the structure of which was first indexed as tetragonal by Mukherjee et al. [17] and then refined as hexagonal by Mattern [16].

Finally, two phases were reported to be stable down to room temperature: γ -(Cu,Si) (also denoted as Cu_5Si), having the $cP20$ β -Mn crystal structure, forming peritectoidally at 729°C and stable in a narrow composition range (17.2-17.6 at% Si), and ϵ - $\text{Cu}_{15}\text{Si}_4$, (sometimes denoted as Cu_4Si) a line compound at 21.05 at% Si forming peritectoidally at 800°C. The ϵ - $\text{Cu}_{15}\text{Si}_4$ crystal structure was first identified as cubic with a body centred lattice by Arrhenius et al. [14] and by Morral et al. [18]. Subsequently Mukherjee [17] obtained more X-ray reflections than Morral et al. [18] and concluded that the structure should be cubic but not bcc. Finally, Mattern et al. [16] refined the structure according to a body centred Bravais lattice, claiming, however, to be in agreement with [17]

Experimental

Samples have been prepared separately by the groups in Genova and in Vienna, in particular with respect to the investigation of the stability of $\varepsilon\text{-Cu}_{15}\text{Si}_4$ (see below). In Vienna the samples were prepared from copper wire (99.95 and 99.999%, Alfa Aesar) and Silicon lump (99.9999%, Alfa Aesar). The samples, each with a total weight of 1000 mg, were prepared by arc-melting the elements under an argon atmosphere on a water cooled copper plate with a tungsten electrode and a zirconium piece as oxygen getter. In order to obtain proper homogenization, the sample beads were turned over and re-melted at least two times. The weight loss during sample preparation process was smaller than 0.5 mass% and was considered not to affect the sample composition considerably. After preparation the samples were placed in alumina crucibles or wrapped in Mo-foil and sealed in quartz glass tubes under vacuum. Depending on the sample, annealing was carried out at temperatures between 500 and 810 °C for three weeks.

In Genova the samples were prepared from copper sheet (99.999%, Newmet Kock, Waltham Abbey, UK) and silicon granules (99.99, Newmet Kock, Waltham Abbey, UK). The preparation in the arc furnace was the same as in Vienna. The samples were placed in high purity alumina crucibles or wrapped in degassed Mo-foil and sealed in quartz glass tubes under an Argon atmosphere. The annealing took place at temperatures between 500 and 780 °C for time periods ranging from a few days to several weeks.

In both cases the samples were quenched in cold water and prepared for further analysis.

The experimental investigation was carried out using powder X-ray diffraction (XRD) analysis, light optical microscopy (LOM), scanning electron microscopy (SEM) equipped with electron probe microanalysis (EPMA-EDX) and differential thermal analysis (DTA).

For powder X-ray analysis a Bruker D8 ADVANCE system ($r = 250.0$ mm), equipped with a copper X-ray tube (operated at 40 kV, 40 mA) and a LynxEye position sensitive detector (PSD) was used in Bragg-Brentano reflection setting. The high temperature powder X-ray diffraction was realized with an Anton Paar XRK900 reactor chamber in combination with an automated alignment stage. The samples were smoothly ground in an agate mortar and pressed as approx. 0.5 mm thick layers (15 mm diameter) on the Macor sample holder. The temperature-resolved measurements were performed under evacuated conditions (< 5 Pa) from 500(5) to 810(10) °C at different intervals depending on the sample. At each temperature the system was equilibrated for 10 min before a continuous scan over the range $10\text{--}100^\circ 2\theta$ with a physical resolution of $0.0103^\circ 2\theta$. An overall counting time of 2.5 h was performed. The resulting diffractograms for the ambient and the high temperature measurements were evaluated using TOPAS software [19].

Polished sections of the annealed samples were analysed by LOM using a Leica DM 4000 M and a Zeiss Axiotech 100 microscope. The composition of the coexisting phases and the overall composition of the samples were determined using SEM (Zeiss EVO 40) equipped with an energy dispersive X-ray spectroscopy (EDX, Oxford INCA Energy 300). SEM imaging in backscattered electron (BSE) mode was performed as well. Quantitative EDX analyses were carried out using an acceleration voltage of 20 kV and a counting time of 50 s using a cobalt standard in order to monitor beam current, gain and resolution of the spectrometer. The measured compositions were finally corrected for ZAF (atomic number, absorption and fluorescence) effects using pure elements as standards. The standard deviation for each element was estimated at 0.5 at.% for phase analysis and at 1.0 at.% for global analysis.

DTA measurements were performed on a Setaram Setsys Evolution 2400 (Setaram Instrumentation, Caluire, France) and a Netzsch DTA 404 PC (Netzsch, Selb, Germany) using open alumina crucibles and employing a slow permanent argon flow. A sample mass of approximately 20 mg was used for the experiments. The possible mass loss during the DTA investigations was checked routinely and

no relevant mass changes were observed. Using a heating rate of $5 \text{ K} \cdot \text{min}^{-1}$, two heating and cooling curves were recorded for each sample. The Pt/Pt10%Rh thermocouple (Type S) of the DTA instrument was calibrated at the melting points of pure Sn, Au and Ni.

Results

Stability of $\epsilon\text{-Cu}_{15}\text{Si}_4$

The equilibrium Cu-Si phase diagram assessed by Olesinski and Abbaschian [5], based on literature data prior to 1984, includes $\epsilon\text{-Cu}_{15}\text{Si}_4$ as an equilibrium phase forming peritectoidally at 800°C from $\eta\text{-Cu}_3\text{Si}$ and $\delta\text{-(Cu,Si)}$. After that, several authors investigated both stability and formation kinetics of this and other Cu-Si intermediate phases, mainly by studying solid state reactions either in diffusion couples or between thin or thick films of the constituent elements.

A number of investigations [20, 21, 22] on Cu-Si diffusion couples, reacted at different temperatures between 250 and 550 °C, reported the formation of Cu_3Si but not of $\gamma\text{-(Cu,Si)}$ and $\epsilon\text{-Cu}_{15}\text{Si}_4$. Similar results were obtained by Levin et al. [23]. They annealed at 470 °C several diffusion couples between Cu and Si, $\gamma\text{-(Cu,Si)}$ and Si, Cu and $\gamma\text{-(Cu,Si)}$, Cu and Cu_3Si , respectively. Analysis revealed the formation of only Cu_3Si in the first two couples, while in the other two couples Cu penetrated along the $\gamma\text{-(Cu,Si)}$ and Cu_3Si grain boundaries caused the fragmentation of the reaction area.

The influence of impurities (especially phosphorous) on the reaction kinetics in Cu-Si diffusion couples was investigated by Van Loo et al. [24, 25]. They considered that $\gamma\text{-(Cu,Si)}$ and $\epsilon\text{-Cu}_{15}\text{Si}_4$ could be absent either for kinetic reasons (which means that the layers are present in principle, but are too small to be observed) or because of impurities (e.g. phosphorous) which change the phase diagram in such a way that $\gamma\text{-(Cu,Si)}$ or $\epsilon\text{-Cu}_{15}\text{Si}_4$ are not involved any more. Based on their observations they concluded that, being Cu diffusion in $\gamma\text{-(Cu,Si)}$ and $\epsilon\text{-Cu}_{15}\text{Si}_4$ about 1000 times slower than in Cu_3Si , the virtual absence of $\gamma\text{-(Cu,Si)}$ and $\epsilon\text{-Cu}_{15}\text{Si}_4$ is mainly due to kinetics and not to impurities.

Solid state reactions between thin or thick films of the constituent elements were also investigated. Stolt et al. [26] prepared Si-Cu bilayers by deposition on

thermally oxidized silicon wafers of 100 nm Si layers followed by Cu layers of appropriate thickness in order to obtain the desired composition. After heat treating the bilayers at different temperatures between 200 and 750°C, they found that in all cases Cu_3Si was the first phase formed, while $\epsilon\text{-Cu}_{15}\text{Si}_4$ was never formed except in the sample at 20 at% composition, where it resulted from the reaction between Cu_3Si and $\gamma\text{-(Cu,Si)}$.

Cu-Si bilayers (100 nm Cu layers deposited on thermally oxidized silicon and followed by Si layers of different thickness, between 40 and 120 nm) were prepared by Shpilewsky et al. [27]. Some of them were subjected to implantation of Ar ions. By comparing implanted and non-implanted samples after annealing at different temperatures between 100 and 700 °C they observed that $\epsilon\text{-Cu}_{15}\text{Si}_4$ is only formed in implanted samples where the maximum density of implanted Ar is close to the Cu/Si interface. They concluded that initiation of $\epsilon\text{-Cu}_{15}\text{Si}_4$ during irradiation and subsequent annealing may then be attributed to a change in thermodynamic and kinetic parameters of phase formation on ion implantation [27].

Yang et al. [28] deposited Cu layers on a Si(100) substrate in three different ways: by physical vapour deposition (PVD), by ion beam assisted deposition (IBAD) and by a combined method consisting in a thin IBAD film followed by a thicker PVD layer. Samples were investigated before and after annealing at 300 °C. It was found that $\epsilon\text{-Cu}_{15}\text{Si}_4$ never forms in the PVD samples (which include only $\gamma\text{-(Cu,Si)}$ and Cu_3Si) while it is formed in IBAD samples (even before annealing) and in combined samples, only after annealing at 300 °C. So they concluded that nucleation behaviour of $\epsilon\text{-Cu}_{15}\text{Si}_4$ is the key factor determining the formation of this phase.

On the other hand, Chromik et al. [29] investigated thermodynamics and kinetics Cu-Si multi-layers obtained by sputtering alternate Cu and Si thin films on a NaCl substrate. Sputtering rate was controlled in order to form samples with different stoichiometries (those of the Cu-Si intermediate phases) and layer modulation (between 5 and 160 nm). After removing the NaCl substrate samples

were subjected to repeated DSC measurements in Al pans by heating them at 10-20 °C/min up to 330-380°C, annealing 10-20 min at high temperature and cooling. They used high purity elements (99.999 mass%) but unquantified contamination by Ar, H, O, N during sputtering was not excluded [30].

They found that, upon initial heating, Cu_3Si appeared first, while $\epsilon\text{-Cu}_{15}\text{Si}_4$ and $\gamma\text{-(Cu,Si)}$ were formed at higher temperature ($> 250^\circ\text{C}$). They were not able to obtain $\epsilon\text{-Cu}_{15}\text{Si}_4$ single phase samples and for this reason they were not able to evaluate its enthalpy of formation.

Moreover, Gillot et al. [31], while studying kinetics of the reactions between CuCl and Si , Si_2Ca , Si_2Fe , $\text{Si}_2\text{Al}_2\text{Ca}$, $\text{Si}_8\text{Al}_6\text{Fe}_4\text{Ca}$ at 200-300°C, obtained Cu , $\gamma\text{-(Cu,Si)}$ and Cu_3Si phases, but not $\epsilon\text{-Cu}_{15}\text{Si}_4$.

Finally in a recent work by part of the present authors [32], dedicated to the investigation of the 500°C Al-Cu-Si phase equilibria, a few Cu-Si binary samples at the $\epsilon\text{-Cu}_{15}\text{Si}_4$ composition were also investigated. Samples were synthesized by arc melting under Ar atmosphere with zirconium pieces as oxygen getter from silicon granules (99.99 mass%) and copper sheet (99.999 mass%). As cast samples placed inside high purity alumina crucibles or degassed Mo foils were enclosed under vacuum in silica ampoules and annealed for generally one month at 500, 700 and 780 °C. Both as cast and annealed samples did not show $\epsilon\text{-Cu}_{15}\text{Si}_4$, while it was readily formed in a sample synthesized from lower purity (99.98 mass%) copper.

Experiments independently performed by the group in Vienna provided different results. For this reason the authors decided to merge all the results and start a common investigation of the Cu-rich part of the system, with a special attention to the $\epsilon\text{-Cu}_{15}\text{Si}_4$ phase and the experimental procedures or conditions which can promote or prevent its formation. Many samples were prepared and exchanged between the two laboratories in order to cross-check results and take advantage from the complementary instrumentation.

As for the formation of $\epsilon\text{-Cu}_{15}\text{Si}_4$, we observed that it *was not formed*:

- a1) in as-cast samples, cooled inside the arc melting furnace,
- a2) during cooling in DTA at different cooling rates, generally between 0.5 and 10 °C/min (with one exception discussed later at point b3),
- a3) in samples prepared with high purity component elements and annealed for different times (from 4 up to 90 days) in new high purity and smooth containers of alumina or degassed molybdenum,
- a4) in selected samples prepared with component elements contaminated by small quantities of other metals (such as Fe and Ca) and annealed for different times in new high purity and smooth alumina containers.

However, we observed that it *was formed*:

- b1) in samples prepared with lower purity component elements,
- b2) in most samples prepared with high purity component elements and annealed for different times (from 5 hours to 20 days) in recycled high purity alumina or non degassed molybdenum containers,
- b3) in one sample cooled in DTA at 5 °C/min. The DTA plot was similar to those obtained for similar samples except for a large peak in the cooling curve at about 660 °C, which could be ascribed to the formation of $\epsilon\text{-Cu}_{15}\text{Si}_4$ in significant under-cooling conditions,
- b4) in samples intentionally contaminated with oxygen by sealing them under air (instead of vacuum) prior to annealing.

Selected samples, either with or without $\epsilon\text{-Cu}_{15}\text{Si}_4$, were analysed for the presence of light elements such as C, H, N and S using a Perkin Elmer 2400 Series II CHNS/O System Elemental Analyzer. Between 3 and 14 mg of sample material was burned off at a temperature between 970 and 980 °C. The combustion products were analyzed by gas chromatography and quantitatively evaluated. Neither significant quantity of such elements was observed nor significant difference between samples with and without $\epsilon\text{-Cu}_{15}\text{Si}_4$ appeared.

All our observations suggest that in the prepared samples:

- Contamination by light elements is very low and probably not enough to explain a thermodynamic stabilisation / destabilisation of the phase. However it is not excluded that they can affect the kinetics.
- Contamination by small quantities of other metals (e.g. Ca, Fe) seems not directly related to the formation of $\epsilon\text{-Cu}_{15}\text{Si}_4$.

Moreover:

- Growth rate seems not the main responsible for $\epsilon\text{-Cu}_{15}\text{Si}_4$ formation: it was not formed in selected samples after 3 months annealing, but it appeared in other samples after only 5 h annealing at 500°C.
- The observation that $\epsilon\text{-Cu}_{15}\text{Si}_4$ was either formed or not formed in samples prepared by the same procedure and in apparently identical conditions suggests that nucleation may be responsible for the phase formation. Actually nucleation rate may be favoured by small, not controllable quantities of compounds formed by light elements (such as oxides, carbides, etc. acting as nucleation seeds) and by large under-cooling.

Then, it may be concluded, also in agreement with most of the available literature information, that $\epsilon\text{-Cu}_{15}\text{Si}_4$ is most probably thermodynamically stable, but kinetically inhibited, mainly due to nucleation difficulties.

High temperature phases β and δ

The β -phase

According to the assessed phase diagram [5] the β -phase ($Im\text{-}3m$, W-type) with composition between 82.8 and 85.8 at.% Cu is supposed to be stable between 785 and 852 °C. The authors in [5] refer to the work of Isawa [33] (written in Japanese), but do not give any detailed information on the performed experiments.

In the present study, the authors tried to confirm the structure of β -(Cu,Si) from samples with the nominal composition $\text{Cu}_{83.7}\text{Si}_{16.3}$ and $\text{Cu}_{84.1}\text{Si}_{15.9}$. These samples were annealed at 810 °C for 21 days and subsequently quenched in water. X-ray powder diffraction analysis showed single phase γ -(Cu,Si) for $\text{Cu}_{83.7}\text{Si}_{16.3}$ and a mixture of γ -(Cu,Si) and κ -(Cu,Si) for $\text{Cu}_{84.1}\text{Si}_{15.9}$. Thus it was not possible to preserve the β -phase by quenching.

In order to confirm the structure of β -(Cu,Si), additional samples with the nominal composition $\text{Cu}_{83.6}\text{Si}_{16.4}$ and $\text{Cu}_{84.0}\text{Si}_{16.0}$ were annealed at 810 and 500 °C, respectively, then quenched in cold water and finally analyzed by means of high temperature powder X-ray diffraction. Sample $\text{Cu}_{84.0}\text{Si}_{16.0}$ was analyzed at room temperature and at 550, 650, 700, 750 and 800°C; the same temperatures were chosen to analyze the samples while cooling down. The results of the high-temperature X-ray powder analysis of this sample are shown in Table 1. At room temperature the sample shows γ -(Cu,Si) as major phase and traces of (Cu). Between 550 and 700 °C the diffractograms show γ -(Cu,Si), traces of (Cu) and an increasing amount of κ -(Cu,Si). This is in good agreement with the proposed stability range of κ in the assessed phase diagram. At 750 °C additional peaks appear which disappear again at 800 °C and are assumed to be related to the δ -phase (see below). These peaks were fitted with a mathematical model so they do not contribute to the calculated error R_{wp} . The measurement at 800°C shows β -(Cu,Si), (Cu) and κ -(Cu,Si). When cooling down the sample, at 750 °C the same peaks, which are assumed to be related to δ -phase, reappear. At 550°C a different set of peaks appears which does not match any of the intermetallic compounds in the system and might be due to oxides formed during the long stay in the sample chamber. Contrary to expectations, a small amount of the β -phase was still present at room temperature, although initially it was not possible to quench this phase. Thus, the assessed formation temperature as well as the crystal structure of the β -phase could be confirmed by the high temperature XRD experiments. The observed inconsistencies are most likely due to surface oxidation of the powder particles during the experiment. The shift in composition (the sample should be single phase β at 800 °C but it was found to contain β and κ) is probably due to

the preferred oxidation of Si yielding a shift towards the Cu-rich side. The stabilization of β to room temperature after the experiment may also be related to interaction with oxygen.

In order to improve the results by accelerating the heating process, sample $\text{Cu}_{83.6}\text{Si}_{16.4}$, annealed at 810 °C, was analyzed at room temperature and then immediately heated up to 810 °C, where every 30 minutes a total of 6 measurements was performed. Table 2 shows the results of some of the measurements. At room temperature the sample shows γ -(Cu,Si) as major phase and traces of κ -(Cu,Si) are still present. It was again not possible to quench β -(Cu,Si). The measurements at 810 °C show only β -(Cu,Si) in equilibrium with κ -(Cu,Si); no extra phases or peaks occur. Between the first and the 6th measurement no alteration occurs and therefore only these two measurements are shown in Table 2. After cooling down the sample, traces of β -(Cu,Si) still remain present.

Thus, the high temperature XRD experiments confirm the range of existence as well as the crystal structure of the β -phase as given in [5].

The δ -phase

A sample with the nominal composition $\text{Cu}_{81.5}\text{Si}_{18.5}$ was prepared to study the formation of δ -(Cu,Si) by means of high temperature XRD. The sample was annealed at 780°C for 21 days and quenched in cold water. Then it was analyzed by XRD at room temperature, subsequently heated to 780°C where it was analyzed six times by high-temperature XRD. Finally it was cooled to room temperature where another diffractogram was taken. The results are shown in Table 3. At room temperature the sample is formed by almost pure γ -phase, ε -(Cu,Si) is found in traces. After heating up to 780 °C, the pattern does show neither γ -(Cu,Si) nor ε -(Cu,Si). We were able to describe major parts of the pattern with the structural model for δ -(Cu,Si) as given by Mattern et. al. [16] with the lattice parameters $a = 4.094(1) \text{ \AA}$ and $c = 5.004(1) \text{ \AA}$, (compared to 4.036 Å and 4.943 Å in [16]). Nevertheless several peaks remain unexplained. The most intense peaks are at $43.62(1)^\circ 2\theta$ and $43.94(1)^\circ 2\theta$, the other peaks show very

little intensity. It has to be mentioned that the peak at $51.521(1)^\circ 2\theta$ matches the position of the (020)-reflex of δ -(Cu,Si) as given by Mattern et. al. [16], but it was not possible to fit the peak intensity with the Mattern model. Five more measurements were taken at the same temperature, which do not differ from the first except for a broad peak at $30.81(1)^\circ 2\theta$ which appears at the second measurement and does not change position or intensity until the last measurement. The results of the sixth measurement are shown in Table 3, too. After cooling down, a final measurement was taken at room temperature. Major phase is again γ -(Cu,Si), κ -(Cu,Si) is present in traces and, against expectations δ -(Cu,Si) is still present, too. Several peaks remain unexplained (see Table 3) which are probably due to oxide formation.

A comparison of the diffractogram of $\text{Cu}_{81.5}\text{Si}_{18.5}$ at 780°C and $\text{Cu}_{84.0}\text{Si}_{16.0}$ at 750°C (Table 1) shows that the observed additional peaks in Table 1 correspond to those observed in $\text{Cu}_{81.5}\text{Si}_{18.5}$ and can be considered to represent the δ -phase.

The situation can thus be summarized as follows: major parts of the high temperature diffractogram of $\text{Cu}_{81.5}\text{Si}_{18.5}$ at 780°C can be explained by the application of the hexagonal structural model given by Mattern [16], but the observation of several additional peaks that appear and disappear at the same temperature suggest that the structural model for δ is not fully correct. However, we were not able to find a unit cell explaining all reflexes observed for δ .

Phase diagram

More than 50 samples have been prepared and analysed to investigate Cu-Si phase equilibria in the 72 to 100 at% Cu composition range. Many of them have been exchanged between the two laboratories in order to cross-check results and to take advantage from the use of the best instrumentation available in both labs. A selection of the most significant and representative results obtained in this work is reported in Table 4. Other results have been obtained which confirm those reported in Table 4 without adding new information: these have been omitted for

brevity. Thanks to these results, stable and metastable Cu-Si phase equilibria have been determined. They are presented and commented in the following.

Stable phase equilibria

The equilibrium phase diagram is shown in Fig. 3. Due to the composition of binary compounds in the system the current work is limited to a Cu-content of more than 72 at.%. The phase diagram presented in this work does confirm the general aspects of the phase diagram assessed by Olesinski and Abbaschian [5]. However, several details concerning reaction temperatures, reaction types and homogeneity ranges of selected phases have been modified. An overview of the samples used for determining the phase diagram including a list of the relevant reaction temperatures is shown in Table 4. An overview of the invariant reactions according to this study is given in Table 5.

Based on EPMA and SEM measurements, the composition of the Cu_3Si phases (η , η' and η'') has been determined ~ 1 at.% richer in Si compared to the previous phase diagram version. According to DTA measurements the transition from η - Cu_3Si to η' - Cu_3Si occurs at 555 °C in the Si-rich side and at 620 °C in the Cu-rich side of Cu_3Si . It was not investigated if the $\eta \rightleftharpoons \eta'$ transition is of first or second order so the transition is drawn as dotted line similar to the phase diagram given by Olesinski and Abbaschian [5]. Two different pieces of sample 22 with the nominal composition $\text{Cu}_{72.5}\text{Si}_{27.5}$ were annealed at 500 (equilibrium between η' and Si) and 650 °C (equilibrium between η and Si) and then quenched in water. The powder X-ray diffraction of both samples shows exactly the same pattern and the DTA measurements show the same effects at the same temperatures. This indicates that it was not possible to quench the high-temperature phase η - Cu_3Si . DTA analysis of the samples show very small thermal effects related to the transition between η' and η . In sample 19 with the nominal composition $\text{Cu}_{78}\text{Si}_{22}$ the effect was too small to be observed at all.

For the ϵ - $\text{Cu}_{15}\text{Si}_4$ phase the stoichiometric composition $\text{Cu}_{78.95}\text{Si}_{21.05}$ was assumed, instead of the analytical composition $\text{Cu}_{78.5}\text{Si}_{21.5}$ resulting from the average of the SEM measurements. The stoichiometric composition is still within

the statistical spread of the SEM measurements and there is no indication of a change in composition in this line compound.

The equilibrium between $\varepsilon\text{-Cu}_{15}\text{Si}_4$ and Cu_3Si is shown in Fig. 4 where a microphotograph of sample 20 (at 78.0 at% Cu) after 120 h annealing at 780 °C is reported. The large and round $\varepsilon\text{-Cu}_{15}\text{Si}_4$ crystals are due to the high temperature annealing. The peritectoidic formation of $\varepsilon\text{-Cu}_{15}\text{Si}_4$ is confirmed by the microphotograph reported in Fig. 5. It shows sample 15 (79.5 at% Cu) after 720 h annealing at 500 °C. $\varepsilon\text{-Cu}_{15}\text{Si}_4$, the darker phase, has grown from the $\delta\text{-(Cu,Si)} + \eta\text{-(Cu,Si)}$ eutectic. Subsequently, during quenching, $\delta\text{-(Cu,Si)}$ transformed into $\gamma\text{-(Cu,Si)}$ without any appreciable change in composition.

The two invariant reactions $L + \beta \rightleftharpoons \delta$ and $L \rightleftharpoons \delta + \eta$ are very close concerning their reaction temperature. Nevertheless, the high number of samples showing these reactions allows the determination of the reactions temperatures of 821 and 818 °C, respectively, with reasonable margins of error. The first heating curve in the DTA measurement of sample 14 with the nominal composition $\text{Cu}_{80}\text{Si}_{20}$ situated in the two-phase field $\varepsilon + \gamma$ is shown in Fig. 6. Three invariant effects including the transition $L \rightleftharpoons \delta + \eta$ at 817 °C are labelled. Fig. 7 shows the first heating curve of sample 10 with the nominal composition $\text{Cu}_{83}\text{Si}_{17}$. The peak with an onset temperature of 821 °C represents the invariant reaction $L + \beta \rightleftharpoons \delta$.

Previously, the transition from $\delta\text{-(Cu,Si)}$ to $\gamma\text{-(Cu,Si)}$ was described to be of peritectoidic type at 729 °C ($\delta + \kappa \rightleftharpoons \gamma$) and of eutectoidic type at 710 °C ($\delta \rightleftharpoons \gamma + \varepsilon$) [5]. According to the DTA-measurements in the present work the transition temperature is essentially the same at both sides of the γ -phase, so the authors assumed a congruent transformation ($\gamma \rightleftharpoons \delta$) and two eutectoidic reactions at 735 °C as indicated in Fig. 3. The DTA curve showing the first heating of sample 8 with the nominal composition $\text{Cu}_{84}\text{Si}_{16}$ is shown in Fig. 8 indicating the reaction $\delta \rightleftharpoons \gamma + \kappa$ at 734 °C.

The formation of the β -phase in the reaction $\beta \rightleftharpoons \kappa + \delta$ is found in various samples. Furthermore it was possible to determine several non-invariant effects connected with the crossing of phase boundaries involving the β -(Cu,Si) and κ -(Cu,Si) high temperature phases, so the respective phase boundaries could be fixed quite accurately. As an example, the DTA curve of sample 8 with the nominal composition $\text{Cu}_{86}\text{Si}_{14}$ is shown in Fig. 8. The invariant reactions $L + (\text{Cu}) \rightleftharpoons \beta$ at 849 °C and $\beta + (\text{Cu}) \rightleftharpoons \kappa$ at 842 °C show again a very small temperature difference but the two effects are well separated in DTA curves.

Since it was not possible to detect the reaction temperature of the invariant reaction $\kappa \rightleftharpoons \gamma + (\text{Cu})$ and the authors of the current work did not find any contradicting results, the temperature (552 °C) and the composition of the reactants are taken from Olesinski and Abbaschian [5]. Similarly, equilibria related to the $\eta'' \rightleftharpoons \eta'$ transformation, not detected in this work, were accepted from literature [5].

Metastable phase equilibria

Several samples prepared in the composition range where $\varepsilon\text{-Cu}_{15}\text{Si}_4$ should be stable did not show the phase, but resulted to be constituted by η -(Cu,Si) and γ -(Cu,Si) in various proportions, depending on the global composition. In such samples the composition of γ -(Cu,Si) in metastable equilibrium with η -(Cu,Si) at 500°C resulted to be about 20 at% Si, which means about 2 at% richer in Cu than in the stable phase diagram. On the other hand the composition of η -(Cu,Si) in metastable equilibrium with γ -(Cu,Si) at the same temperature resulted to be about 23.5 at% Si, only 1 at% richer in Si than in the stable phase diagram. It was not possible to determine experimentally the metastable equilibria between δ -(Cu,Si) and η -(Cu,Si), due to the non-quenchability of the δ -(Cu,Si) phase. Presumably the composition range of the δ -(Cu,Si) phase is also increased in the Cu rich side when $\varepsilon\text{-Cu}_{15}\text{Si}_4$ is suppressed.

Conclusions

Cu-Si phase equilibria have been investigated at compositions greater than 72 at% Cu. Stable phases and phase equilibria already reported in literature have been substantially confirmed in their general trends, but selected composition ranges and the nature of a few invariant equilibria have been modified on the basis of our experiments. In particular stability ranges of the β -(Cu,Si), δ -(Cu,Si) and η -(Cu,Si) phases have been slightly modified as well as temperature and nature of the invariant equilibria related to the $\gamma \rightleftharpoons \delta$ transformation.

Stability of the ϵ -(Cu₁₅Si₄) phase has been especially investigated concluding that it is thermodynamically stable but kinetically inhibited by nucleation difficulties which become especially effective when samples are synthesised from very high purity elements using high purity crucibles.

Investigation of crystal structure and composition ranges of the high temperature β -(Cu,Si) and δ -(Cu,Si) was particularly difficult, due to the non-quenchability of these phases. Stability ranges were determined mainly by DTA, while high temperature XRD was used to investigate crystal structures. The structure of β -(Cu,Si) was confirmed, while for δ -(Cu,Si) some uncertainties still remain.

Acknowledgements

Financial support from the Austrian Science foundation (FWF) under the project number P19305 is gratefully acknowledged. Furthermore, the authors wish to thank Christian Lengauer for his support with the high-temperature X-Ray diffraction and Johannes Theiner for the elemental analysis.

Tables

Table 1

High-temperature X-ray powder diffraction of a sample with the nominal composition $\text{Cu}_{84.0}\text{Si}_{16.0}$, annealed at 500°C.

T (°C)	phase	amount ^a (%)	lattice parameters (Å)		additional reflections ° 2θ	R _{wp}
			a	c		
25	γ	99(1)	6.2210(1)			3.64
	(Cu)	1(1)	3.622(1)			
550	γ	85(1)	6.284(1)			4.096
	(Cu)	14(1)	3.6595(1)			
	κ	1(1)	2.5881(1)	4.2253(1)		
650	γ	58(1)	6.296(1)			4.104
	(Cu)	3(1)	3.6674(1)			
	κ	39(1)	2.5940(1)	4.235(1)		
700	γ	43(1)	6.3011(1)			4.221
	(Cu)	1(1)	3.6684(1)			
	κ	56(1)	2.598(1)	4.2371(1)		
750	(Cu)	2(1)	3.676(1)			5.17
	κ	89(1)	2.604(1)	4.2401(1)		
	β	8(1)	2.894(1)			
					35.85(1)	
					36.54(1)	
					43.51(1)	
800					43.90 (1)	δ ^{b)}
					44.34(1)	
	(Cu)	3(1)	3.6815(1)			
	κ	62(1)	2.6064(1)	4.248(1)		
	β	35(1)	2.9234(1)			
750	(Cu)	3(1)	3.676(1)			5.03
	κ	85(1)	2.6032(1)	4.2403(1)		
	β	12(1)	2.8932(1)			

					35.90(1)
					36.55(1)
					43.51(1)
					43.90(1)
					44.35(1)
550	(Cu)	2(1)	3.661(1)		4.707
	β	12(1)	2.8741(1)		
	γ	11(1)	6.2835(1)		
	κ	74(1)	2.591(1)	4.2245(1)	
					26.84(1)
					36.05(1)
					37.20(1)
					39.60(1)
					51.92(1)
25	β	15(1)	2.5624(1)	4.184(1)	5.47
	γ	9(1)	6.2223(1)		
	κ	76(1)	2.847(1)		
					27.15 (1)
					36.50(1)
					37.60(1)
					39.43(1)
					50.31(1)

^a amount calculated on basis if the peak area in the X-Ray powder diffractogram by TOPAS [19]

^b Peaks are assumed to be related to the formation of the δ -phase

Table 2

High-temperature X-ray powder diffraction of a sample with the nominal composition $\text{Cu}_{83.6}\text{Si}_{16.4}$, annealed at 810 °C. Only the first and the sixth measurements at 810 °C are shown, the other four do not show any significant difference.

Temperature °C	phase	amount ^a (%)	lattice parameters (Å)		R_{wp}
			a	c	
25	γ	98(1)	6.2225(1)		3.37
	κ	2(1)	2.5605(1)	4.1831(1)	
810	β	91(1)	2.9215(1)		4.64
	κ	9(1)	2.6064(1)	4.248(1)	
810	β	90(1)	2.922(1)		4.57
	κ	10(1)	2.6061(1)	4.2493(1)	
25	β	4(1)	2.8455(1)		4.19
	γ	80(1)	6.2205(1)		
	κ	16(1)	2.5615(1)	4.1836(1)	

Table 3

High-temperature X-ray powder diffraction of a sample with the nominal composition $\text{Cu}_{81.5}\text{Si}_{18.5}$ annealed at 780 °C. Only the first and the sixth measurements at 780 °C are shown, the other four do not show any significant difference.

Temperature °C	phase	amount ^a (%)	lattice parameters (Å)		additional reflections (° 2θ)	R_{wp}
			a	c		
25	γ	99(1)	6.2233(1)			3.56
	ε	1(1)	9.836(1)			
780	δ^{*j}	100	4.094(1)	5.01(1)		5.46
					36.40(1)	
					38.54(1)	
					43.62(1)	
					43.94(1)	
					48.58(1)	
					49.34(1)	
					51.53(1)	
					75.10(1)	
780	δ^{*j}	100	4.095(1)	5.01(1)		5.56
					30.81(1)	
					32.38(2)	
					36.42(1)	
					38.55(1)	
					43.50(1)	
					43.90(1)	
					48.56(1)	
					49.32(1)	
					51.41(1)	
					75.05(2)	
25	δ^{*j}	5(1)	4.0296(1)	4.926(1)		5.19
	γ	93(1)	6.2213(1)			

κ	2(1)	2.562(1)	4.1824(1)	
				32.63 (1)
				37.58(1)
				44.40(1)
				50.20(1)

^{*)} δ according to the structural model of [16]

Table 4 – Selection of experimental results used to determine stable phase equilibria.

Sample number	Annealing temperature (°C)	Global composition ^(a) (at%Cu)	Phase analysis from EPMA (compositions and amounts) (at%Cu, volume%)	Phase analysis from XRD (amounts) (volume%)	DTA peaks on heating (on cooling) (°C)	Remarks
1	500	88.0	---	γ (60%)	839	$\beta + (\text{Cu}) \rightleftharpoons \kappa$
				(Cu) (40%)	848	$\text{L} + (\text{Cu}) \rightleftharpoons \beta$
					945 (943)	$\text{L} \rightleftharpoons \text{L} + (\text{Cu})$
2	500	87.0	---	γ (70%)	822	$\kappa + \beta \rightleftharpoons \kappa$
				(Cu) (30%)	840	$\beta + (\text{Cu}) \rightleftharpoons \kappa$
					849	$\text{L} + (\text{Cu}) \rightleftharpoons \beta$
					923 (921)	$\text{L} \rightleftharpoons \text{L} + (\text{Cu})$
3	500	86.5	γ (83.0, 55%) (Cu) (90.0, 45%)	γ (84%)	806	$\kappa + \beta \rightleftharpoons \kappa$
				(Cu) (16%)	838	$\beta + (\text{Cu}) \rightleftharpoons \kappa$
					844	$\text{L} + (\text{Cu}) \rightleftharpoons \beta$
					920	$\text{L} \rightleftharpoons \text{L} + (\text{Cu})$
4	500	86.0	---	γ (86%)	734	$\delta \rightleftharpoons \kappa + \gamma$
				(Cu) (14%)	793	$\kappa + \beta \rightleftharpoons \kappa$
					842	$\beta + (\text{Cu}) \rightleftharpoons \kappa$
					849	$\text{L} + (\text{Cu}) \rightleftharpoons \beta$

			896 (896)		L \rightleftharpoons L + (Cu)
5	650	85.5	κ (86.5, 55%) γ (82.5, 45%)	κ γ	
6	500	85.0	---	γ (89%) (Cu) (11%)	$\delta \rightleftharpoons \kappa + \gamma$ $\beta \rightleftharpoons \delta + \kappa$ $\beta \rightleftharpoons \beta + \kappa$ $\beta + L \rightleftharpoons \beta$ $L + (\text{Cu}) \rightleftharpoons \beta$ $L \rightleftharpoons L + (\text{Cu})$
7	500	84.5	γ (83.0, 90%) (Cu) (90.0, 10%)	---	$\delta \rightleftharpoons \kappa + \gamma$ $\beta \rightleftharpoons \delta + \kappa$ $\beta \rightleftharpoons \beta + \kappa$ $L + \beta \rightleftharpoons \beta$ $L + (\text{Cu}) \rightleftharpoons \beta$ $L \rightleftharpoons L + (\text{Cu})$
8	500	84.0	---	γ (98%) (Cu) (2%)	$\delta \rightleftharpoons \kappa + \gamma$ $\beta \rightleftharpoons \delta + \kappa$ $L + \beta \rightleftharpoons \beta$ $L + (\text{Cu}) \rightleftharpoons \beta$

9	500	83.5	γ (83.0, 97%) (Cu) (90.0, 3%)	γ (Cu)	733 779 794 820 845 (842)	$\delta \rightleftharpoons \kappa + \gamma$ $\beta \rightleftharpoons \delta + \kappa$ $\beta \rightleftharpoons \beta + \delta$ $L + \beta \rightleftharpoons \delta$ $L \rightleftharpoons L + \beta$
10	500	83.0	---	γ	733 741 782 821 835 (831)	$\delta \rightleftharpoons \kappa + \gamma$ $\delta + \kappa \rightleftharpoons \delta$ $\beta \rightleftharpoons \delta + \kappa$ $L + \beta \rightleftharpoons \delta$ $L \rightleftharpoons L + \beta$
11	500	82.0	γ (82.5, 80%) ϵ (78.0, 20%)	γ ϵ	735 760 821 826 (815)	$\delta \rightleftharpoons \epsilon + \gamma$ $\delta \rightleftharpoons \epsilon + \delta$ $L + \beta \rightleftharpoons \delta$ $L \rightleftharpoons L + \beta$
12	500	81.0	γ (82.0, 50%) ϵ (78.0, 50%)	γ (50%) ϵ (50%)	736 801 820 827 (815)	$\delta \rightleftharpoons \epsilon + \gamma$ $\eta + \delta \rightleftharpoons \epsilon$ $L \rightleftharpoons \delta + \eta$ $L \rightleftharpoons L + \delta$
13	760	81.0	γ (δ) (82.0, ---)	γ (57%)	---	

14	500	80.0	ε (78.5, ---)	ε (43%)	735	$\delta \rightleftharpoons \varepsilon + \gamma$
			γ (82.0, ---)	ε (78%)		$\eta + \delta \rightleftharpoons \varepsilon$
			ε (78.5, ---)	γ (22%)	800	$L \rightleftharpoons \eta + \delta$
					817	$L \rightleftharpoons L + \eta$
					827 (823)	
15	500	79.5	ε (78.0, 80%)	ε (78%)	732	$\delta \rightleftharpoons \varepsilon + \gamma$
			γ (82.5, 20%)	γ (22%)	799	$\eta + \delta \rightleftharpoons \varepsilon$
					815	$L \rightleftharpoons \delta + \eta$
					832 (828)	$L \rightleftharpoons L + \eta$
16	500	79.0	ε (78.0, 98%)	ε (100%)	801	$\eta + \delta \rightleftharpoons \varepsilon$
			η (75.5, 2%)		819	$L \rightleftharpoons \eta + \delta$
					842 (829)	$L \rightleftharpoons L + \eta$
17	500	78.5	ε (78.0, 85%)	---	618	$\eta + \varepsilon \rightleftharpoons \eta'$
			η (76.0, 15%)		798	$\eta + \delta \rightleftharpoons \varepsilon$
					815	$L \rightleftharpoons \delta + \eta$
					845 (837)	$L \rightleftharpoons L + \eta$
18	500	78	ε (78.5, 75%)	---	---	
			η (75.5, 25%)			
19	500	78.0	ε (78.5, 70%)	ε	802	$\eta + \delta \rightleftharpoons \varepsilon$

20	780	77.5	η (75.0, 30%)	η	821	$L \rightleftharpoons \delta + \eta$
					855 (842)	$L \rightleftharpoons L + \eta$
				ε	---	
			ε (78.5, 70%)			
			η (76.0, 30%)	η		
21	500	77	---	ε	670	$\eta + \varepsilon \rightleftharpoons \eta'$
				η	844	$L + \eta \rightleftharpoons \eta$
					861 (840)	$L \rightleftharpoons L + \eta$
22	500	72.5	η (76.0, 90%)	η	554	$\eta \rightleftharpoons \eta' + \text{Si}$
			(Si) (1, 10%)	Si	807	$L \rightleftharpoons \text{Si} + \eta$
					839 (828)	$L \rightleftharpoons L + \eta$

(a) This is the nominal composition of the prepared samples. For selected samples the global composition measured by EPMA resulted to be equal to the nominal composition, within the EPMA error limits.

Table 5

Invariant reactions as determined in this work.

Reaction	Temperature (°C)	Phase	Composition (at.% Cu)
$L + (Cu) \rightleftharpoons \beta$	849±2	L	84.0(5)
		(Cu)	89(a)
		β	85.8(5)
$(Cu) + \beta \rightleftharpoons \kappa$	839±2	(Cu)	89 (a)
		β	85.5(5)
		κ	87.5(5)
$L + \beta \rightleftharpoons \delta$	821±2	L	80.8(5)
		β	83.5(5)
		δ	82.5(5)
$L \rightleftharpoons \eta + \delta$	818±3	L	80.2(5)
		η	76.8(5)
		δ	82.3(5)
$L \rightleftharpoons (Si) + \eta$	807±2	L	70 (a)
		(Si)	0 (b)
		η	74 (a)
$\eta + \delta \rightleftharpoons \varepsilon$	800±2	η	76.5(5)
		δ	81.5(5)
		ε	78.9(5)
$\beta \rightleftharpoons \delta + \kappa$	781±2	β	83.8(5)
		δ	83.0(5)
		κ	85.8(5)
$\delta \rightleftharpoons \varepsilon + \gamma$	735±2	δ	82.1(5)
		ε	78.9 (b)
		γ	82.2(5)
$\delta \rightleftharpoons \gamma + \kappa$	734±2	δ	83.1(5)
		γ	82.5(5)

		κ	86.8(5)
$\eta + \varepsilon \rightleftharpoons \eta'$	618 \pm 3	η	75.8(5)
		ε	78.9 (b)
		η'	75.8(5)
$\eta' + \varepsilon \rightleftharpoons \eta''$	570 (a)	η'	75.6(5)
		ε	78.9 (b)
		η''	75.6(5)
$\eta \rightleftharpoons (\text{Si}) + \eta'$	555 \pm 3	(Si)	0 (b)
		η	74 (a)
		η'	74 (a)
$\kappa \rightleftharpoons \gamma + (\text{Cu})$	552 (a)	κ	89 (a)
		γ	83 (a)
		(Cu)	90 (a)
$\eta' \rightleftharpoons \eta'' + (\text{Si})$	467 (a)	(Si)	0 (b)
		η'	74 (a)
		η''	74 (a)

a) value from literature [5]

b) stoichiometric composition

Figures

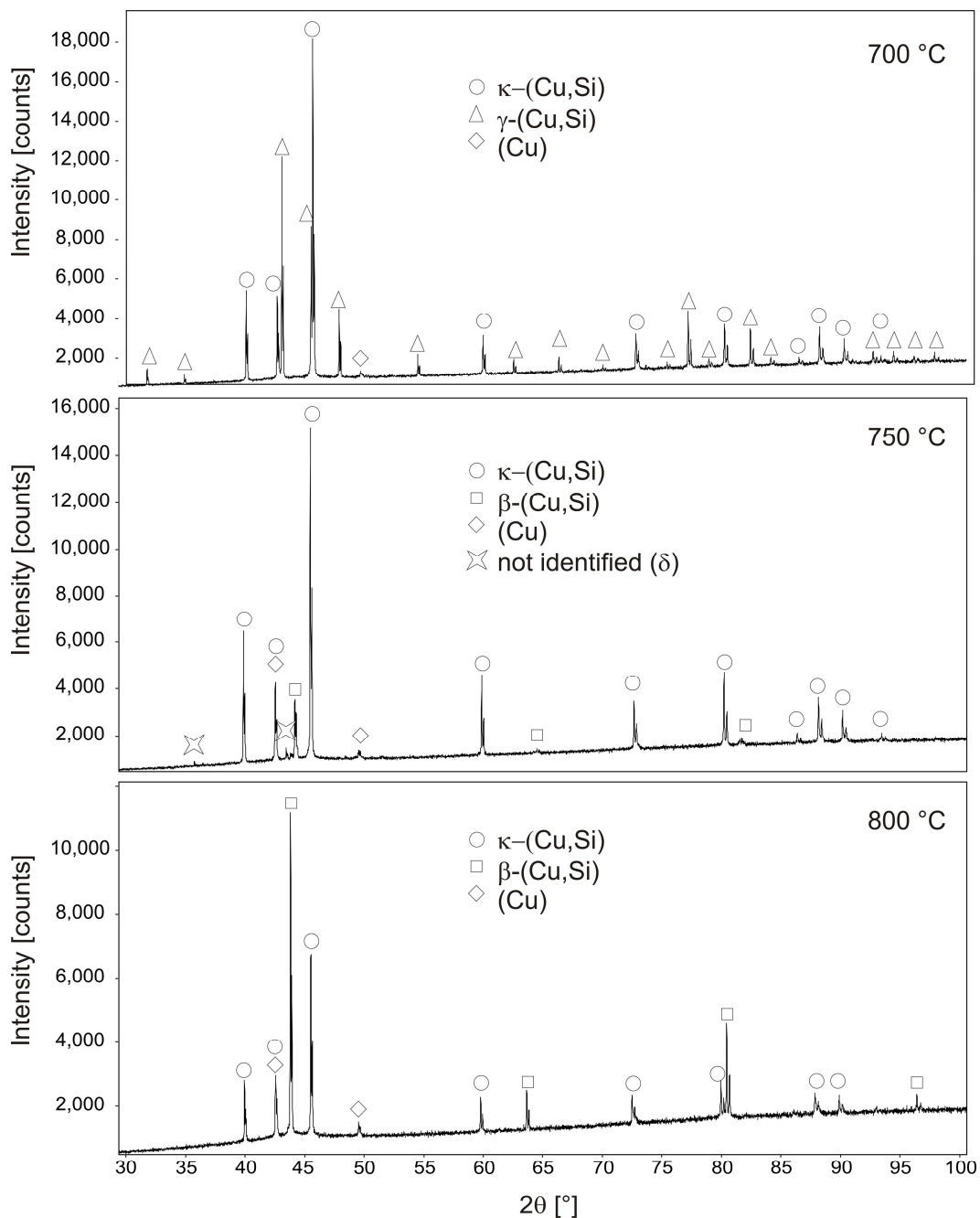


Fig. 1: Comparison of high temperature X-ray diffractograms of a sample with the nominal composition $\text{Cu}_{84}\text{Si}_{10}$ obtained at different temperatures.

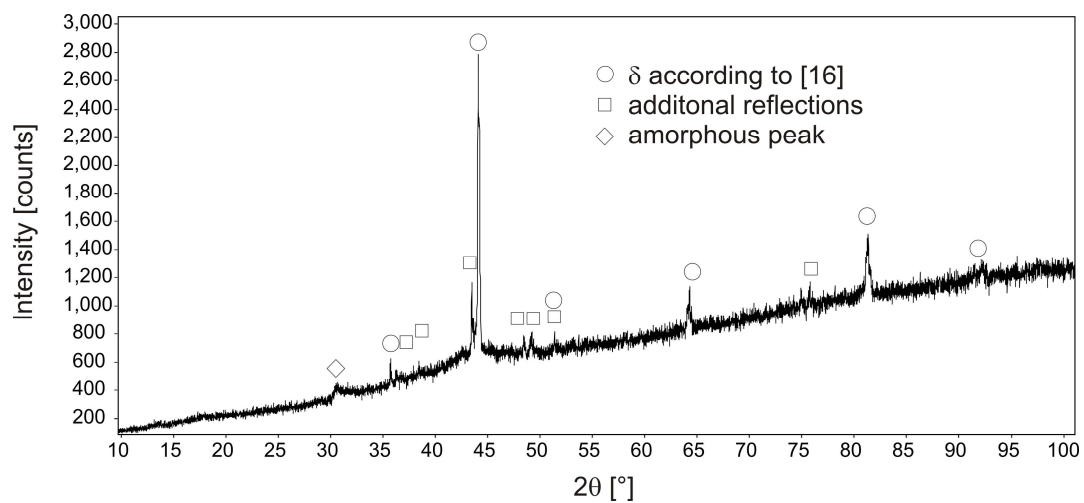


Fig. 2: Powder X-ray diffractogram of a sample with the nominal composition $\text{Cu}_{81.5}\text{Si}_{18.5}$ at 780°C

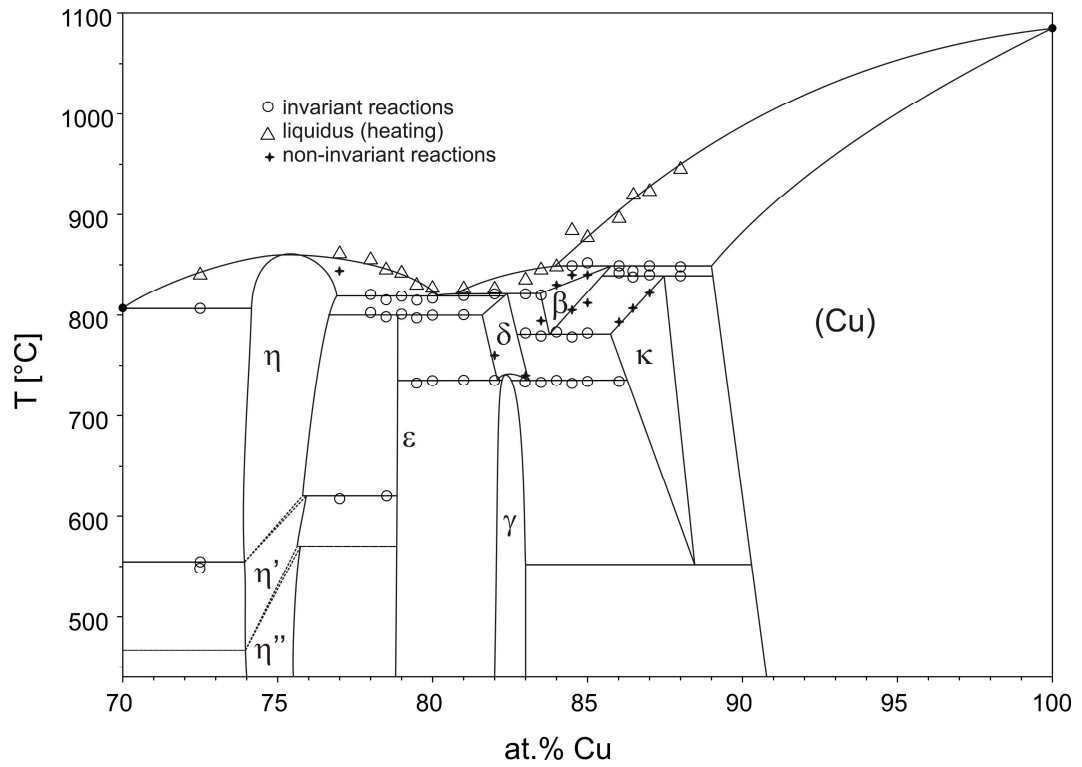


Fig. 3: Equilibrium phase diagram of the Cu-Si system between 70 and 100 at% Cu with experimental data points from DTA measurements

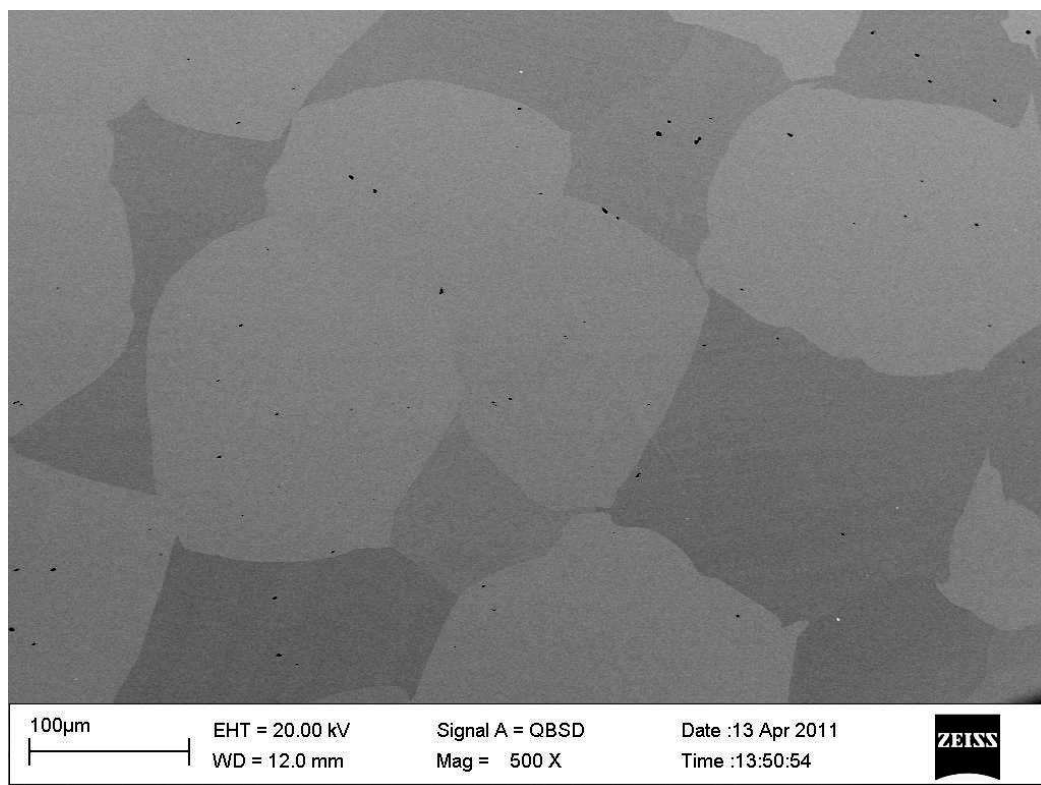


Fig. 4: Microphotograph of sample 20 (78.0 at% Cu) after 120 h annealing at 780 °C. Dark phase is Cu_3Si and bright phase is $\epsilon\text{-Cu}_{15}\text{Si}_4$.

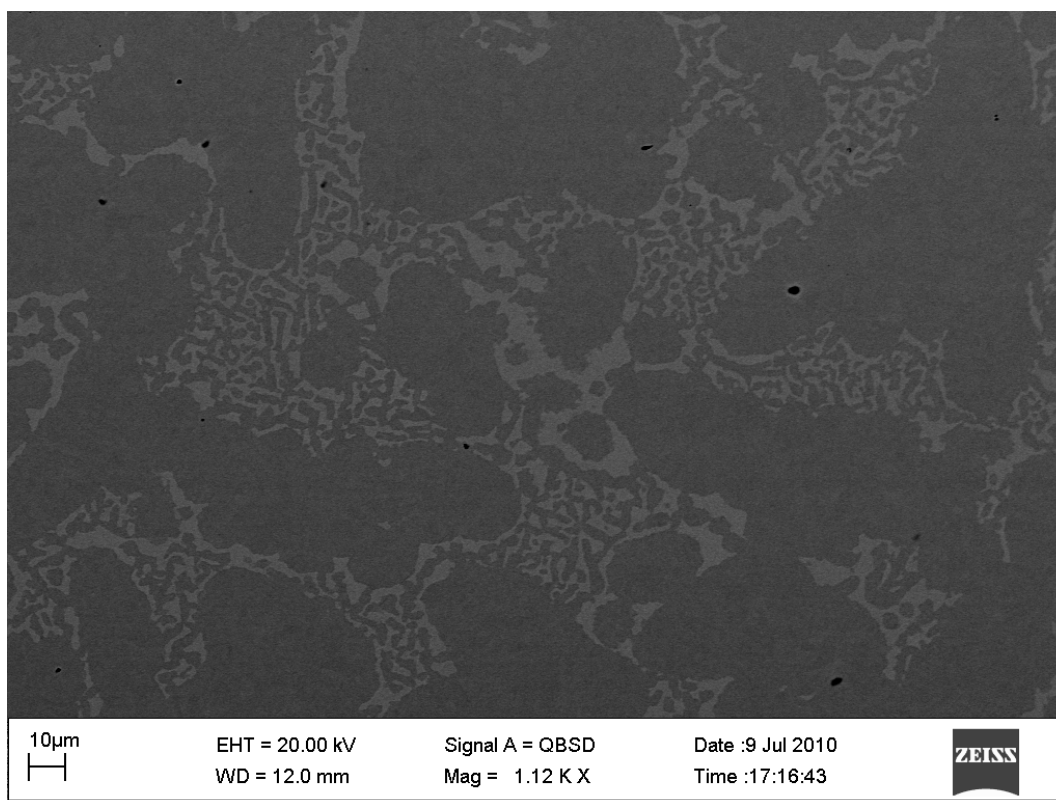


Fig. 5: Microphotograph of sample 15 (79.5 at% Cu) after 720 h annealing at 500 °C. Dark phase is $\epsilon\text{-Cu}_{15}\text{Si}_4$ and bright phase is $\gamma\text{-(Cu,Si)}$.

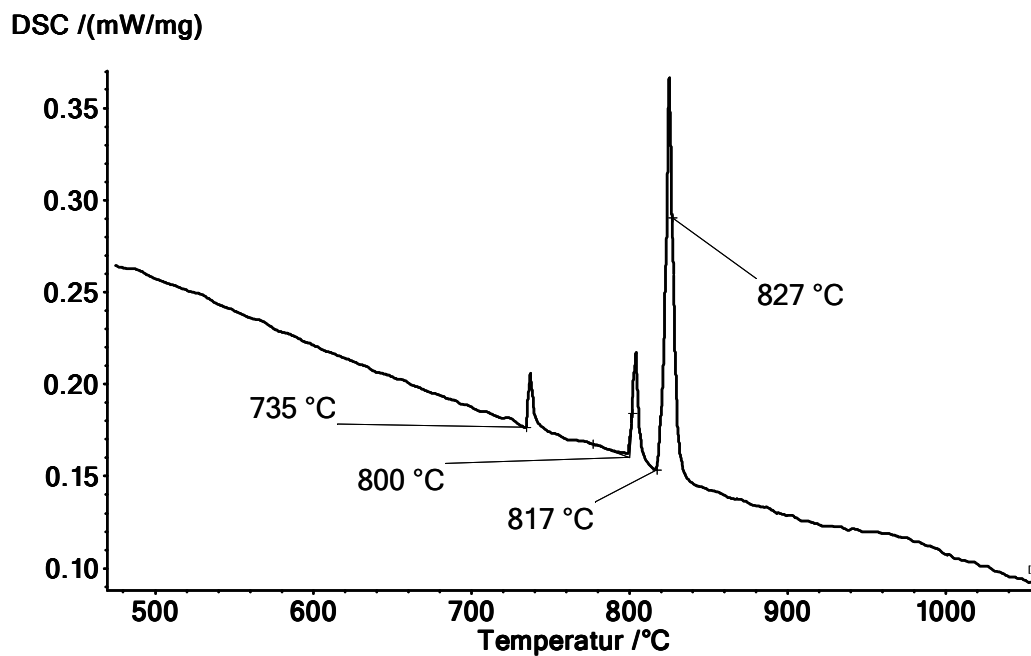


Fig. 6: First cycle of the DTA measurement of sample 14 with the nominal composition $\text{Cu}_{80}\text{Si}_{20}$

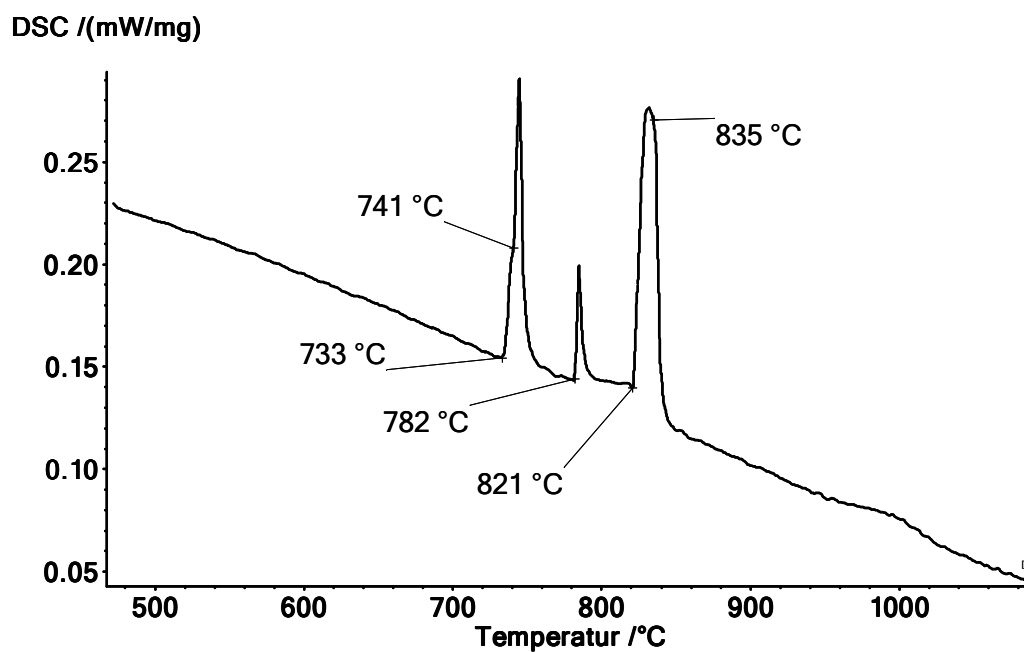


Fig. 7: First cycle of the DTA measurement of the sample 10 with the nominal composition $\text{Cu}_{83}\text{Si}_{17}$

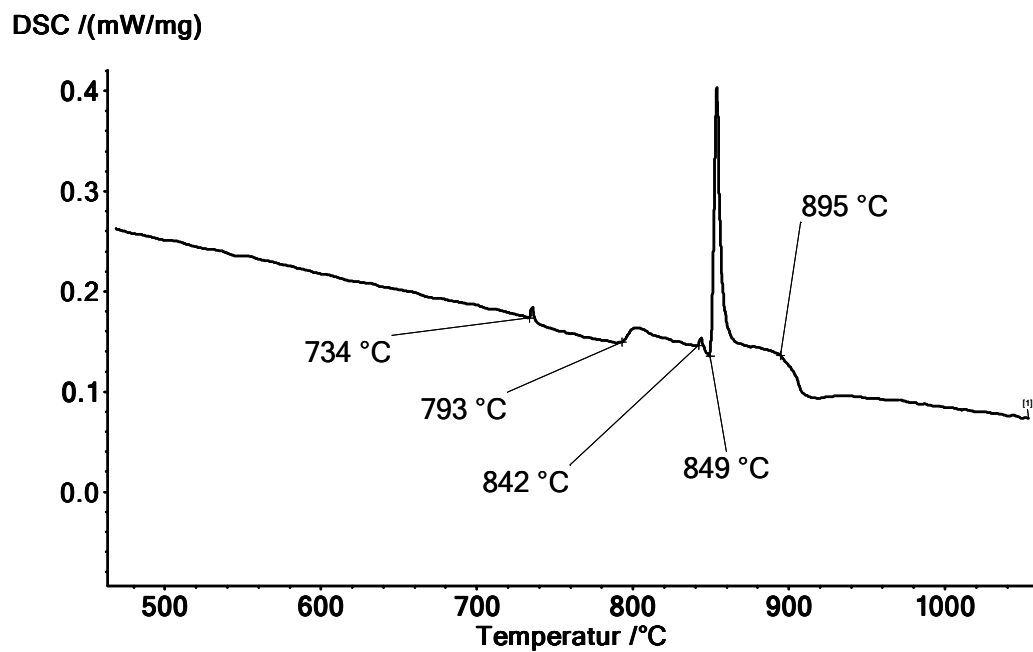


Fig. 8: First cycle of the DTA measurement of the sample 8 with the nominal composition $\text{Cu}_{86}\text{Si}_{14}$

References

- [1] O. Parajuli, N. Kumar, D. Kipp, J.-I. Hahm, *Applied Physics Letters* 90 (2007) num. 173107
- [2] Y. Liu, S. Song, D. Mao, H. Ling, M. Li, *Microelectronic Engineering* 75(3) (2004) 309-315
- [3] H.-J. Ahn, Y.-S. Kim, W.B. Kim, Y.-E. Sung, T.-Y. Seong, *J. Power Sources* 163 (2006) 211–214
- [4] D.C. Johnson, J.M. Mosby, S.C. Riha, A.L. Prieto, *J. Materials Chemistry* 20 (2010) 1993-1998
- [5] R.W. Olesinski, G.J. Abbaschian, in: P.R. Subramanian, D.J. Chakrabarti, D.E. Laughlin (Eds.), *Phase Diagrams of Binary Copper Alloys*, ASM International, Materials Park, OH, 1994, 398-405
- [6] E. Rudolphi, *Z. Anorg. Chem.* 53 (1907) 216-227 (in German)
- [7] C.S. Smith, *J. Inst. Met.* 40 (1928) 359-370
- [8] C.S. Smith, *Trans. AIME* 83 (1929) 414-439
- [9] C.S. Smith, *Trans. AIME* 137 (1940) 313-329
- [10] A.G.H. Andersen, *Trans. AIME* 137 (1940) 331-350
- [11] W.R. Hibbard, Jr., G.H. Eichelman, Jr., W.P. Saunders, *Trans. AIME* 180 (1949) 92-100
- [12] A.D. Hopkins, *J. Inst. Met.* 82 (1953-54) 163-165
- [13] B.J.K. Solberg, *Acta Cryst.* A34 (1978) 684-698
- [14] S. Arrhenius, A. Westgren, *Z. Phys. Chem.* B14 (1931) 66-79
- [15] K. Schubert, G. Brandauer, *Z. Metallk.* 43 (1952) 267
- [16] N. Mattern, R. Seyrich, L. Wilde, C. Baetz, M. Knapp, J. Acker, *J. Alloys Compd.* 429 (2007) 211-215
- [17] K.P. Mukherjee, J. Bandyopadhyaya, K.P. Gupta, *Trans. Metall. Soc. AIME* 245 (1969) 2335-2338
- [18] F.R. Morral, A. Westgren, *Ark. Kemi, Mineral. Geol.* 11 (1934) 1
- [19] TOPAS, Version 3.0, Brucker AXS Inc., Karlsruhe, Germany, (1999)

- [20] F.A. Veer, B.H. Kolster, W.G. Burgers, Trans. Metall. Soc. AIME 242 (1968) 669
- [21] M. Onishi, H. Muira, Trans. Jpn. Inst. Met. 18 (1977) 107
- [22] W.J. Ward, K.M. Carroll, J. Electrochem. Soc 129 (1982) 227
- [23] L. Levin, Z. Atzmon, A. Katsman, T. Werber, Mater. Chem. Phys. 77 (1995) 4399
- [24] J.G.M. Becht, F.J.J. van Loo, R. Metselaar, Reactivity of Solids, P. Barret, L.C. Dufour (Eds.), Elseviers Publishers B.V., Amsterdam, 1985, pp.941
- [25] F.J.J. van Loo, P.J.C. Vosters, J.G.M. Becht, R. Metselaar, Mater. Sci. Forum 29 (1988) 261-274
- [26] L. Stolt, F.M. D'Heurle, J.M.E. Harper, Thin Solid Films 200 (1991) 147-156
- [27] E.M. Shpilewsky, M.E. Shpilewsky, M.A. Andreev, Surface and Coatings Technology 74-75 (1995) 937-940
- [28] J. Yang, H.B. Zhang, K. Tao, Y. Fan, Appl. Phys. Lett. 64 (1994) 1800-1802
- [29] R.R. Chromik, W.K. Neils, E.J. Cotts, J. Appl. Phys. 86(8) (1999) 4273-4281
- [30] R.R. Chromik, personal communication, 2010
- [31] B. Gillot, G. Weber, H. Souha, M. Zenkour, J. Alloys Compd. 270(1-2) (1998) 275-280
- [32] P. Riani, K. Sufryd, G. Cacciamani, Intermetallics 17 (2009) 154-164
- [33] T. Isawa, Nippon Kinzoku Gakkaishi, 2 (1938) 400-409

3.3 New investigation of phase equilibria in the system Al-Cu-Si

*Norbert Ponweiser and Klaus W. Richter**

University of Vienna, Department of Inorganic Chemistry/Materials Chemistry
Waehringer Strasse 42, 1090 Wien, Austria

* corresponding author

Email: klaus.richter@univie.ac.at

Submitted: *Journal of Alloys and Compounds*, Sept. 1st, 2011

Contributions to this paper:

N.P. sample preparation, analysis and interpretation, wrote the paper

K.W.R.: proofreading, general advice and helpful comments

Contribution of N. Ponweiser to the article: 80 %

Abstract

The phase equilibria and invariant reactions in the system Al-Cu-Si were investigated by a combination of optical microscopy, powder X-ray diffraction (XRD), differential thermal analysis (DTA) and electron probe micro analysis (EPMA). Isothermal phase equilibria were investigated within two isothermal sections. The isothermal section at 500 °C covers the whole ternary composition range and largely confirms the findings of previous phase diagram investigations. The isothermal section at 700 °C describes phase equilibria only in the complex Cu-rich part of the phase diagram. A new ternary compound τ was found in the region between (Al,Cu)- γ_1 and (Cu,Si)- γ and its solubility range was determined. The solubility of Al in κ -CuSi was found to be extremely high at 700°C. In contrast, no ternary solubility in the β -phase of Cu-Al was found, although this phase is supposed to form a complete solid solution according to previous phase diagram assessments. Two isopleths, at 10 and 40 at.% Si, were investigated by means of DTA and a partial ternary reaction scheme (Scheil diagram) was constructed, based on the current work and the latest findings in the binary systems Al-Cu and Cu-Si. The current study shows that the high temperature equilibria in the Cu-rich corner are still poorly understood and additional studies in this area would be favorable.

1. Introduction and literature review

Due to its importance in industry, the ternary system Al-Cu-Si has been heavily investigated over the last decades. Al-Cu-Si alloys are, for example, of growing importance for automotive industry due to its lightweight. The ternary alloys show higher strength than Al-Si alloys and their corrosion resistance is better than in Al-Cu alloys [1]. For designing ternary alloys matching specific requirements, fundamental understanding of the phase relationships and solidification behavior is essential. The Cu-rich corner of Al-Cu-Si and even of the binary subsystems Al-Cu and Cu-Si, is highly complex. Despite various studies of phase equilibria the ternary system is still not fully understood. Therefore we decided to perform a new re-investigation of the entire ternary system. A detailed literature review of existing phase diagram information on Al-Cu-Si and its binary subsystems is given below.

1.1 The binary Al-Cu system

The latest complete assessment of the system Al-Cu was done by Murray [2]. His work describes the equilibrium phase diagram and provides some information on metastable phase equilibria as well. According to Murray, the system contains 12 intermetallic compounds, 7 of them are only stable at elevated temperatures. More recently, phase diagram investigations have been performed by Liu et al. [3] and Ponweiser et al. [4]. Riani et al. [5] published a phase diagram combining the results of Murray and Liu. In the Cu-poor phase diagram all the authors agree very well. The binary compound θ -Al₂Cu shows a composition around 33 at.% Cu and crystallizes tetragonally [6]. It decomposes peritectically between 590(1) [4] and 592 °C [7]. At the composition of around AlCu, phase equilibria are more complicated. In the 1930ies, Preston [8] found an orthorhombic structure in a sample quenched from 602 °C. Slowly cooled samples investigated by Bradley et al. [9] proposed an allotropic transformation $\text{Al}_{1.8}\text{Cu}-\eta_1 \rightarrow \text{AlCu}-\eta_2$. Based on the comparison with the work of Preston, an orthorhombic or monoclinic structure

was suggested for the low temperature phase. El-Boragy [10] showed that the structure of the low-temperature phase was monoclinic. Murray does not explicitly mention the order of the transition from the high- to the low-temperature phase but according to the phase diagram given in [2] he assumes a higher order transition. Investigations by high-temperature X-ray diffraction worked out recently by the authors revealed the structure of the high-temperature η_1 -phase to be of the *Cmmm*-type ($\text{Al}_{1.8}\text{Cu}$ -type) [4]. Based on differential thermal analysis (DTA) as well as structural analysis, Ponweiser et al. [4] indicate that the transition $\eta_1 \rightarrow \eta_2$ is a first order transition.

Compounds with the proximate composition Al_3Cu_4 were also found to show a high- and a low-temperature modification [8, 9]. Murray suggests a transition temperature between 530 and 570 °C depending of the composition of the phase. Dong et al. [11, 12] investigated annealed and as-cast samples with a composition of Al_3Cu_4 . The as-cast samples exhibit a mixture of an orthorhombic face-centered and an orthorhombic body-centered structure and a minimum amount of $\gamma\text{-Al}_4\text{Cu}_9$. After annealing at 500 °C the orthorhombic face-centered structure became the major phase. The authors therefore suggested a transition $\gamma\text{-Al}_4\text{Cu}_9 + "oI" = "oF"$. EPMA measurements indicated compositions of $\text{Al}_{43.2}\text{Cu}_{56.8}$, $\text{Al}_{41.3}\text{Cu}_{58.7}$ and $\text{Al}_{39.6}\text{Cu}_{60.4}$ for *oF*, *oI* and $\gamma\text{-Al}_4\text{Cu}_9$, respectively. In the assessment of Murray, "*oI*" is labeled ζ_1 and "*oF*" is labeled ζ_2 . Gulay and Harbrecht determined the structures of ζ_1 (*Fmm2*, structure type Al_3Cu_4) [13] and ζ_2 (*Imm2*, structure type $\text{Al}_3\text{Cu}_{4.8}$) [14]. Contrary to Dong et al., Gulay and Harbrecht dedicate the face-centered structure to the phase with the higher Cu-content. Additional thermal analysis showed that Cu-rich phase ζ_1 (sample composition $\text{Al}_{42.5}\text{Cu}_{57.5}$) is stable at 400 °C [13] and the Cu-poorer phase ζ_2 (sample composition $\text{Al}_{43.2}\text{Cu}_{56.8}$) is stable at elevated temperatures (530 °C) and does not resist thermal treatment at 400 °C [14]. This is not in agreement with Murray who describes a low temperature phase ζ_2 and a high temperature phase ζ_1 with a slightly higher Cu-content [2]. As mentioned above, the transition temperature is supposed to be between 530 and 570 °C. Our own new

investigations find ζ_1 not to be stable at 500 °C, indicating a transition temperature $\zeta_2 = \zeta_1 + \eta_2$ above 500 °C.

The high temperature phases ε_1 and ε_2 were determined by Stockdale [15], the structure of ε_2 was found to be hexagonal [10]. The structure of the ε_1 -phase, stable at elevated temperatures, is still unknown. The order of the transition ε_1 - ε_2 is not mentioned specifically in literature but according to established phase diagrams it is a higher order transition [2, 4].

The region between 60 to 70 at.% Cu shows according to Murray two different compounds stable at room temperature, δ and γ_1 [2], while a third phase with unknown structure was not included in the assessment due to non-consensus in literature. The structure of δ was determined by Kisi and Brown [16], γ_1 was revealed by Arnberg and Westman [17]. The high temperature structure γ_0 was investigated by Liu et al. who found a bcc structure of the Cu_5Zn_8 -type. The assessment of Murray proposes a two-phase field between γ_0 and γ_1 based on the work of Hisatsune [18, 19]. Liu et al. investigated the Cu-rich part by differential scanning calorimetry (DSC), high-temperature X-ray diffraction and diffusion couples and did not find a two-phase field between γ_0 and γ_1 thus proposing a higher order transition between the two phases. This finding was confirmed recently by Ponweiser et al. [4].

The assessment of Murray claims that a high temperature phase β_0 is formed peritectically from β and liquid at 1037 °C. The phase was determined by Dawson [20] metallographically and by dilatometry measurements but has, according to Murray, never been reconfirmed. New diffusion couple experiments of Liu [3] did not confirm the existence of β_0 either. Additional investigations by DSC measurements revealed only an effect at 1019 °C which is rather connected to the solidus of β than the eutectoid reaction $\beta_0 = \beta + \gamma_0$. This interpretation was confirmed by Ponweiser et al. [4].

The two-phase region between β and (Cu) was heavily investigated and the assessment of Murray [2] gives a broad overview about the results of this research. The temperature of the eutectoid reaction $\beta = \gamma_1 + (\text{Cu})$ was found

between 560 and 575 °C which can be explained by the sluggishness of the reaction.

The α_2 -phase, stable below 363 °C [2]. According to Murray's assessment α_2 has an ordered fcc structure with a long period superlattice based on Cu₃Au and Al₃Ti. Adorno et al. [21] give a more detailed description of the phase α_2 .

An overview about the invariant reactions in the system used in the current study is given in Table 1.

1.2 The binary Al-Si system

The binary Al-Si system is a simple eutectic system and was assessed by Murray and McAlister extensively [22].

1.3 The binary Cu-Si system

The system Cu-Si has been investigated intensively in the last decades. A critical assessment was done by Olesinski and Abbaschian [23] giving an extensive overview about the work done in solid and liquid solutions as well as on metastable phases reported in literature up to the 1980ies. A more recent thermodynamic description of the system has been given by Yan and Chang [24], experimental investigations with focus on the Cu-rich part have recently been performed by Sufryd et al. [25]. An overview about the invariant reactions in the system is given in Table 1.

The binary compounds are all formed in the Cu-rich part of the phase diagram, starting with Cu₃Si. This phase shows three different modifications, the high-temperature η -phase, an intermediate phase η' and the low temperature phase η'' . It must be noted that the nomenclature of the phases is not consistent in old literature. The high temperature phase melts congruently at 859 °C and the transition temperatures between the phases differ highly with composition. The transition temperature of η to η' takes place between 558 and 620 °C, the transition temperature between η' and η'' differs between 467 and 570 °C, for the Cu-poor and Cu-rich side, respectively. According to the assessed phase diagram, the phases η and η' [26] show a rhombohedral structure ($R-3m$ and $R-3$) whereas

η'' is orthorhombic [26] or tetragonal [27]. Solberg [26] claims that η' has an ordered superstructure and η'' exhibits a long-period superstructure which is derived from the η' -structure by periodic displacement. The high-temperature phase η shows a disordered structure. More recent transmission electron investigations by Wen and Spaepen indicate $P-3m1$ and $R-3$ as space groups for η and η' [28]. Rapid quenching experiments performed by Mattern et al. [29] confirm the structure type of η .

The existence of the phase with the nominal composition $\text{Cu}_{15}\text{Si}_4$, designated ϵ , is widely discussed in literature. The assessment included the phase in the stable binary phase diagram [23], even though previous authors found different results. The phase was described first by Arrhenius and Westgren [30], Mukherjee et al. described a possible phase transition around 600 °C which was not confirmed. Diffusion couple experiments showed only one intermetallic phase, Cu_3Si [31, 32]. The authors suspected retarded nucleation of the other phases. By contrast, thin film diffusion couple experiments prepared by sputter deposition exhibit all three expected intermetallic compounds, Cu_3Si , ϵ and γ [33, 34]. Rapidly quenched samples do not show ϵ but after subsequent annealing at 500 °C ϵ is present [29]. In their study about the ternary Al-Cu-Si system Riani et al. claim that ϵ is stabilized by impurities and not present in the binary if very pure basic materials are used [35]. This conclusion was later withdrawn by the same authors in a recent study of the Cu-Si binary system by Sufryd et al. [25]. The authors conclude that the formation of ϵ is only inhibited kinetically but that the phase is stable in the binary Cu-Si system [25].

The third intermetallic compound stable at low temperature is Cu_5Si , designated as γ . It is cubic, showing the β -Mn structure, and it forms peritectically at 729 °C [23]. Although the phase does not occur in some diffusion couple experiments [31, 32], the phase is considered stable at the indicated temperature.

Three phases are reported to be stable at elevated temperature, κ , β and δ . The phase κ forms at 842 °C and decomposes eutectically at 552 °C. The compound crystallizes hexagonally in the Mg-type structure [23, 29]. β forms peritectically from (Cu) and liquid at 852 °C and decomposes at eutectically into δ and γ at 785

°C. It crystallizes cubic in a W-type structure [23]. According to the assessment of Olesinski and Abbaschian, the phase δ forms peritectically from β and liquid at 824 °C and decomposes at 710 °C eutectically into ε and γ [23]. New investigations by Sufryd et al. [25] indicate a congruent transformation from γ to δ and two eutectoidic reactions at 735 °C. High-temperature X-ray diffraction experiments performed by Mukherjee et al. described the phase as tetragonal [27]. Splat cooling experiments of Mattern et al. [29] lead to the hexagonal symmetry P63/mmc but the structure could not be confirmed by recent investigations [25].

1.4 The ternary system Al-Cu-Si

The first investigations of the whole system have been performed by Matsuyama [36] and Hisatsune [18]; a critical assessment is given by Lukas and Lebrun [37]. The authors give an overview about the present phases in the binaries as well as information invariant ternary equilibria including a liquidus surface projection. According to this assessment, no ternary compounds are present. An isothermal section at 400 °C based on the work of Hisatsune [18] together with a tentative reaction scheme (Scheil diagram) completes the assessment.

The largest part of the ternary system is dominated by phase equilibria with (Si), since binary phases only occur in the Cu-rich part and there are no ternary phases reported. At 400 °C γ_1 -Al₄Cu₉ shows the highest solubility into the ternary. The phase is stable up to the approximate composition Al₁₇Cu₇₂Si₁₁. The compounds δ -Al₄Cu₉ (~1 at.% Si), γ -Cu₅Si (~2 at.% Al), ε -Cu₁₅Si₄ (~2 at.% Al) and η'' -Cu₃Si (~5 at.% Si) show solubilities, too [37]. There is no information given on the solubility of ζ_1/ζ_2 -Al₃Cu₄, η_2 -AlCu and θ -Al₂Cu since the isothermal section given by Lukas and Lebrun only covers the section with a Cu-content higher than 60 at.%. The three phase fields in the Cu-rich corner present at 400 °C are: {(Cu) + (Al,Cu)- γ_1 + (Cu,Si)- κ }, {(Cu,Si)- η'' + (Al,Cu)- γ_1 + (Cu,Si)- κ }, {(Cu,Si)- ε + (Cu,Si)- η'' + (Cu,Si)- κ }, {(Cu,Si)- ε + (Cu,Si)- η'' + (Cu,Si)- γ } and {(Cu,Si)- γ + (Cu,Si)- κ + (Cu)} [37].

Additional isothermal sections at 500 and 600 °C are given by He et al. [38]. According to He et al. the three phase fields in the Cu-rich corner present at 500 °C are: $\{(Cu) + (Al,Cu)-\gamma_1 + (Cu,Si)-\kappa\}$, $\{(Cu,Si)-\eta + (Al,Cu)-\gamma_1 + (Cu,Si)-\varepsilon\}$, $\{(Cu,Si)-\varepsilon + (Al,Cu)-\gamma_1 + (Cu,Si)-\kappa\}$, $\{(Cu,Si)-\varepsilon + (Cu,Si)-\gamma + (Cu,Si)-\kappa\}$ and $\{(Cu,Si)-\gamma + (Cu,Si)-\kappa + (Cu)\}$. The solubilities change slightly compared to the isothermal section at 400 °C. The phase γ_1 -Al₄Cu₉ for example is stable up to the composition Al₁₅Cu₇₄Si₁₁. At 600°C, the additional three phase field $\{(Cu) + (Al,Cu)-\beta + (Al,Cu)-\gamma_1\}$ appears, where (Al,Cu)- β shows a solubility of about 4 at.% Si. Both at 500 and 600 °C, He et al. allocate the binary phase Cu₃Si to Cu₃Si- η , which is contradicting to the binary Cu-Si system [23, 29, 39].

He et al. also present several calculated vertical sections and a Scheil diagram which differs from the one proposed by Lukas and Lebrun [37] concerning the reactions temperatures as well as the reactions itself. Further thermodynamic measurements and assessments have been performed by various authors [1, 40-44].

The latest experimental investigation was done by Riani et al. [35]. The extensive study consists of an isothermal section at 500 °C and a detailed description of the existence of ε -Cu₁₅Si₄ in the binary and ternary system. As mentioned above, Sufryd et al. [25] give a more detailed study on the ε -Cu₁₅Si₄ phase, which is considered to be stable in the binary. Considering the findings of Sufryd et al.[25] the isothermal section given by Riani et al. [35] shows the same three phase fields like described by He et al. [38] although the solubility ranges especially for (Cu), κ -Cu₇Si and γ_1 -Al₄Cu₉ are quite different.

2. Experimental

The samples were prepared from Aluminum slug (99.999%), Copper wire (99.95%) and Silicon lump (99.9999%), all supplied by Alfa Aesar, Karlsruhe, Germany. For cleaning from oxides, the Cu wire was treated in a H₂-flow at 300 °C for approximately 3 hours. The calculated amounts of aluminum, copper and silicon were weighted to an accuracy of 0.05 mg. Sample homogenization was done in an Edmund Buehler MAM-1 arc furnace with a water-cooled copper plate and zirconium as a getter material. The resulting slug was turned and re-melted two times for homogenization. In order to prevent reactions with the quartz glass surface, the resulting bead was wrapped in Molybdenum foil (99.97%, Plansee SE, Reutte, Austria) before placing it in a quartz glass tube. The ampoules were sealed under vacuum and placed in a muffle furnace for 28 days. After annealing, the samples were quenched in cold water and prepared for further investigation. The occurring mass loss during the whole sample preparation procedure usually was below 1% and therefore not considered to affect the sample composition significantly. Representative sections of the annealed samples were investigated by means of optical microscopy using a Zeiss Axiotech 100 microscope. For phase determination, X-Ray powder diffraction analysis was performed using a Bruker D8 ADVANCE Diffractometer operating in reflection mode (Cu K α_1 radiation, Lynxeye silicon strip detector). For evaluation of the resulting diffractograms the software TOPAS [45] was used.

Selected samples showing three phases in powder X-Ray analysis or two-phase samples required for the definition of specific tie-lines were analyzed by means of Electron Probe Micro Analysis (EPMA). EPMA measurements were carried out using a Cameca SX electron probe 100 (Cameca, Courbevoie, France) operating with wavelength dispersive spectroscopy (WDS) for quantitative analysis. The measurements were carried out at 15 kV using a beam current of 20 nA with pure elements as standard materials. Conventional ZAF matrix correction was used to calculate the final composition from the measured X-ray intensities. In order to rule out inhomogeneity, measurements of the composition of the respective

phases usually were performed at three different spots. The measured sample composition did not depend on the location within the sample.

DTA measurements were performed on a Setaram Setsys Evolution 2400 (Setaram Instrumentation, Caluire, France) and a Netzsch DTA 404 PC (Netzsch, Selb, Germany). Both measurement devices are operated using Pt/Pt-10%Rh thermocouples (Type S) which were calibrated using the melting points of pure Sn, Au and Ni. The samples with a weight of approximately 20 mg were placed in open alumina crucibles and measured employing a slow permanent argon flow. Applying a heating rate of 5 K·min⁻¹, two heating- and cooling-curves were routinely recorded for each sample to check reproducibility of thermal effects. The possible mass loss during the DTA investigations was checked routinely and no relevant mass changes were observed.

3. Results and Discussion

3.1 Isothermal section at 500°C

The isothermal section of the phase diagram is shown in Fig. 1. The composition of the limiting phases in the three phase fields colored in dark grey are determined by EPMA measurements. The three phase fields in light grey have been determined by measuring samples in the limiting two phase fields because of lack of a sample in the respective three phase field. An overview about three phase fields and selected tie-lines measured by EPMA is given in Table 2. A selection of images in the back scattered electron mode (BSE) showing the microstructures of annealed samples is shown in Fig. 2.

The Cu-poor region of the isothermal section shows Si in equilibrium with various binary Al-Cu compounds. The binary Al-Cu compounds in this region show very limited solubility of Si. (Al,Cu)- θ shows the highest solubility of Si with about 1 at.%. The phases (Al,Cu)- η_2 , (Al,Cu)- ζ_1 and (Al,Cu)- δ do not show any solubility of Si at all. Two of the three phase fields in this region, $\{\eta_2 + (\text{Si}) + \zeta_1\}$ and $\{\delta + \gamma_1 + (\text{Si})\}$ could not be determined by EPMA due to the lack of samples in the respective three phase field. However, their existence is well documented by measurements in adjacent two phase fields (comp. Table 2).

The most Cu-rich phase field with Si is $\{\gamma_1 + \text{Cu}_3\text{Si}-\eta' + \text{Si}\}$. Phases with the composition Cu_3Si show three isomorphic structures which transform very easily and therefore it was not possible to quench the respective phases stable at high temperature. Identification of the respective powder-XRD pattern was done by comparison with a sample in the two-phase region $\text{Cu}_3\text{Si}-(\text{Si})$. Following the binary phase diagram [25], the three phase field contains the phase $\text{Cu}_3\text{Si}-\eta'$, rather than the low temperature phase $\text{Cu}_3\text{Si}-\eta''$ or the high temperature phase $\text{Cu}_3\text{Si}-\eta$.

The Cu-rich part of the isothermal section shows a more complicated situation dominated by extended solid solutions. The only three phase field determined directly by EPMA measurements is $\{\varepsilon + \gamma_1 + \kappa\}$. The limiting compounds of the

remaining three phase fields as well as their solubility ranges have been determined by analysis of several samples in the respective two phase regions. The remaining three phase fields are: $\{(Cu) + \gamma_1 + \kappa\}$, $\{(Cu) + \gamma + \kappa\}$, $\{\varepsilon + \gamma + \kappa\}$ and $\{\varepsilon + \gamma_1 + \eta''\text{-Cu}_3\text{Si}\}$. A very narrow three phase field $\{\eta' + \eta'' + \gamma_1\}$ should also be present but was not included in the isothermal section due to reasons of clarity.

The binary compounds in the Cu-rich part of the phase diagram show a considerable ternary solubility of Si and Al, respectively. The phase γ_1 is stable up to the composition $\text{Al}_{18}\text{Cu}_{72.2}\text{Si}_{9.8}$. $\eta''\text{-Cu}_3\text{Si}$, ε and γ show a solubility of 2.4, 2 and 2 at.% Al, respectively.

In the binary, the compound (Cu,Si)- κ is only stable between 570 and 839 °C [25]. By addition of (Al) it is stable at 500 °C between $\text{Al}_8\text{Cu}_{74}\text{Si}_8$, $\text{Al}_{14}\text{Cu}_{68}\text{Si}_8$ and $\text{Al}_{17}\text{Cu}_{78.5}\text{Si}_{4.5}$. Pure Cu shows a high solubility of Al and Si as indicated by the binary phase diagrams [4, 25].

The determined three phase fields in general in good agreement with Riani et al. [35], although the composition of the limiting phases is slightly different. Contrary to Riani, the phase (Cu,Si)- ε is shown as stable binary compound in agreement with recent literature [25].

The phase (Al,Cu)- γ_1 is was found to be stable up to the composition $\text{Al}_{18}\text{Cu}_{72.2}\text{Si}_{9.8}$ compared to $\text{Al}_{14.5}\text{Cu}_{74}\text{Si}_{11.5}$ found by [35]. The phase with the composition Cu_3Si shows a solubility of 2.4 at.% Al in the current work compared to 4.8 at.% in [35]. The solubility ranges of (Cu,Si)- ε are in the same range in both cases (2 at.% Al compared to 1.5 at.% Al in [35]). The phase (Cu,Si)- γ shows a broader solubility range in the binary (from 17 to 20 at.% Cu) in the work of Riani which is not in agreement with recent literature (16 to 18 at.% Cu in [25]). The phase dissolves up to 2 at.% Al in both, the current work as well as in the isothermal section published by Riani et al. [35].

Riani et. al. propose a two phase field of about 1.5 at.% width [35] between (Cu) and (Cu,Si)- κ in the ternary phase diagram. In the current work, samples with the nominal composition $\text{Al}_{11}\text{Cu}_{82}\text{Si}_7$, $\text{Al}_{13}\text{Cu}_{81}\text{Si}_6$ and $\text{Al}_{15}\text{Cu}_{80}\text{Si}_5$ were placed in this region. X-Ray powder diffraction of the respective samples shows

pure (Cu,Si)- κ for the sample with the nominal composition $\text{Al}_{11}\text{Cu}_{82}\text{Si}_7$, and a mixture of (Cu,Si)- κ and (Cu) for the other two samples. Due to the very low amount of Cu in the samples, implied by the low intensity of the Cu-related peaks in the diffractograms, it was not possible to analyze these samples properly by means of EPMA. Therefore, the Si-poor boundary of the phase (Cu,Si)- κ was estimated using the sample $\text{Al}_{11}\text{Cu}_{82}\text{Si}_7$ in the single phase field (Cu,Si)- κ and the sample $\text{Al}_{13}\text{Cu}_{81}\text{Si}_6$ and $\text{Al}_{15}\text{Cu}_{80}\text{Si}_5$ in the two phase field {(Cu,Si)- κ + (Cu)} with a very low Cu-content. The solubility of (Al) and (Si) in Cu were estimated based on the solubility of (Al) and (Si) in Cu in the binary sub-systems and tie-lines in the two phase field {(Cu,Si)- γ + (Cu)}. The phase (Cu,Si)- κ is stable up to the composition $\text{Al}_{15}\text{Cu}_{85.5}\text{Si}_{9.5}$ in the work of Riani et al. [35] compared to $\text{Al}_8\text{Cu}_{84}\text{Si}_8$ in the current work.

3.2 Isothermal section at 700 °C

According to the binary phase diagram [25], at 700 °C Cu_3Si shows the high temperature structure η . Fine black lines in Fig. 3 indicate tie-lines as measured by EPMA analysis of different samples. These measurements allow determining the remaining three phase fields as well as the approximate composition of the limiting phases. A selection of measured tie-lines at 700 °C is given in Table 2.

The solubility of Al and Cu in the binary phases is noticeable higher than at 500 °C. The phase γ_1 is stable up to the composition $\text{Al}_{13}\text{Cu}_{76}\text{Si}_{11}$. The binary phase (Al,Cu)- β was not found in any of the ternary samples. In contrast, the binary phase (Cu,Si)- κ shows a continuous solubility extending almost to the binary Al-Cu system. The phases η , ϵ and γ show a solubility of 2, 3 and 5 at.% Al, respectively.

EPMA analyses of samples in the region between (Al,Cu)- γ_1 and (Cu,Si)- γ indicate a second phase with a composition between $\text{Al}_4\text{Cu}_{81}\text{Si}_{15}$ and $\text{Al}_{10}\text{Cu}_{78.5}\text{Si}_{11.5}$. Powder XRD analysis of this phase show a very well crystallized structure not known in the limiting binary phase diagrams. A sample with the nominal composition $\text{Al}_{12}\text{Cu}_{77}\text{Si}_{11}$ shows (Cu,Si)- κ and the unknown phase, referred to as τ from now on, in equilibrium at 700 °C. The powder XRD pattern

of the sample is shown in Fig. 4. A piece of this sample was re-annealed at 500 °C for three weeks. Powder XRD analysis of this piece shows ϵ , γ_1 and κ in equilibrium. The pattern of τ completely disappeared. This indicates a eutectoid decomposition of $\tau = \epsilon + \gamma_1 + \kappa$ between 700 and 500 °C. A sample with the nominal composition of $\text{Al}_{10}\text{Cu}_{77}\text{Si}_{13}$, located in the three phase field $\{\epsilon + \gamma_1 + \kappa\}$ was annealed at 500 °C and subsequently investigated by DTA. It did not show any thermal effect in the region between 500 and 700 °C. The lack of a thermal effect can be interpreted either by the fact that the heat exchange during the eutectoid decomposition $\tau = \epsilon + \gamma + \kappa$ is too small to be detected by DTA analysis, or that it is too slow to occur at a heating rate of 5 K·min⁻¹ at all. Nevertheless, the annealing results indicate that a ternary compound τ is formed in the ternary system between 500 and 700 °C. This contradicts previous authors [38] who do not indicate a ternary compound in the system Al-Cu-Si. Determination of the crystal structure of τ will be attempted by the authors in the near future.

Considering the measured tie-lines and the XRD analysis of the respective samples listed in Table 2, the remaining three phase fields present at 700 °C are: $\{\gamma + \kappa + \tau\}$, $\{\epsilon + \gamma + \tau\}$, $\{\gamma_1 + \kappa + \tau\}$, $\{\epsilon + \gamma_1 + \tau\}$, $\{\epsilon + \gamma_1 + \eta\}$ and $\{(\text{Cu}) + \gamma_1 + \kappa\}$ as indicated in Fig. 3.

Powder XRD analysis of samples with their nominal composition in the vicinity of $\text{Al}_{20}\text{Cu}_{78}\text{Si}_2$ show several very broad peaks which can not be derived from any neighboring structure. The most intense peaks are at 26.2, 27.2, 44.9 and 46.2 °2 θ . A sample with the nominal composition $\text{Al}_{20}\text{Cu}_{78}\text{Si}_2$ annealed at 700 °C shows (Cu) and the additional peaks. After re-annealing of the sample at 500 °C, (Cu) and κ are present, but the additional peaks mentioned before are still present with considerable intensity (see Fig 5). As cast samples in this region reach equilibrium without this phase at 500 °C after 3 weeks of annealing. A sample with the nominal composition $\text{Al}_{25}\text{Cu}_{72.5}\text{Si}_{2.5}$ shows the three phase field $\{(\text{Cu}) + \gamma_1 + \kappa\}$ after annealing at 500 °C. This may indicate a ternary compound which is stable at 700 °C but the annealing time at 500 °C (3 weeks) was not enough to re-establish the equilibrium at 500 °C. EPMA analysis of samples showing the additional peaks do not indicate an additional phase indicating very small

precipitates. Contrary to the peaks assigned to τ in Fig. 3, the possible ternary phase in this region does not crystallize very well, making it very difficult to determine its structure. It should be pointed out, that this particular part of the phase diagram is in conflict with earlier interpretations. On the one hand, the assessed phase diagram by Lukas and Lebrun [37] assumes a complete solid solubility between the W-type β -phases of Cu-Si and Al-Cu, on the other hand our results at 700 °C do not show any significant solubility of Si in (Al,Cu)- β , a very extended (Cu,Si)- κ phase field, and a possible ternary phase very close to binary (Al,Cu)- β . This area definitely needs additional investigations at high temperatures to clarify phase equilibria and crystal structures.

3.2 Isopleths and ternary reaction scheme

Since the transitions ε_1 - ε_2 and γ_0 - γ_1 in the binary system Al-Cu were determined to be of higher order [3, 4], the distinction between the high temperature phases ε_1 and γ_0 and the low temperature phase ε_2 and γ_1 in the reaction scheme is not appropriate. Therefore the respective phases will be designated as $\varepsilon_{1,2}$ and $\gamma_{0,1}$ in the following section.

The isopleth at 40 at.% Si is shown in Fig. 6. Continuous horizontal lines indicate reactions determined by invariant effects in DTA measurements. Dashed horizontal lines indicate solid state reactions which have to be present due to adjacent invariant reactions and participating three phase fields, but were not determined experimentally. An overview of the determined and estimated invariant reactions including the reaction temperatures as well as the estimated composition of the participating phases is given in Table 3. Some solid state reactions at approximately 25 at.% Al were not determined by thermal analysis of samples in this isopleth but by samples in the isopleth at 10 at.% Si (see below). The invariant reactions determined in the Al-rich part of the isopleth are well determined and in good agreement with the limiting binary system Al-Cu [4]. In the Cu-rich part of the isopleth, some inconsistencies remain. Samples between 4 and 8.5 at.% Al show extremely weak non-invariant effects around 512 °C which could not be assigned to any reaction. The sample with the nominal composition

$\text{Cu}_{60}\text{Si}_{40}$ shows two peaks with low and equal intensity at the onset temperatures 546 and 555 °C. Despite the fact that there are two distinct peaks, they can only be assigned to the reaction $\eta = \eta' + (\text{Si})$ in the binary Cu-Si system.

The isopleth shown in Fig. 6 matches the isothermal sections experimentally determined in this work at 500 and 700 °C as well as the isothermal section at 400 °C published by Lukas and Lebrun [37]. The high solubility of Al in the low temperature phase $\text{Cu}_3\text{Si}-\eta''$ compared to the solubility of Al in the high temperature phases $\text{Cu}_3\text{Si}-\eta'$ and $\text{Cu}_3\text{Si}-\eta$ is originated in the isothermal section at 400 °C. In accordance with the liquidus projection surface published by Lukas and Lebrun [37], (Si) primarily crystallizes over the whole composition range.

The isopleth at 10 at.% Si is shown in Fig 7. The Al-rich part down to approx. 20 at.% Al shows the same reactions like in the 40 at.% Si isopleth. Due to the low Si-content in the isopleth, the primary crystallization fields are different, however (see Fig 7).

The Cu-rich part of the isopleth shows a more complicated situation. The high solubility ranges of the binary compounds in this region as well as the thermal stabilization of (Cu,Si)- κ and the existence of the ternary phase τ provide a complex sequence of two- and three phase fields stable at 500 and 700 °C. The boundaries of the phase fields corresponding to the isothermal sections are drawn by continuous lines in Fig. 7 in the respective temperature range. Comparison of the three phase fields present at 400, 500 and 700 °C shows that several solid state reactions occur in this region, but only two of them were determined experimentally: U11 at 579 °C and E2 at 663 °C (see Table 3). It was not possible to determine the reaction temperatures of the invariant reactions U15: $\varepsilon + \gamma_{0,1} = \eta'' + \kappa$, P2: $\varepsilon + \eta' + \gamma_{0,1} = \eta$ and U3: $\delta + \text{Si} = \gamma_{0,1} + \eta$.

Above 700 °C, the Cu-rich part of the isopleth shows a high number of thermal effects but it was not possible to construct the isopleth and reaction scheme in this region. Additional reliable information on phase equilibria at higher temperature in this region is needed solve this part of the isopleth.

A partial ternary reaction scheme (Scheil diagram) is shown in Fig. 8. The fundament of this diagram is the reaction scheme given by Lukas and Lebrun

[37]. New data on the limiting binary systems [4, 25] as well as experimental results obtained in the current work were integrated in the reaction scheme. Several invariant reactions indicated by dotted lines were not determined experimentally in this work, but are required due to the existence of neighboring invariant reactions and three phase fields. Missing parts of the reaction scheme are indicated by question marks.

4. Conclusions

The largest part of the Al-Cu-Si system, in particular the isothermal phase equilibria at 400 and 500°C and the reaction sequence in the Cu-poor part of the system, is now well characterized. However, in spite of the numerous experimental studies performed by different authors, phase equilibria in the complex Cu-rich part of the system at higher temperatures are still questionable and require additional attention. The current study revealed the existence of a previously unknown ternary high-temperature compound, whose structure has not been solved up to now. Its equilibria with the liquid phase have to be investigated and the phase relations of the extended solid solutions of κ and β at high temperatures should be subject of additional investigations. Our results at 700°C raise some doubts regarding the complete solid solubility of the β -phase of Al-Cu and Cu-Si proposed previously, so an independent study of the liquidus projection including extended primary crystallization studies would be favorable. Last but not least, most of the proposed solid state reactions in this area are not accessible by DTA investigations and further annealing studies would be helpful to confirm these and to better fix the respective reaction temperatures.

Supplementary material

A table with experimental DTA data is available as supplementary material.

5. Acknowledgement

The authors thank the Austrian Science Found FWF for supporting this work under the

project number P19305. Additionally the authors want to thank Theodoros Ntaflos and Franz Kiraly from the Department of Lithospheric Sciences at the University of Vienna for their support in EPMA measurements.

Tables

Table 1: invariant reactions in the binary subsystems used in the current work

Phase Reaction	Composition of the involved phases / at. %	Temperature (°C)	Ref.
Al-Cu			
$L = \beta$	---	1052(5)	[4]
$L = (Cu) + \beta$	83.0(5) Cu	1035(5)	[4]
$\beta + L = \gamma_0$	69.0(5) Cu	993(2)	[4]
$\gamma_0 + L = \varepsilon_1$	65.5(5) Cu	960(2)	[4]
$\gamma_1 + \varepsilon_1 = \varepsilon_2$	64.0(5) Cu	847(1)	[4]
$\varepsilon_1 = \varepsilon_2 + L$	59.5(5) Cu	847(1)	[4]
$\gamma_0 = \gamma_1$	---	~800	[4]
	69.0 Cu		
	65.0 Cu	874(2)	[4]
$\gamma_1 + \varepsilon_2 = \delta$	63.0(5) Cu	684(1)	[4]
$\varepsilon_2 + L = \eta_1$	54.5(5) Cu	625(2)	[4]
$\varepsilon_2 + \eta_1 = \zeta_2$	56.5(5) Cu	597(1)	[4]
$\eta_1 + L = \theta$	51.5(5) Cu	591(2)	[4]
$\zeta_2 + \eta_1 = \eta_2$	54.5(5) Cu	580(1)	[4]
$\varepsilon_2 = \delta + \zeta_2$	57.5(5) Cu	578(2)	[4]
$\eta_1 = \eta_2 + \theta$	52.0(5) Cu	574(3)	[4]
$\beta = (Cu) + \gamma_1$	76.0(5) Cu	567(2)	[4]
$\delta + \zeta_2 = \zeta_1$	60.0(5) Cu	561(2)	[4]
$L = \theta + (Al)$	17(1) Cu	550(2)	[4]
	32.0(5) Cu		

$\gamma_1 + (\text{Cu}) = \alpha_2$	69 Cu	80.3 Cu	77.25 Cu	363	[2]
Al-Si					
L = Al + Si	12.2(1) Si	1.5(1) Si	100 Si	577(1)	[22]
Cu-Si					
L + (Cu) = β	84.0(5) Cu	89(1) Cu	85.8(5) Cu	849(2)	[25]
(Cu) + $\beta = \kappa$	89(1) Cu	85.5(5) Cu	87.5(5) Cu	839(2)	[25]
L + $\beta = \delta$	80.8(5) Cu	83.5(5) Cu	82.5(5) Cu	821(2)	[25]
L = $\eta + \delta$	80.2(4) Cu	76.8(5) Cu	82.3(5) Cu	818(3)	[25]
L = (Si) + η	70(1) Cu	0 Cu	74.0(5) Cu	807(2)	[25]
$\eta + \delta = \varepsilon$	76.5(5) Cu	81.5(5) Cu	78.95 Cu	800(2)	[25]
$\beta = \delta + \kappa$	83.8(5) Cu	83.0(5) Cu	85.8(5) Cu	781(2)	[25]
$\delta = \varepsilon + \gamma$	82.1(5) Cu	78.95(1) Cu	82.2(5) Cu	735(2)	[25]
$\delta = \gamma + \kappa$	83.1(5) Cu	82.5(5) Cu	86.8(5) Cu	734(2)	[25]
$\eta + \varepsilon = \eta'$	75.8(5) Cu	78.95 Cu	75.8(5) Cu	618(3)	[25]
$\eta' + \varepsilon = \eta''$	75.6(5) Cu	78.95 Cu	75.6(5) Cu	570	[25]
$\eta + (\text{Si}) + \eta'$	74(1) Cu	0 Cu	74(1) Cu	555(3)	[25]
$\kappa = \gamma + (\text{Cu})$	89 Cu	83 Cu	90 Cu	552	[25]
(Si) + $\eta' = \eta''$	0 Cu	74(1) Cu	74(1) Cu	467	[25]

Table 2: Overview about selected three- and two-phase fields at 500 and 700 °C determined in the present study

phase field	temperature	nominal composition of the respective sample	Phase composition			
			Phase	Al	Cu	Si
{(Al) + θ + (Si)}	500	Al ₅₀ Cu ₁₀ Si ₄₀	(Al)	96.0(10)	3.0(10)	1.0(10)
			θ	68.0(10)	31.0(10)	1.0(10)
			(Si)	0 ^a	0 ^a	100 ^a
{ η_2 + (Si) + θ }	500	Al ₃₅ Cu ₂₅ Si ₄₀	η_2	49.7(2)	50.2(1)	0.1(1)
			(Si)	0 ^a	0 ^a	100 ^a
			θ	66.6(3)	32.4(3)	1.0(1)
{ η_2 + (Si)}	500	Al ₄₂ Cu ₄₈ Si ₁₀	η_2	46.8(2)	53.2(2)	0.1(1)
			(Si)	0 ^a	0 ^a	100 ^a
{ δ + (Si) + ζ_1 }	500	Al ₃₇ Cu ₅₃ Si ₁₀	δ	41.0(10)	59.0(10)	0.0(10)
			(Si)	0 ^a	0 ^a	100 ^a
			ζ_1	42.0(10)	58.0(10)	0.0(10)
{(Si) + ζ_1 }	500	Al ₂₅ Cu ₃₅ Si ₄₀	(Si)	0 ^a	0 ^a	100 ^a
			ζ_1	42.6(2)	57.3(2)	0.1(1)

$\{\delta + (\text{Si})\}$	500	$\text{Al}_{10}\text{Cu}_{55}\text{Si}_{10}$	δ	39.7(2)	0.1(1)	60.2(1)
			(Si)	0 ^a	0 ^a	100 ^a
$\{\gamma_1 + (\text{Si})\}$	500	$\text{Al}_{20}\text{Cu}_{40}\text{Si}_{40}$	γ_1	33.4(2)	0.6(2)	65.4(2)
			(Si)	0 ^a	0 ^a	100 ^a
$\{\eta' + \gamma_1 + (\text{Si})\}$	500	$\text{Al}_{10}\text{Cu}_{50}\text{Si}_{40}$	η'	3.0(10)	76.0(10)	21.0(10)
			γ_1	25.0(10)	69.0(10)	6.0(10)
			(Si)	0 ^a	0 ^a	100 ^a
$\{\varepsilon + \kappa\}$	500	$\text{Al}_{10}\text{Cu}_{80}\text{Si}_{10}$	ε	1.3(1)	78.5(1)	20.2(1)
			κ	11.4(2)	80.2(2)	8.3(1)
$\{\varepsilon + \gamma_1 + \kappa\}$	500	$\text{Al}_6\text{Cu}_{78}\text{Si}_{16}$	ε	2.0(10)	78.0(10)	20.0(10)
			γ_1	16.4(1)	73.6(1)	10.0(1)
			κ	14.1(1)	77.8(1)	8.1(1)
$\{\gamma_1 + \kappa\}$	500	$\text{Al}_{25}\text{Cu}_{72.5}\text{Si}_{2.5}$	γ_1	28.6(2)	69.1(1)	2.3(1)
			κ	17.2(1)	78.6(2)	4.2(1)
		$\text{Al}_{17}\text{Cu}_{75}\text{Si}_8$	γ_1	18.7(2)	72.8(2)	8.5(1)
			κ	14.6(1)	77.7(1)	7.7(1)

{(Cu) + γ }	500	$\text{Al}_2\text{Cu}_{86}\text{Si}_{12}$	(Cu)	3.3(2)	87.6(3)	9.1(3)
			γ	0.6(1)	82.9(1)	16.5(2)
{ γ + κ }	500	$\text{Al}_3\text{Cu}_{82}\text{Si}_{15}$	γ	2.3(1)	81.1(1)	16.6(1)
			κ	8.5(1)	82.5(1)	9.0(1)
{ ϵ_2 + γ_1 + (Si)}	700	$\text{Al}_{38}\text{Cu}_{60}\text{Si}_2$	ϵ_2	39.6(3)	60.2(3)	0.2(1)
			γ_1	38.3(3)	61.5(2)	0.2(1)
			(Si)	0 ^a	0 ^a	100 ^a
{ γ_1 + (Si)}	700	$\text{Al}_{30}\text{Cu}_{60}\text{Si}_{10}$	γ_1	33.2(3)	65.9(2)	0.9(2)
			(Si)	0 ^a	0 ^a	100 ^a
		$\text{Al}_{25}\text{Cu}_{60}\text{Si}_{15}$	γ_1	28.1(3)	68.2(2)	3.7(1)
			(Si)	0 ^a	0 ^a	100 ^a
{ η + γ_1 + (Si)}	700	$\text{Al}_{10}\text{Cu}_{60}\text{Si}_{30}$	η	1.8(1)	76.4(1)	21.8(2)
			γ_1	19.5(2)	71.2(1)	9.2(2)
			(Si)	0 ^a	0 ^a	100 ^a
{ η + γ_1 }	700	$\text{Al}_{10}\text{Cu}_{75}\text{Si}_{15}$	η	2.5(1)	76.7(1)	20.8(1)
			γ_1	16.0(10)	74.0(10)	10.0(10)

{ $\varepsilon + \tau$ }	700	$\text{Al}_5\text{Cu}_{77}\text{Si}_{18}$	ε	2.9(1)	76.9(1)	20.2(1)
			τ	9.1(3)	77.2(1)	13.7(2)
{ $\gamma + \kappa$ }	700	$\text{Al}_4\text{Cu}_{78}\text{Si}_{18}$	ε	2.3(1)	77.2(1)	20.5(2)
			τ	6.0(2)	78.8(1)	15.2(2)
		$\text{Al}_3\text{Cu}_{82}\text{Si}_{15}$	γ	2.6(1)	80.9(3)	16.5(3)
			κ	3.6(1)	83.7(2)	12.7(1)
{ $\kappa + \tau$ }	700	$\text{Al}_5\text{Cu}_{80}\text{Si}_{15}$	γ	4.9(1)	79.7(2)	15.4(1)
			κ	6.1(1)	82.2(1)	11.7(1)
		$\text{Al}_7\text{Cu}_{80}\text{Si}_{13}$	κ	7.7(1)	81.2(2)	11.1(1)
			τ	6.6(1)	79.0(1)	14.4(1)
{ $\gamma_1 + \kappa$ }	700	$\text{Al}_{12}\text{Cu}_{77}\text{Si}_{11}$	κ	13.0(1)	79.1(1)	7.9(2)
			τ	11.8(2)	76.5(1)	11.7(1)
		$\text{Al}_{20}\text{Cu}_{75}\text{Si}_5$	γ_1	22.1(2)	71.8(2)	6.1(1)
			κ	19.2(2)	76.6(3)	4.2(1)
{ $\gamma_1 + \kappa$ }	700	$\text{Al}_{26}\text{Cu}_{72}\text{Si}_2$	γ_1	23.3(1)	75.1(1)	1.6(1)
			κ	28.0(1)	69.9(2)	2.1(1)

{(Cu) + κ }	700	Al ₁₈ Cu ₈₀ Si ₂	(Cu)	16.5(1)	81.8(2)	1.7(1)
			κ	20.1(1)	77.7(1)	2.2(2)
		Al ₅ Cu ₈₆ Si ₉	(Cu)	5.4(2)	86.3(3)	8.3(2)
			κ	4.8(2)	85.4(2)	9.8(2)

^a no considerable solubility of Al or Cu in Si

Table 3

Invariant reactions in the system Al-Cu-Si and the estimated composition of the reactants

Reaction	T / °C	Phase	Composition / at.%		
			Al	Cu	Si
Max: $L = \gamma_{0,1} + \text{Si}$	778	L	27.0	57.0	16.0
		$\gamma_{0,1}$	26.0	72.0.	2.0
		Si	0	0	100
U1: $L + \gamma_{0,1} = \varepsilon_{1,2} + \text{Si}$	747	L	37.0	50.0	13.0
		$\gamma_{0,1}$	36.0	62.5	1.5
		$\varepsilon_{1,2}$	40.0	59.5	0.5
		Si	0	0	100
U2: $L + \gamma_{0,1} = \delta + \text{Si}$	740	L	13.5	66.0	20.5
		$\gamma_{0,1}$	21.0	72.5	6.5
		δ	15.5	73.5	11.0
		Si	0	0	100
E1: $L = \delta + \eta + \text{Si}$	730	L	11.0	68.0	21.0
		δ	15.0	72.0	13.0
		η	2.0	75.0	23.0
		Si	0	0	100
U3: $\delta + \text{Si} = \gamma_{0,1} + \eta$	579<T<730	δ	14.0	75.0	11.0
		Si	0	0	100
		$\gamma_{0,1}$	21.5	71.5	7.0

		η	2.0	76.0	22.0
U4: $\varepsilon_{1,2} + \gamma_{0,1} = \delta + \text{Si}$	679	$\varepsilon_{1,2}$	40.0	59.5	0.5
		$\gamma_{0,1}$	36.0	62.5	1.5
		δ	38.5	61.0	0.5
		Si	0	0	100
U5: $\text{L} + \varepsilon_{1,2} = \eta_1 + \text{Si}$	603	L	60.0	32.0	8.0
		$\varepsilon_{1,2}$	42.5	57.0	0.5
		η_1	48.5	51.0	0.5
		Si	0	0	100
U6: $\varepsilon_{1,2} + \eta_1 = \text{Si} + \zeta_2$	599	$\varepsilon_{1,2}$	42.0	57.5	0.5
		η_1	47.5	52.0	0.5
		Si	0	0	100
		ζ_2	44.5	55.0	0.5
U7: $\varepsilon + \eta = \gamma_{0,1} + \eta'$	583	ε	2.0	78.0	20.0
		η	2.0	75.5	22.5
		$\gamma_{0,1}$	24.5	70.0	5.5
		η'	1.5	76.0	22.5
U8: $\eta_1 + \zeta_2 = \eta_2 + \text{Si}$	579	η_1	47.5	52.0	0.5
		ζ_2	45.0	54.5	0.5
		η_2	46.0	53.5	0.5
		Si	0	0	100
U9: $\text{L} + \eta_1 = \text{Si} + \theta$	573	L	67.0	26.5	6.5
		η_1	48.5	51.0	0.5

		Si	0	0	100
		θ	67.0	32.0	1.0
E2: $\tau = \varepsilon + \gamma_{0,1} + \kappa$	663	τ	10.5	77.0	12.5
		ε	2.5	77.5	20.0
		$\gamma_{0,1}$	18.0	74.0	8.0
		κ	11.0	80.0	9.0
E4: $\eta_1 = \text{Si} + \eta_2 + \theta$	500<T<573	η_1	48.0	51.5	0.5
		Si	0	0	100
		η_2	48.5	50.5	1.0
		θ	66.5	32.5	1.0
U11: $\eta + \gamma_{0,1} = \eta' + \text{Si}$	579	η	2.0	75.0	23.0
		$\gamma_{0,1}$	24.0	70.0	6.0
		η'	2.5	75.0	22.5
		Si	0	0	100
P1: $\varepsilon + \eta' + \gamma_{0,1} = \eta''$	570<T<583	ε	2.0	78.0	20.0
		η'	1.5	76.0	22.5
		$\gamma_{0,1}$	25.0	69.0	6.0
		η''	2.0	75.5	22.5
E3: $\varepsilon_{1,2} = \delta + \text{Si} + \zeta_2$	570	$\varepsilon_{1,2}$	42.0	57.5	0.5
		δ	40.0	59.5	0.5
		Si	0	0	100
		ζ_2	44.0	55.5	0.5
U12: $\delta + \zeta_2 = \text{Si} + \zeta_1$	557	δ	40.0	59.5	0.5

		ζ_2	44.0	55.5	0.5
		Si	0	0	100
		ζ_1	43.0	56.5	0.5
<hr/>					
U13: $\eta' + \gamma_{0,1} = \eta'' +$ Si	550	η'	1.5	76.0	22.5
		$\gamma_{0,1}$	24.5	69.0	6.5
		η''	2.0	76.0	22.0
		Si	0	0	100
<hr/>					
U14: $\text{Si} + \zeta_2 = \eta_2 + \zeta_1$	500<T<558	Si	0	0	100
		ζ_2	44.5	55.0	0.5
		η_2	45.0	54.0	1.0
		ζ_1	43.0	56.5	0.5
<hr/>					
U15: $\varepsilon + \gamma_{0,1} = \eta'' + \kappa$	400<T<500	ε	2.0	78.0	20.0
		$\gamma_{0,1}$	18.0	72.5	9.5
		η''	2.5	76.0	21.5
		κ	14.0	78.0	8.0
<hr/>					
E4: $\text{L} = \text{Al} + \text{Si} + \theta$	522	L	80.5	13.5	6.0
		Al	96.0	2.5	1.5
		Si	0	0	100
		θ	68.0	31.0	1.0

Figures

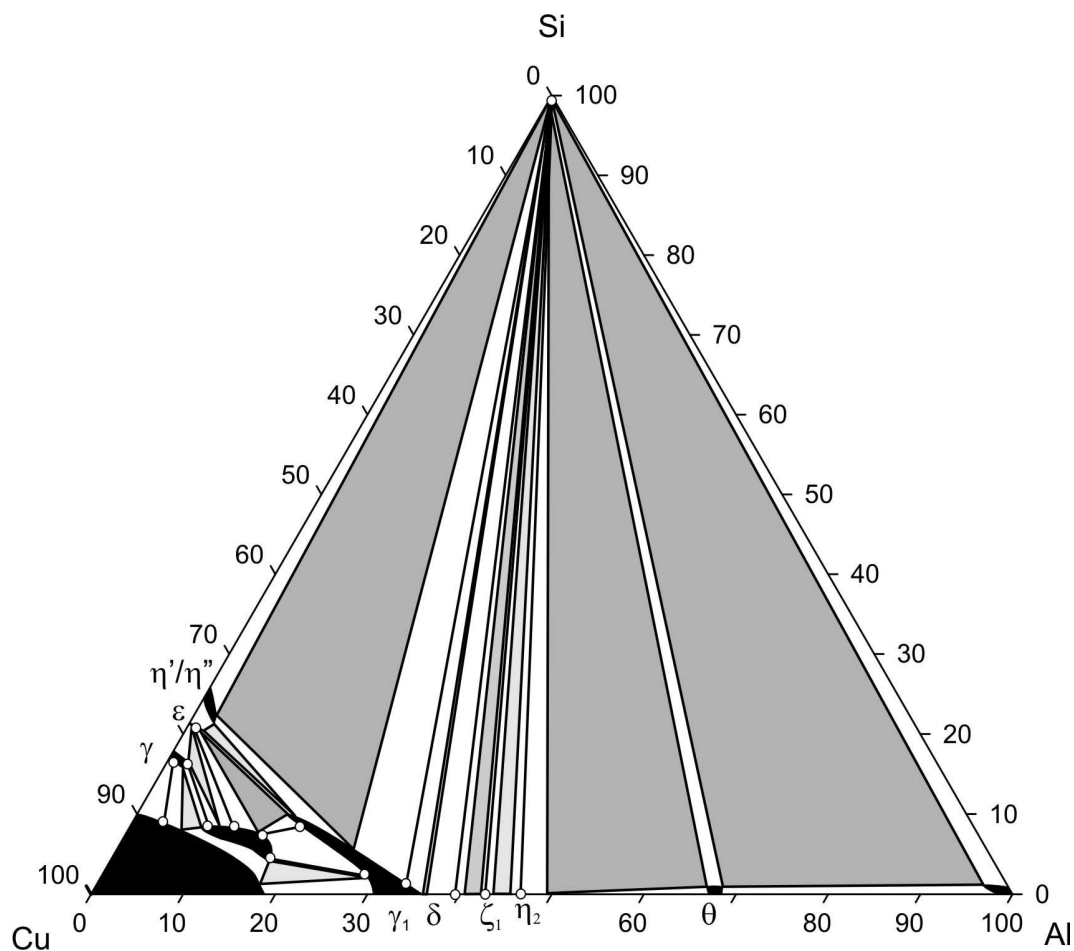


Fig. 1: Isothermal section at 500 °C

Black: single phase fields, dark grey: three phase fields determined by EPMA measurements, light grey fields: three phase fields determined by analysis of the neighboring two phase fields, black lines: tie-lines measured by EPMA

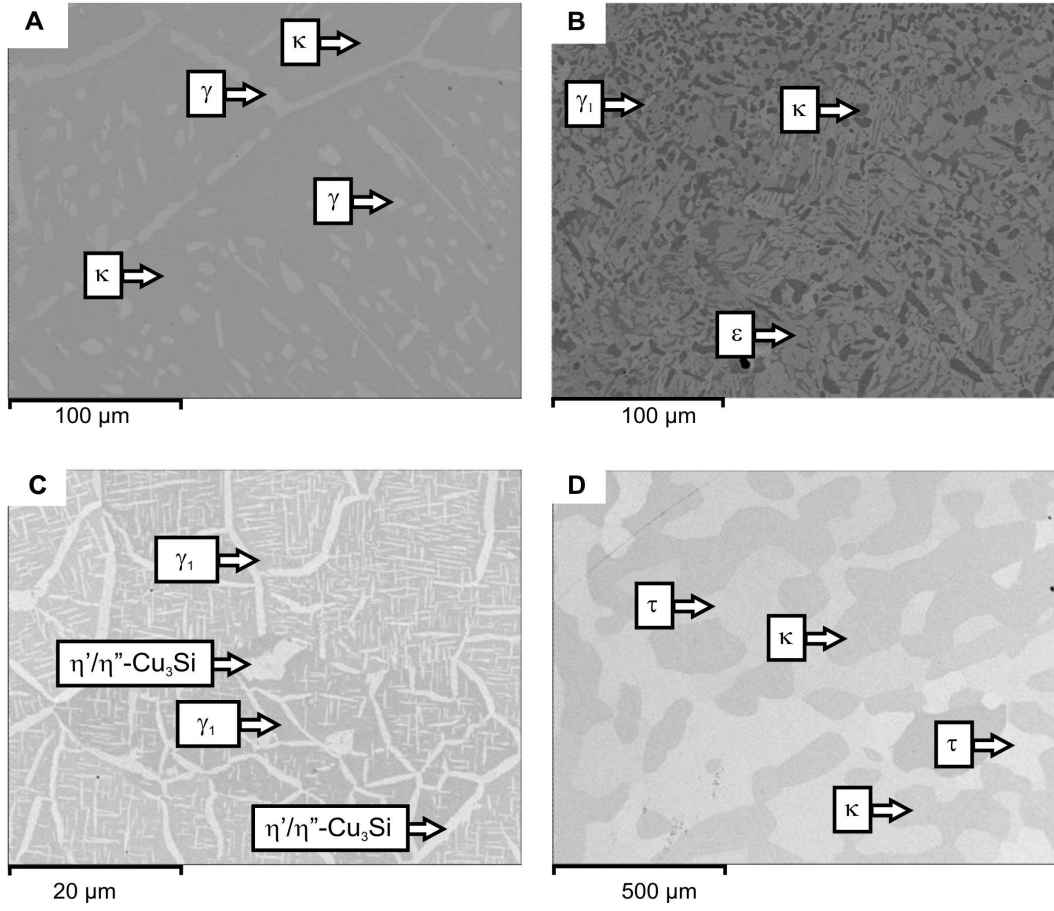


Fig. 2: BSE images of samples with the nominal composition A) $\text{Al}_{10}\text{Cu}_{80}\text{Si}_{10}$ (500 °C), B) $\text{Al}_6\text{Cu}_{78}\text{Si}_{16}$ (500 °C), C) $\text{Al}_{17}\text{Cu}_{73}\text{Si}_{10}$ (500 °C) and D) $\text{Al}_7\text{Cu}_{80}\text{Si}_{13}$ (700 °C)

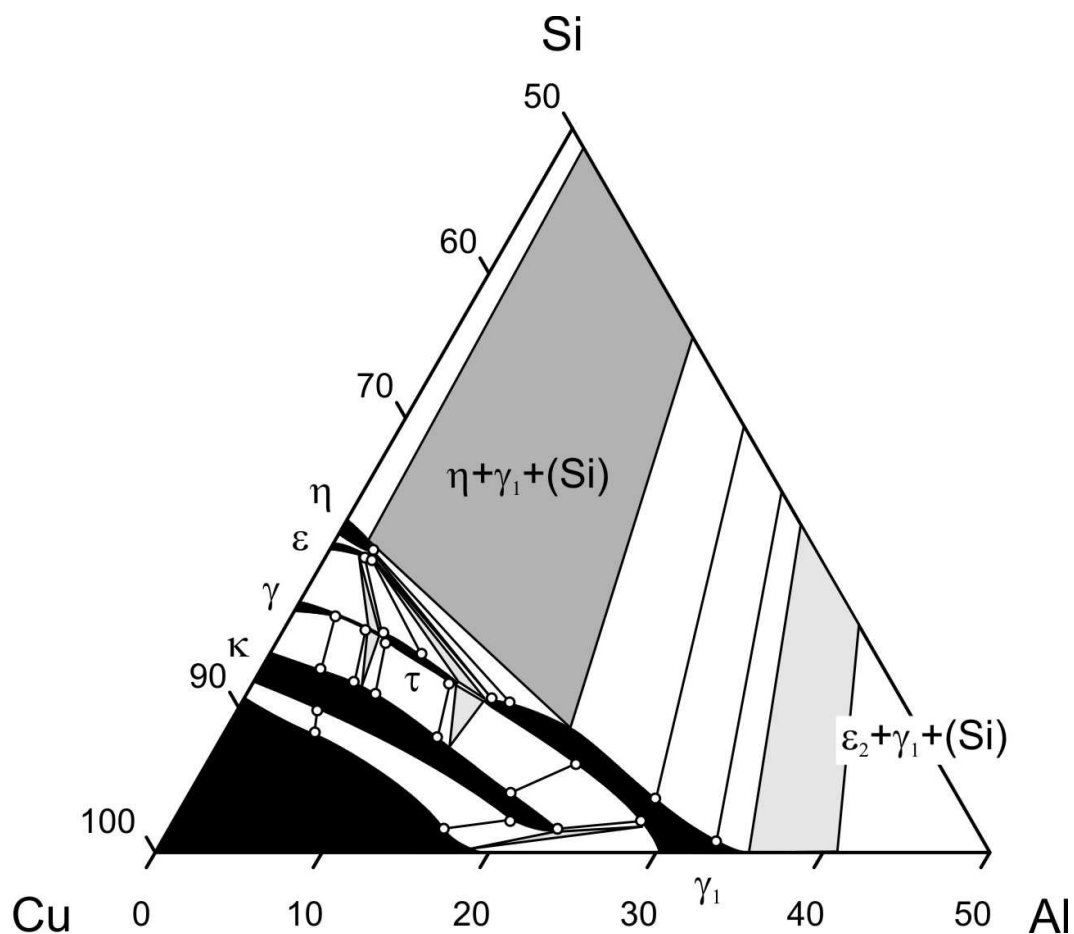


Fig 3: Isothermal section at 700 °C

Black: single phase fields, dark grey: three phase fields determined by EPMA measurements, light grey: three phase fields determined by analysis of the neighboring two phase fields, black lines: tie-lines measured by EPMA

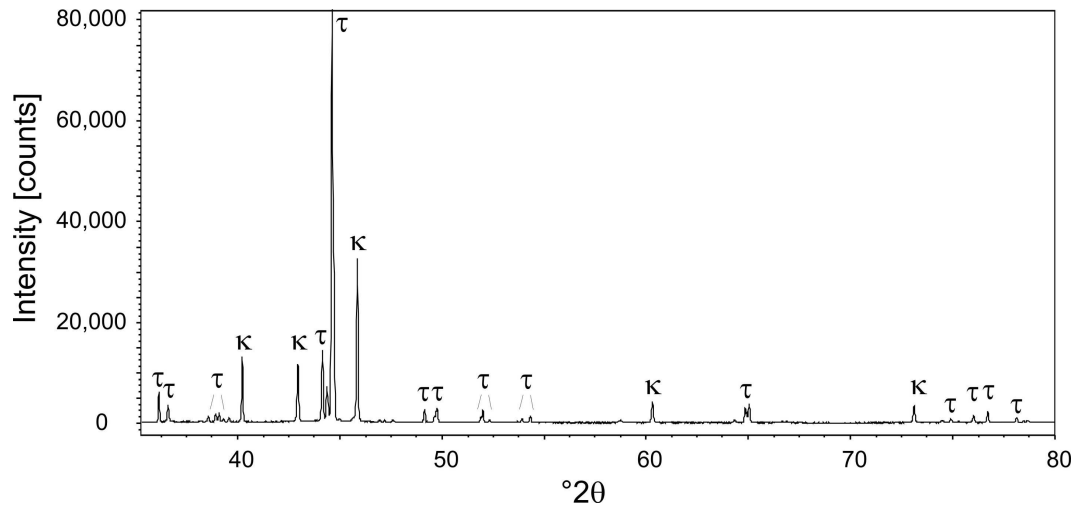


Fig. 4: powder XRD pattern of a sample with the nominal composition of $\text{Al}_{12}\text{Cu}_{77}\text{Si}_{11}$ annealed at 700 °C. Note that the diffractogram was recorded in the 2θ -range between 10 and 120°, but is only shown between 35 and 80 ° 2θ for the sake of clarity of representation.

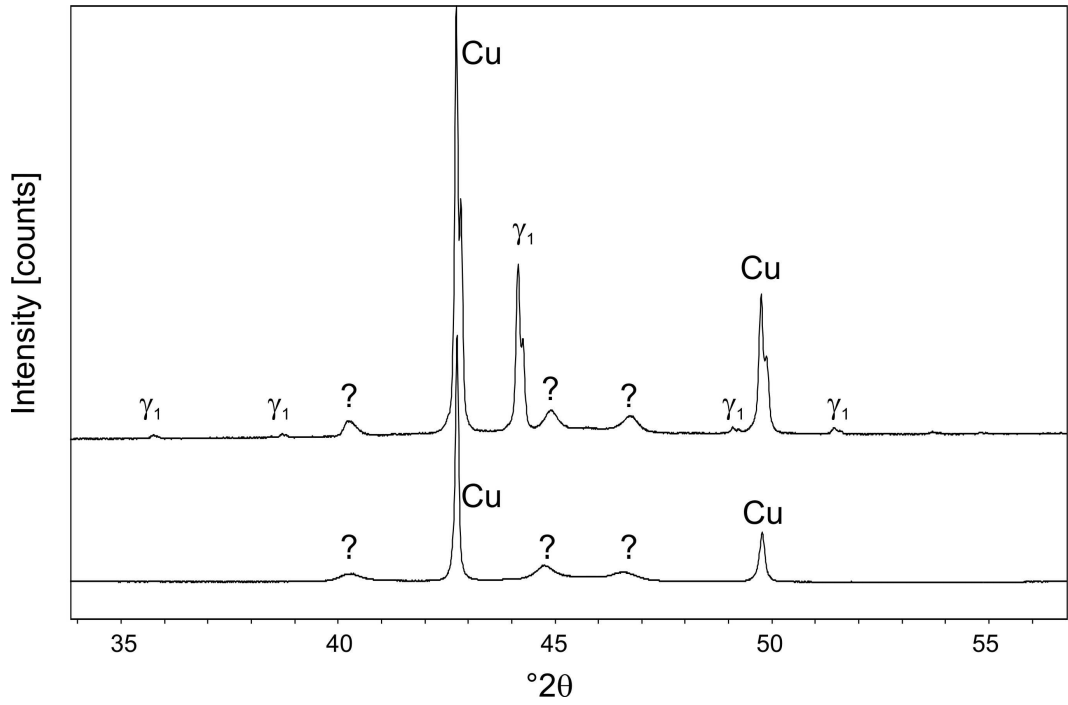


Fig. 5: Comparison of the powder XRD pattern of a sample with the nominal composition $\text{Al}_{20}\text{Cu}_{78}\text{Si}_2$, annealed at 700 °C (bottom) and re-annealed at 500 °C (top). Note that the diffractograms were recorded in the 2θ -range between 10 and 120°, but are only shown between 34 and 56 ° 2θ for the sake of clarity of representation.

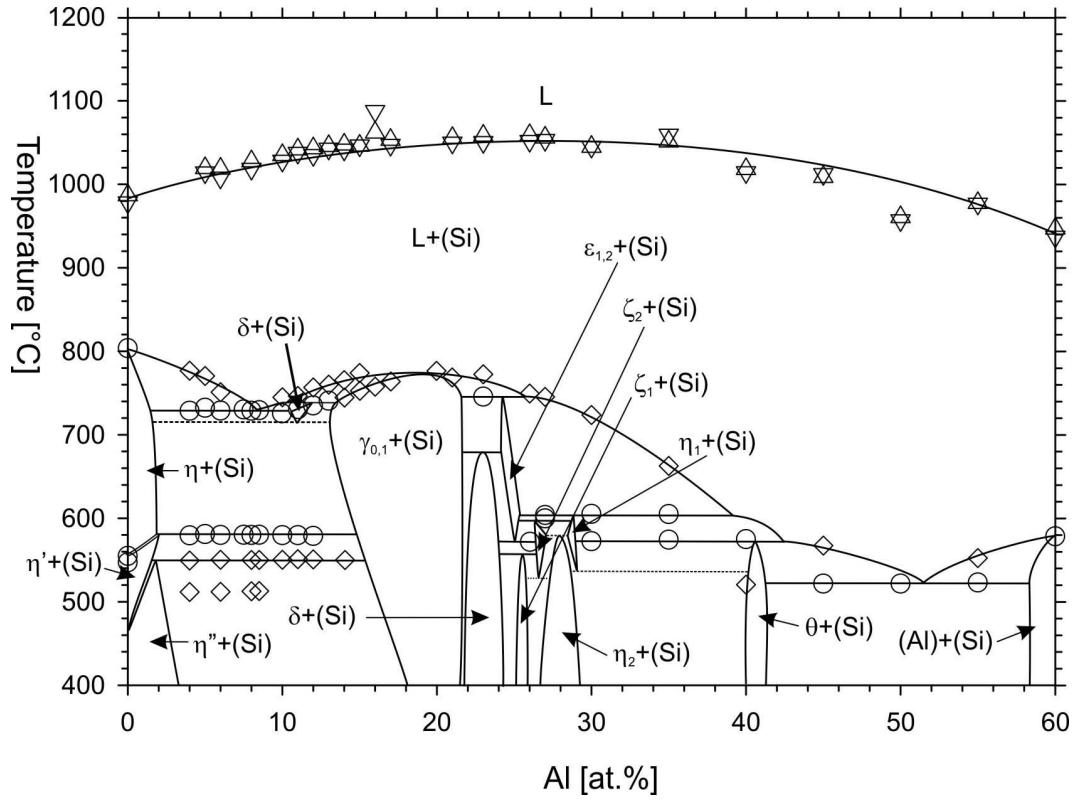


Fig. 6: Isopleth at 40 at.% Cu.

Circles: invariant reactions, diamonds: non-invariant reactions, triangle up: liquidus on heating, triangles down: liquidus on cooling

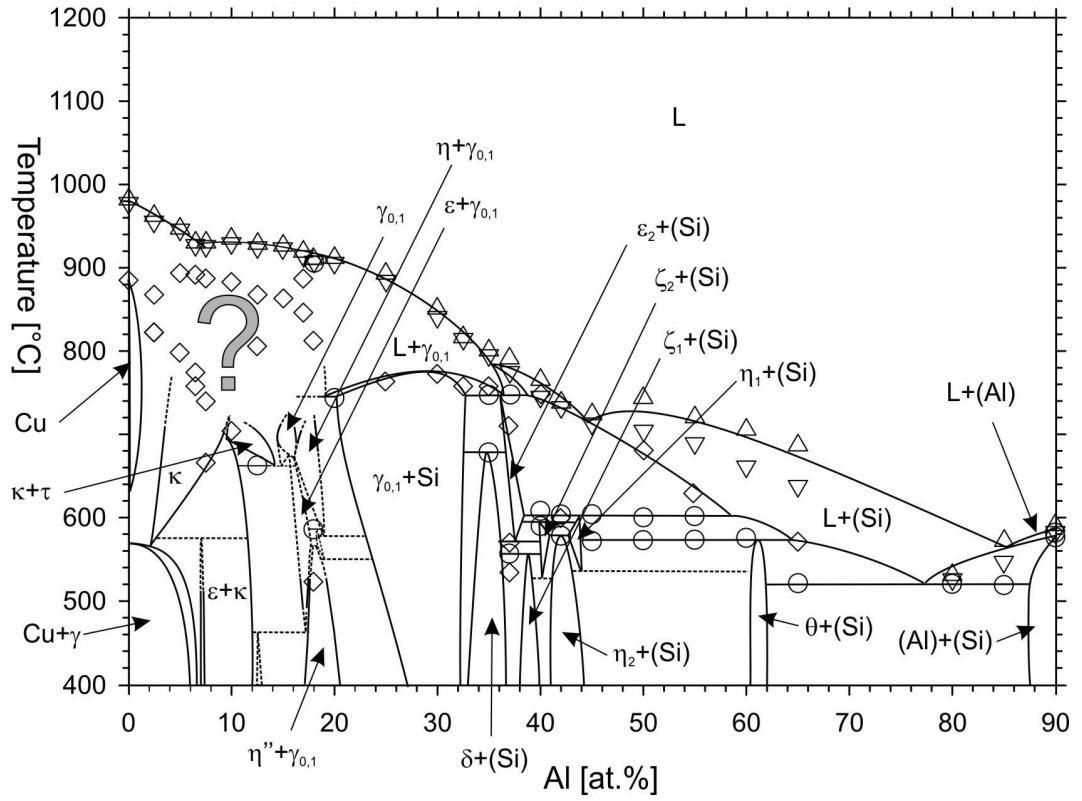


Fig. 7: Isopleth at 10 at.% Cu.

Circles: invariant reactions, diamonds: non-invariant reactions, triangle up: liquidus on heating, triangles down: liquidus on cooling

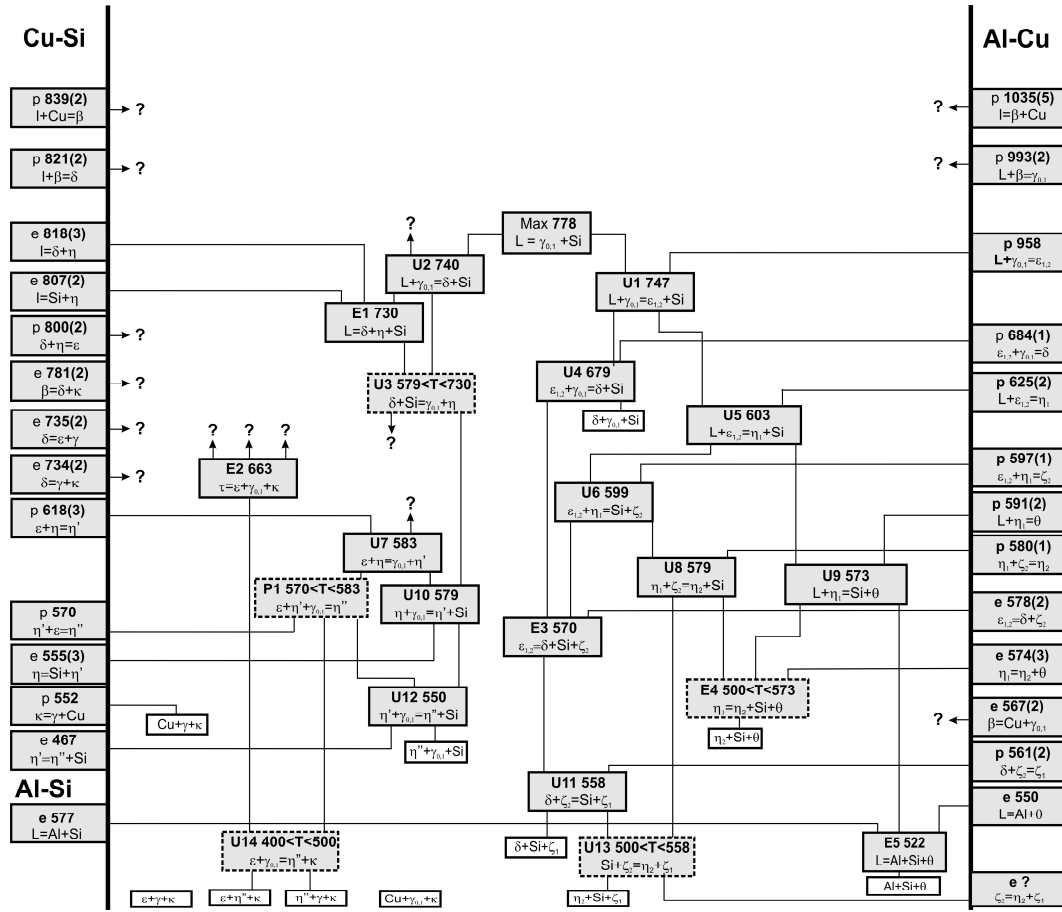


Fig. 8: Partial reaction scheme (Scheil diagram) for the Al-Cu-Si system.

Dashed invariant reaction: temperature not determined experimentally. Open ends with question marks indicate missing parts of the reaction scheme.

References

- [1] X.M. Pan, C. Lin, J.E. Morral, H.D. Brody, An assessment of thermodynamic data for the liquid phase in the Al-rich corner of the Al-Cu-Si system and its application to the solidification of a 319 alloy, *J. Phase Equilib. Diffus.*, 26 (2005) 225-233.
- [2] J.L. Murray, The aluminium-copper system, *Int. Met. Rev.*, 30 (1985) 211-233.
- [3] X.J. Liu, I. Ohnuma, R. Kainuma, K. Ishida, Phase equilibria in the Cu-rich portion of the Cu-Al binary system, *J. Alloys Compd.*, 264 (1998) 201-208.
- [4] N. Ponweiser, C.L. Lengauer, K.W. Richter, Re-investigation of phase equilibria in the system Al-Cu and structural analysis of the high-temperature phase ϵ -Al(1- δ)Cu, *Intermetallics*, 19 (2011) 1737-1746.
- [5] P. Riani, L. Arrighi, R. Marazza, D. Mazzone, G. Zanocchi, R. Ferro, Ternary rare-earth aluminum systems with copper: A review and a contribution to their assessment, *J. Phase Equilib. Diffus.*, 25 (2004) 22-52.
- [6] J.B. Friauf, The crystal structure of two intermetallic compounds, *J. Am. Chem. Soc.*, 49 (1927) 3107-3114.
- [7] T. Goedecke, F. Sommer, Solidification behavior of the Al_2Cu phase, *Z. Metallk.*, 87 (1996) 581-586.
- [8] G.D. Preston, An x-ray investigation of some copper-aluminum alloys, *Philos. Mag.*, 12 (1931) 980-993.
- [9] A.J. Bradley, H.J. Goldschmidt, H. Lipson, The intermediate phases in the aluminium-copper system after slow cooling, *J. Inst. Met.*, 63 (1938) 149-162.
- [10] M. El-Boragy, R. Szepan, K. Schubert, Crystal structure of Cu_3Al_2 (h) and CuAl (r), *J. Less-Common Met.*, 29 (1972) 133-140.
- [11] C. Dong, Q.H. Zhang, D.H. Wang, Y.M. Wang, Al-Cu approximants in the Al_3Cu_4 alloy, *Eur. Phys. J. B*, 6 (1998) 25-32.
- [12] C. Dong, Q.H. Zhang, D.H. Wang, Y.M. Wang, Al-Cu approximants and associated B2 chemical-twinning modes, *Micron*, 31 (2000) 507-514.

- [13] L.D. Gulay, B. Harbrecht, The crystal structure of zeta(1)-Al₃Cu₄, *J. Alloys Compd.*, 367 (2004) 103-108.
- [14] L.D. Gulay, B. Harbrecht, The crystal structure of zeta(2)-Al₃Cu₄-delta, *Z. Anorg. Allg. Chem.*, 629 (2003) 463-466.
- [15] D. Stockdale, The aluminium-copper alloys of intermediate composition, *J. Inst. Met.*, 31 (1924) 275-294.
- [16] E.H. Kisi, J.D. Browne, Ordering and Structural Vacancies in Nonstoichiometric Cu-Al Gamma Brasses, *Acta Crystallogr., Sect. B: Struct. Sci.*, 47 (1991) 835-843.
- [17] L. Arnberg, S. Westman, Crystal Perfection in a Non-Centrosymmetric Alloy - Refinement and Test of Twinning of Gamma-Cu₉Al₄ Structure, *Acta Crystallogr., Sect. A: Found. Crystallogr.*, 34 (1978) 399-404.
- [18] C. Hisatsune, Constitution Diagram of the Copper-Silicon-Aluminium System, *Memb. Coll. Eng. Kyoto Imp. Univ.*, 9 (1936) 18-47.
- [19] C. Hisatsune, The constitution of alloys of copper, aluminum and silicon. I. The equilibrium diagrams of three binary systems, *Tetsu to Hagane*, 21 (1935) 726-742.
- [20] A.G. Dawson, *J. Inst. Met.*, 61 (1937) 197-204.
- [21] A.T. Adorno, M.R. Guerreiro, A.V. Benedetti, Thermal behavior of Cu-Al alloys near the alpha-Cu-Al solubility limit, *J. Therm. Anal. Calorim.*, 65 (2001) 221-229.
- [22] J.L. Murray, A.J. McAlister, The Al-Si (aluminum-silicon) system, *Bull. Alloy Phase Diagr.*, 5 (1984) 74-84, 89-90.
- [23] R.W. Olesinski, G.J. Abbaschian, The copper-silicon system, *Bull. Alloy Phase Diagr.*, 7 (1986) 170-178, 193-176.
- [24] X.Y. Yan, Y.A. Chang, A thermodynamic analysis of the Cu-Si system, *J. Alloys Compd.*, 308 (2000) 221-229.
- [25] K. Sufryd, N. Ponweiser, P. Riani, K.W. Richter, G. Cacciamani, Experimental investigation of the Cu-Si phase diagram at $x(\text{Cu}) > 0.72$, *Intermetallics*, 19 (2011) 1479-1488.

- [26] J.K. Solberg, Crystal-Structure of Eta-Cu₃Si Precipitates in Silicon, *Acta Crystallogr., Sect. A: Found. Crystallogr.*, 34 (1978) 684-698.
- [27] K.P. Mukherje, J.P. Bandyopadhyaya, K.P. Gupta, Phase Relationship and Crystal Structure of Intermediate Phases in Cu-Si System in Composition Range of 17 at Pct Si to 25 at Pct Si, *Trans. Metall. Soc. AIME*, 245 (1969) 2335-2338.
- [28] C.-Y. Wen, F. Spaepen, In situ electron microscopy of the phases of Cu₃Si, *Philos. Mag.*, 87 (2007) 5581-5599.
- [29] N. Mattern, R. Seyrich, L. Wilde, C. Baetz, M. Knapp, J. Acker, Phase formation of rapidly quenched Cu-Si alloys, *J. Alloys Compd.*, 429 (2007) 211-215.
- [30] S. Arrhenius, A. Westgren, X-radiation analysis of copper-silicon alloys, *Z. Phys. Chem.*, 14 (1931) 66-79.
- [31] F.A. Veer, W.G. Burgers, W.G. Burgers, Diffusion in the Cu₃Si phase of the copper-silicon system, *Trans. Am. Inst. Min. Metall. Pet. Eng.*, 242 (1968) 669-673.
- [32] W.J. Ward, K.M. Carroll, Diffusion of copper in the copper-silicon system., *J. Electrochem. Soc.*, 129 (1982) 227-229.
- [33] R.R. Chromik, W.K. Neils, E.J. Cotts, Thermodynamic and kinetic study of solid state reactions in the Cu-Si system, *J. Appl. Phys.*, 86 (1999) 4273-4281.
- [34] R.R. Chromik, W.K. Neils, E.J. Cotts, Erratum: "Thermodynamic and kinetic study of solid state reactions in the Cu-Si system" [*J. Appl. Phys.* 86, 4273 (1999)], *J. Appl. Phys.*, 87 (2000) U3-U3.
- [35] P. Riani, K. Sufryd, G. Cacciamani, About the Al-Cu-Si isothermal section at 500 DegC and the stability of the epsilon.-Cu₁₅Si₄ phase, *Intermetallics*, 17 (2009) 154-164.
- [36] K. Matsuyama, Ternary Diagram of the Al-Cu-Si System, *Kinzuko no Kenkyu* (in Japanese), 11 (1934) 461-490.
- [37] H.L. Lukas, N. Lebrun, Al-Cu-Si (Aluminium-Copper-Silicon), in: G. Effenberg, S. Ilyenko (Eds.) *SpringerMaterials - The Landolt-Börnstein Database*, 2005, pp. 135-147.

- [38] C.-Y. He, Y. Du, H.-L. Chen, H. Xu, Experimental investigation and thermodynamic modeling of the Al-Cu-Si system, *CALPHAD*, 33 (2009) 200-210.
- [39] C.-Y. Wen, F. Spaepen, Filling the voids in silicon single crystals by precipitation of Cu₃Si, *Philos. Mag.*, 87 (2007) 5565-5579.
- [40] J. Miettinen, Thermodynamic description of the Cu-Al-Si system in the copper-rich corner, *CALPHAD*, 31 (2007) 449-456.
- [41] F. Cziple, D. Frunzaverde, D. Nedelcu, I. Padurean, Thermodynamic characterization of regular solutions in the Al-Cu-Si system, *Metalurgia* (Bucharest, Rom.), (2008) 33-38.
- [42] D.S. Kanibolotsky, O.A. Bieloborodova, V.A. Stukalo, N.V. Kotova, V.V. Lisnyak, Thermodynamics of liquid aluminium-copper-silicon alloys, *Thermochim. Acta*, 412 (2004) 39-45.
- [43] V.T. Witusiewicz, I. Arpshofen, H.J. Seifert, F. Aldinger, Enthalpy of mixing of liquid Al-Cu-Si alloys, *J. Alloys Compd.*, 297 (2000) 176-184.
- [44] T. Yoshikawa, K. Morita, Thermodynamics of solid silicon equilibrated with Si-Al-Cu liquid alloys, *J. Phys. Chem. Solids*, 66 (2005) 261-265.
- [45] A.X.S. BRUKER, TOPAS V3: General profile and structure analysis software for powder diffraction data, in: *Users's Manual*, Bruker AXS, Karlsruhe, Germany, 2005.

3.4 Phase equilibria in the Al-Mo-Si system

*Norbert Ponweiser^a, Werner Paschinger^a, Anna Ritscher^a, Julius C. Schuster^b and Klaus W. Richter^a **

^a University of Vienna, Department of Inorganic Chemistry/Materials Chemistry,
Währinger Straße 42, 1090 Wien, Austria

^b University of Vienna, Innovative Materials Group, Währinger Straße 42, 1090
Wien, Austria

* Corresponding author: Klaus Richter

Email: klaus.richter@univie.ac.at

Published: *Intermetallics* (2011), 19(3), 409-418

Contributions to this paper:

N.P. sample preparation, analysis and interpretation for the isothermal section at 1400 °C and the liquidus surface projection, supervision of sample preparation, analysis and interpretation of samples for the 600 °C isothermal section, supervision preparation and analysis of samples in the vicinity of MoSi₂, half the DTA measurements, interpretation of all DTA results to determine the reaction scheme, wrote the paper

W.P, A.R.. sample preparation, analysis and interpretation of samples for the isothermal section at 600 °C, preparation and analysis of samples in the vicinity of MoSi₂

J.C.S, K.W.R.: proofreading, general advice and helpful comments

Contribution of N. Ponweiser to the article: 75 %

Abstract

The ternary Al-Mo-Si phase diagram was investigated by a combination of optical microscopy, powder X-ray diffraction (XRD), differential thermal analysis (DTA), electron probe microanalysis (EPMA) and scanning electron microscopy (SEM). Ternary phase equilibria were investigated within two isothermal sections at 600 °C for the Mo-poor part and 1400 °C for the Mo-rich part of the phase diagram. The solubility ranges of several phases including MoSi_2 (C11_b) as well as $\text{Mo}(\text{Si},\text{Al})_2$ with C40 and C54 structure were determined. The binary high temperature phase Al_4Mo was found to be stabilized at 600 °C by addition of Si. DTA was used to identify 9 invariant reactions and thus constructing a ternary reaction scheme (Scheil diagram) in the whole composition range. A liquidus surface projection was constructed on basis of the reaction scheme in combination with data for primary crystallization from as-cast samples determined by SEM-measurements.

Introduction

Structural materials with high temperature oxidation resistance are needed for many applications today, including for example gas turbine engines [1] missile nozzles and industrial gas burners [2]. A detailed review about molybdenum disilicide, its alloys and their properties compared with aluminides and ceramics for high temperature application is given by Vasudevan and Petrovic [1].

Given the excellent properties of molybdenum disilicide, the system Mo-Si-system is of high technological importance. It was assessed by Gokhale and Abbaschian [3]. In the first investigations of phase equilibria in this system [4] three intermetallic phases were described: Mo_3Si ($Pm-3n$, $cP8$, CrSi-type), Mo_3Si_2 and MoSi_2 ($I4/mmm$, $tI6$, MoSi_2 -type). Later it was found that Mo_3Si_2 actually shows the composition Mo_5Si_3 ($I4/mcm$, $tI32$, Si_3W_5 -type) [5]. The authors also claimed that MoSi_2 undergoes a transition from a low-temperature tetragonal form ($\alpha\text{-MoSi}_2$) to a high-temperature hexagonal form ($\beta\text{-MoSi}_2$) at around 1900 °C. Later investigations in the quasi-binary system MoSi_2 and TiSi_2 indicate, that the mentioned transition of MoSi_2 does not occur in the binary [6]. The hexagonal form of MoSi_2 is supposed to be metastable which explains why it occurs in rapid cooling [7]. For the present investigation the tetragonal form ($I4/mmm$, $tI6$, MoSi_2 -type) was considered to be the only stable modification of MoSi_2 .

MoSi_2 has a high potential as material for high temperature structural applications because of its high melting point (2020 °C) [3] in combination with low density ($6.24 \text{ g}\cdot\text{cm}^{-3}$ [8]) and a high oxidation resistance. Nevertheless, a high creep rate at elevated temperatures has inhibited a wide range of application for this compounds but gave rise to a wide field of research in MoSi_2 -based alloys [2]. The compound Mo_5Si_3 , shows also interesting properties, like a better creep resistance than MoSi_2 [9] but it has poor oxidation resistance at high temperatures. Undoped Mo_5Si_3 shows pest oxidation at 800 °C but its oxidation resistance can be improved by 5 orders of magnitude by adding 1-2 wt% Boron [10].

The Al-Mo binary system was assessed by Saunders [11] and contains, according to this author, 7 intermetallic phases: AlMo_3 ($Pm-3n$, $cP8$, CrSi-type), AlMo ($Im-3m$, $cI2$, W-type), $\text{Al}_{63}\text{Mo}_{37}$ (unknown structure), Al_8Mo_3 ($C2/m$, $mC22$, Al_8Mo_3 -type), Al_4Mo (Cm , $mC30$, Al_4W -type), Al_5Mo ($P6_3$, $hP12$, Al_5W -type), and Al_{12}Mo ($Im-3$, $cI26$, Al_{12}W -type). AlMo and $\text{Al}_{63}\text{Mo}_{37}$ are stable only at elevated temperatures and were reported by Rexer [12]. The eutectoid decomposition of $\text{Al}_{63}\text{Mo}_{37}$ could not be inhibited and thus the author did not give any structural information. Although Rexer suggested a congruent melting of AlMo , Saunders replaced it by a peritectic decomposition because of thermodynamic reasons. Contrary to the assessment by Saunders, calculations of Cupuid et. al. [13] indicate congruent melting for the phase AlMo , as suggested by Rexer [12].

The results of Schuster and Ipsier [14] who investigated the Al-rich part of the binary system, did not find their way into Saunders' assessment. These authors introduced four additional compounds to the binary system: Al_3Mo (Cm , $mC32$, Al_3Mo -type), $\text{Al}_{17}\text{Mo}_4$ ($C2$, $mC84$, $\text{Al}_{17}\text{Mo}_4$ -type), $\text{Al}_{22}\text{Mo}_5$ ($Fdd2$, $oF216$, $\text{Al}_{22}\text{Mo}_5$ -type) and $\text{Al}_{(3+x)}\text{Mo}_{(1-x)}$ ($Pm3n$, $cP8$, WO_3 -type. For Al_5Mo , two additional high temperature modifications were introduced: $\text{Al}_5\text{Mo}(h')$ ($P3$, $hP60$) and $\text{Al}_5\text{Mo}(r)$ ($R-3c$, $hR12$). Eumann et. al. re-evaluated the Al-rich part and confirmed the existence of the phases introduced by Schuster and Ipsier [14] with exception of $\text{Al}_{(3+x)}\text{Mo}_{(1-x)}$. The temperatures of the invariant reactions were slightly corrected (see Table 1) and the phase $\text{Al}_{22}\text{Mo}_4$ was found to exist at 600 °C as well, although this was not confirmed by diffusion couple experiments at 630 °C [15]. Okamoto [16] presents a phase diagram combining the results of Rexer [12], Saunders [11] and Eumann [15].

The binary Al-Si system is a simple eutectic system with limited solid solubility in Al and Si [17]. A complete list of the binary invariant reactions used in this study can be found in Table 1.

The ternary system Al-Mo-Si has been investigated for the past forty years to overcome some of the disadvantages of MoSi_2 . The addition of Al lead to a new ternary compound $\text{Mo}(\text{Si},\text{Al})_2$ with CrSi₂-type structure (Strukturbericht

designation: C40) [18]. Further replacement of Si by Al lead to the TiSi_2 -type structure (Strukturbericht designation: C54) which forms peritectically from C40 and the liquid [19]. In the current study the Strukturbericht designations will be used to indicate the phases MoSi_2 (MoSi_2 -type, C11_b), $\text{Mo}(\text{Si},\text{Al})_2$ (CrSi_2 -type, C40) and $\text{Mo}(\text{Si},\text{Al})_2$ (TiSi_2 -type, C54).

Most research activities in the ternary system were dealing with properties of C40 due to its importance for technical application and its advantages compared to C11_b. For example, contrary to C11_b, C40 does not show pest oxidation at intermediate temperature. Therefore, C40 is considered to have definite advantages over C11_b for oxidation resistance coatings at service temperatures up to about 1673 K [20]. Some of these papers show isothermal sections of the phase diagram as a byproduct, e.g. by Yanigahara et. al.[21] at 1853 K. However, their suggestion does not include C54 but indicates a wide solubility range for C40. Eason et. al. [22] gave an isothermal section at 1400 °C including the C54-phase, but only estimated the composition of the limiting compounds in the three phase field [C40+C54+ Mo_5Si_3]. The investigation of the Mo_5Si_3 -phase – designated as T1- Mo_5Si_3 by the authors – revealed a solubility up to 12.5 at.% Al [22].

Liu et.al present calculated isotherms between 1273 and 1873 K as well as a predicted liquidus surface projection [8], including binary Al-Mo compounds from Al_4Mo to AlMo_3 , with exception of AlMo . A list of the invariant reactions predicted by the calculation of the liquidus surface projection is given in Table 2; no reaction temperatures are given by the authors.

The current work shows a systematic study of phase equilibria at 600 and 1400 °C as well as the reaction scheme and the liquidus surface projection to establish a comprehensive scheme about phase equilibria and reactions in the system Al-Mo-Si.

Experimental

The samples were prepared from Aluminum slug (99.999%), Silicon lump (99.9999%) and Molybdenum wire (99.95%), all supplied by Alfa Aesar, Karlsruhe, Germany. The oxide at the surface of Molybdenum was removed by abrasive paper, followed by cleaning with acetone. The calculated amounts of silicon and molybdenum were weighted to an accuracy of 0.05 mg; the aluminum was weighted to an accuracy of 1 mg (see below). The samples were melted in an arc furnace with a water-cooled copper plate and zirconium as a getter material. Due to the high difference in the melting point of molybdenum (2890 K) compared to aluminum (933.52 K) and silicon (1683 K) [23], achieving homogeneity was a challenge. Melting of all three components at once and re-melting the reguli three times lead to remaining pieces of pure molybdenum inside the sample, so a different approach was chosen.

Flat aluminum pieces (between 20 and 240 mg depending on the sample) were placed on the copper plate, covered with small molybdenum pieces and melted two times at power. The resulting bead was melted together with the rest of the aluminum and the silicon and re-melted two times for homogenization. Significant weight loss was considered to be due to evaporating aluminum and was tried to compensate by adding up to 50 mg extra aluminum for a 1000 mg sample. Electron probe microanalysis (EPMA) of samples used to determine the isothermal sections, however, sometimes showed significant change of composition and therefore it was not possible to investigate consistent isopleths. Determination of phase composition was not affected.

Samples annealed at low temperature (550 – 600 °C) were placed into alumina crucibles, sealed into evacuated quartz glass ampoules and annealed in a muffle furnace. The samples were heated up to 800 °C for assuring good homogeneity, slowly cooled to 600 °C and annealed for 21 days. After quenching in cold water, the samples were cut into several pieces and analyzed by powder-XRD, optical microscopy, differential thermal analysis (DTA) and EPMA. Due to the number of peritectic reactions in the Al-rich part of the Al-Mo phase diagram, several

samples were not well equilibrated and therefore not considered in further investigations.

Samples in the Mo-rich part of the phase diagram were sealed under an argon atmosphere in tantalum crucibles and annealed at 1400 °C for 96 hours. The samples were quenched in a water cooled steel vessel under argon. For the determination of the liquidus surface projection several as-cast samples were analyzed by Scanning Electron Microscopy (SEM).

Powder-XRD was performed using a Bruker D8 Advance Diffractometer operating in reflection mode (Cu K α radiation, Lynxeye silicon strip detector); the patterns were analyzed using TOPAS software [24]. Polished sections of the annealed samples were investigated by optical microscopy using a Zeiss Axiotech 100 microscope. To determine the composition of the identified phases, EPMA measurements were carried out on selected samples using a Cameca SX electron probe 100 (Cameca, Courbevoie, France) operating with wavelength dispersive spectroscopy (WDS) for quantitative analysis. The measurements were carried out at 15 kV using a beam current of 7 nA with pure elements as standard materials. Conventional ZAF matrix correction was used to calculate the final composition from the measured X-ray intensities. SEM measurements were performed on a Zeiss Supra 55 VP operating with energy dispersive spectroscopy (EDS) for quantitative analysis using the pure elements for calibration. The composition of the respective phases usually was measured at three different spots and it did not depend on the location within the sample.

DTA measurements were performed on a Setaram Setsys Evolution 2400 (Setaram Instrumentation, Caluire, France). The system can be operated at a low-temperature setup using an alumina sample holder and Pt/Pt10%Rh thermocouples (Type S) and a high temperature setup using a tungsten sample holder and a W-5%Re/W-26%Re thermocouple (Type W5). In both cases alumina crucibles were used. For calibration of the low temperature setup the melting points of Sn, Au and Ni were used, the high temperature setup was calibrated using the melting points of Au, Ni and Pt. A heating rate of 5 K·min⁻¹ and an argon flow of 20 ml·min⁻¹ were applied in both cases.

Results and discussion

Isothermal section at 600 °C (550 °C)

Previous investigations in the Al-Mo-Si system had been dealing with phase equilibria at higher temperature than the present work and thus avoiding complicated phase equilibria in the Al-rich corner of the system. The current study refers to the work of Schuster and Ipser [14] as limiting binary system for the investigations of Al-rich alloys.

The isothermal section at 600 °C constructed on the basis of XRD and EPMA measurements is shown in Fig. 1. Three phase fields are indicated by gray triangles, the nominal composition of samples used for EPMA investigations are indicated by black circles; open circles represent samples only investigated by XRD. The microstructure of selected samples is shown in Fig. 2.

Due to the binary eutectic in the Al-Si system at 577 ± 1 °C the liquid phase was found in the corresponding region of the phase diagram. An additional sample in the three phase field [(C40)+(Al)+(Si)] was annealed at 550 °C to avoid equilibrium with the liquid and define this phase field separately. This sample is indicated by a square in Fig. 1. The compositions of the phases in the different three phase fields are given in Table 3.

In the XRD-analysis of the samples $\text{Al}_{79.5}\text{Mo}_{18}\text{Si}_{2.5}$ and $\text{Al}_{78}\text{Mo}_{21}\text{Si}_1$ difficulties occurred during the identification of the phase with the approximate composition $\text{Al}_{81}\text{Mo}_{18.8}\text{Si}_{0.2}$. According to the phase diagram of Schuster and Ipser, this phase is $\text{Al}_{17}\text{Mo}_4$ which is stable at 600 °C [14], while according to Eumann it could be $\text{Al}_{22}\text{Mo}_5$ as well as $\text{Al}_{17}\text{Mo}_4$ [15]. EPMA measurements (see Table 3) showed for this particular phase similar compositions within the limits of error for both samples. Considering this fact, the phase with the approximate composition $\text{Al}_{81}\text{Mo}_{18.8}\text{Si}_{0.2}$ was interpreted to be $\text{Al}_{17}\text{Mo}_4$ although the identification by XRD was only tentative. This interpretation is in accordance with both, the phase

diagram published by Schuster and Ipsen as well as the phase diagram by Eumann et. al.

According to the present investigation, Al_{12}Mo shows the widest solubility range up to 7.2(1) at.% Si at 600 °C with lattice parameters varying from 7.5815(5) Å in the binary [25] to 7.5439(1) in the ternary. The solubility in Al_5Mo (0.9(1) at.% Si), $\text{Al}_{17}\text{Mo}_4$ (0.4(1) at.% Si) and Al_8Mo_3 (2.3(1) at.% Si) is much smaller. The X-ray powder pattern of a sample with the nominal composition $\text{Al}_{83}\text{Mo}_{12}\text{Si}_5$ representing the three phase field of Al_{12}Mo , Al_5Mo and C40 is given in Fig. 3. As expected, Mo does not show any significant solubility in (Al) or (Si), respectively.

In the binary Al-Mo system the phase Al_4Mo does only exist in the temperature range from 942 to 1177 °C [14]. In the present work, four samples show this phase at 600 °C thus implying a stabilization of the phase by addition of silicon. The solubility ranges at 600 °C from 2.4(3) to 6.0(1) at.% Si and the lattice parameters vary from $a = 5.2554(2)$ Å, $b = 17.784(1)$ Å, $c = 5.2245(2)$ Å, $\beta = 100.49(1)^\circ$ to $a = 5.2431(2)$ Å, $b = 17.763(1)$ Å, $c = 5.2200(2)$ Å and $\beta = 100.967(4)^\circ$, respectively, compared to $a = 5.255(5)$ Å, $b = 17.768(5)$ Å, $c = 5.225(5)$ Å and $\beta = 100.88(6)^\circ$ [26] for the binary compound.

The ternary compound $\text{Mo}(\text{Si},\text{Al})_2$ (C40) shows a wide solubility range, from 35.8(1) at 600 °C to at least 57.3(1) at.% Si at 550 °C. The lattice parameters vary from $a = 4.7151(4)$ Å, $c = 6.564(1)$ Å to $a = 4.64471(4)$ Å and $c = 6.5483(1)$ Å, respectively. The exact situation of the phase field [C40+C11_b+(Si)] was not determined, so this tentative phase field is printed with a dotted line in Fig. 1 and the solubility of Al in MoSi_2 (C11_b) remains unclear.

Isothermal section at 1400 °C

The isothermal section at 1400 °C is shown in Fig. 4. Three phase fields are indicated by gray triangles, the nominal composition of samples used for determination of the composition of the respective phases is indicated by black circles; open circles represent samples in the two phase fields. Due to the high

annealing temperature it was – despite the addition of up to 50 mg excess aluminum to cover the expected loss - difficult to obtain samples with the requested composition. The phase equilibria were again determined by means of EPMA and XRD. The sample with the nominal composition $\text{Al}_{37}\text{Mo}_{35}\text{Si}_{28}$ has obviously shifted its composition during sample preparation but the three phase field [C54+C40+ Mo_5Si_3] was identified without doubt. A list of the phase compositions of the various samples can be found in Table 3; the microstructure of selected samples is shown in Fig. 2.

At 1400 °C, homogeneity of the samples was easily established and it was also possible to determine the solubility range of the C11_b. The Mo-content of the phase deviates slightly from the ideal composition of 33.3 at.% for all the ternary $\text{Mo}(\text{Si},\text{Al})_2$ -phases, but this may also be due to a minor systematic error in the ZAF matrix correction used by EPMA analysis. The limiting ternary composition of C11_b is $\text{Al}_{3.0}\text{Mo}_{34.2}\text{Si}_{62.8}$ and the lattice parameters change from $a = 3.2064(2) \text{ \AA}$ and $c = 7.8478(8) \text{ \AA}$ [27] in the binary to $a = 3.2044(1) \text{ \AA}$ and $c = 7.8839(1) \text{ \AA}$ at its solubility limit.

Compared to the work of Eason [22], the current work shows the same expected three phase fields. The solubility ranges are different, especially in the three phase field of [C54+C40+ Mo_5Si_3] where Eason did not place a sample. The authors estimated the phase compositions to be $\text{Al}_{44}\text{Mo}_{33}\text{Si}_{23}$ (C54), $\text{Al}_{37}\text{Mo}_{33}\text{Si}_{30}$ (C40) and $\text{Al}_{10}\text{Mo}_{60}\text{Si}_{30}$ (Mo_5Si_3). In the current work the compositions of the limiting phases were found to be $\text{Al}_{37.7}\text{Mo}_{33.9}\text{Si}_{28.3}$ (C54), $\text{Al}_{32.8}\text{Mo}_{34.2}\text{Si}_{32.9}$ (C40) and $\text{Al}_{6.5}\text{Mo}_{61.3}\text{Si}_{32.3}$ (Mo_5Si_3). The X-ray powder pattern of a sample in this three phase field is shown in Fig. 5.

According to Gokhale and Abbaschian, there is no consensus about the binary solubility range of Mo_5Si_3 and the authors assume a homogeneity range between 60 and 63.2 at.% Mo [3]. In the current investigation, EPMA measurements reveal a range from $\text{Al}_{0.30}\text{Mo}_{62.0}\text{Si}_{37.6}$ to $\text{Al}_{12.8}\text{Mo}_{61.1}\text{Si}_{26.0}$ for the Mo-poor side of the ternary Mo_5Si_3 -phase. These results indicate that the actual homogeneity range of the Mo_5Si_3 -phase in the binary system may be smaller than assumed by Gokhale and Abbaschian.

EPMA and XRD analysis of samples with the nominal composition of $\text{Al}_{15}\text{Mo}_{80}\text{Si}_5$, $\text{Al}_{10}\text{Mo}_{80}\text{Si}_{10}$ and $\text{Al}_5\text{Mo}_{80}\text{Si}_{15}$ indicate a complete series of solid solutions between the two isostructural binary alloys AlMo_3 and Mo_3Si .

Ternary phase reactions and the liquidus surface projection

The determination of the ternary phase reactions in the system Al-Mo-Si was performed by DTA analysis of samples situated in the different three phase fields at 550, 600 and 1400 °C, respectively. The measurements of samples annealed at 550 and 600 °C were carried out to a maximum temperature between 900 in the Al-rich part and 1500 °C in the Al-poor part of the phase diagram. Two heating and two cooling cycles at $5 \text{ K} \cdot \text{min}^{-1}$, respectively, were performed starting 50 °C below the annealing temperature of the respective sample. The samples annealed at 1400 °C were analyzed by applying the high-temperature DTA equipment. Due to the possible reaction of a partially liquid sample with the crucible, the measurements were performed only until the first reaction peak occurred. In these cases it was not possible to determine the liquidus temperature of the samples.

Due to the cascade of peritectic reactions in the Al-rich corner at low temperatures, the phase equilibria determined at 600 °C and the amount of heat exchanged in the occurring invariant reactions in the respective sample, it is approvable to assume that all the invariant reactions observed involve the liquid phase. Based on this assumption, the invariant reactions and the composition of the reactants estimated based on the isothermal sections are given in Table 4. The composition of the phases involved in the invariant reactions was estimated considering the location of relevant three phase fields at lower temperature, the information on melting behaviour in the binary systems and the information on primary crystallization. Furthermore the composition of the liquid in the invariant reactions was chosen to yield a realistic course of the liquidus valleys and fulfil the requirements of the respective type of reaction concerning the composition of the participating phases. A corresponding reaction scheme is shown in Fig. 6.

The two invariant reactions, U3 and U4, were introduced for a full description of the reaction scheme, but they were not determined experimentally. The three phase field $[Al_4Mo + Al_5Mo + Al_{17}Mo_4]$, represented by the sample $Al_{79.5}Mo_{18}Si_{2.5}$, participates in U3, but no recognizable invariant effect was found up to 1207 °C, which might be due to the fact that Al_5Mo -fraction in the sample is very small and therefore the small thermal effect of its melting can not be observed.

The reaction P2: $L + C40 + Al_8Mo_3 = Al_4Mo$ at 1218 °C involves the three phase field $[L + Al_4Mo + Al_8Mo_3]$ which is not connected to any of the ternary reactions in Fig. 6. According to the phase diagram of Schuster, two additional compounds, Al_3Mo and $Al_{(3+x)}Mo_{(1-x)}$ – the latter not confirmed by Euman et. al. [15] – are formed in the binary system Al-Mo which do not occur in the isothermal section at 600 °C. The three phase field $[L + Al_4Mo + Al_8Mo_3]$ is supposed to undergo further ternary invariant reactions with these phases but due to lack of experimental data in this region of the phase diagram it was not possible to determine these reactions.

The reaction U5: $L + C54 = Al_8Mo_3 + C40$ involves the three phase field $[C40 + C54 + Al_8Mo_3]$ which was not observed experimentally but obviously exists in a very narrow composition area. Both reactions, U7 and U8, take place at around 1507 °C and it was not possible to separate the two reaction temperatures. It can be assumed that the composition of the liquid in the two reactions is very similar. The three phase field $[L + Mo_3(Al, Si) + Al_8Mo_3]$ connected to the invariant reaction U8 is drawn with an open end in the reaction scheme in Fig. 6. Considering the phase equilibria in the binary system Al-Mo, it is possible that this phase field undergoes invariant reactions involving $AlMo$ and $Al_{63}Mo_{37}$ which were not found in any of the investigated samples and are probably restricted to a very limited composition area in the vicinity of the binary system.

The temperatures of the occurring invariant reactions were combined with literature data for the binary phase diagrams and investigations of primary crystallization of as-cast samples to construct a liquidus surface projection within the whole phase diagram which is shown in Fig. 7. The liquidus valleys separate the different fields of primary crystallization and are indicated by solid lines;

arrows are directing towards the lower temperature. The composition of the liquid in the respective invariant reactions is listed in Table 4 and is represented by black dots connecting the liquidus valleys in Fig. 7. The dotted lines indicate the isotherms between 600 and 2600 °C. It must be emphasized that most of these isotherms are only extrapolated based on binary liquidus temperatures and the observed invariant reactions because in the current work liquidus temperatures were not determined above 1500 °C. However, isotherms in the Al-rich corner of the primary crystallization field of C40 are based on the liquidus temperatures of 5 samples in this area.

According to our study, the liquidus valley between the invariant reactions P3 and U9 shows a maximum. This assumption was backed up on the one hand by analyzing a sample with the composition $\text{Al}_{12}\text{Mo}_{33.3}\text{Si}_{54.7}$ (annealed at 1400 °C) by DTA. It shows the first effect at 1925 °C which is higher than the reaction temperatures of U9 (1917 °C). On the other hand this maximum is a consequence of the congruent melting behaviour of the C40 phase which was confirmed by microstructure analysis of as-cast alloys.

The congruent melting phase C40 forms a quasi binary system with MoSi_2 (C11_b), which melts congruently in the binary. The quasi binary eutectic between these two phases represents a maximum in the liquidus valley between the reactions U6 and U9. The reaction U6 was not detected experimentally due to the very narrow composition of $[\text{C40}+\text{C11}_b+\text{Si}]$. Table 5 gives an overview of primary crystallization observed in as-cast samples which were investigated by metallographic and SEM analysis.

A few selected microstructures are given in Fig. 8 showing the primary crystallization of $\text{Mo}_3(\text{Al},\text{Si})$ (A), Mo_5Si_3 (B), C54 (C) and C40 (D). Picture (C) is of special importance for verifying the position of the (very narrow) primary crystallization field of C54.

The analysis of a binary sample with nominal composition of $\text{Mo}_{33.3}\text{Si}_{66.7}$ cooled from the liquid state showed only C11_b and not the hexagonal $\beta\text{-MoSi}_2$, presumptive C40 , thus confirming the non-existence of the latter in the binary Mo-Si system.

Summary

The phase equilibria in the system Al-Mo-Si were studied at 600 °C for the Mo-poor part and at 1400 °C for the Mo-rich part. At 600 °C, Al_{12}Mo shows the widest solubility range with up to 7.2(1) at.% Si. The solubility of Si in Al_5Mo (0.9(1) at.% Si), $\text{Al}_{17}\text{Mo}_4$ (0.4(1) at.% Si) and Al_8Mo_3 (2.3(1) at.% Si) is much smaller. The phase Al_4Mo which exist in the binary only at elevated temperatures is stabilized at 600 °C by addition of Si and shows a solubility range from 2.4(3) to 6.0(1) at.% Si at 600 °C.

At 1400°C phase equilibria between MoSi_2 (MoSi_2 -type, C11_b), $\text{Mo}(\text{Si},\text{Al})_2$ (CrSi_2 -type, C40), $\text{Mo}(\text{Si},\text{Al})_2$ (TiSi_2 -type, C54) and their neighbouring phases Al_8Mo_3 , Mo_5Si_3 and $\text{Mo}(\text{Al},\text{Si})_3$ were investigated. The results in the current work show the same three phase fields as found by Eason [22] but the solubility ranges differ significantly.

In combination with data from the binary it was possible to determine the ternary reaction scheme (Scheil diagram) containing the 9 invariant reactions determined by DTA measurements between 574 and 1917 °C, and 4 additional invariant reactions which were not determined experimentally. Additionally, two maxima at temperatures higher than 1917 °C and a quasi binary eutectic between C11_b and C40 were introduced. In combination with primary crystallization analysis the liquidus surface projection was established, showing – besides remaining uncertainties in the Al-rich corner and in the vicinity of AlMo and $\text{Al}_{63}\text{Mo}_{37}$ – the primary crystallization fields of (Al), (Si), Al_{12}Mo , C11_b, C40, C54, Al_8Mo_3 , Mo_5Si_3 , $\text{Mo}_3(\text{Al},\text{Si})$ and (Mo).

Acknowledgement

Financial support from the Austrian science foundation (FWF) under the project number P19305 is gratefully acknowledged. The authors wish to thank Theodoros Ntaflos and Franz Kiraly (Department of Lithospheric Sciences) for their support with EPMA measurements and Stephan Puchegger (Dynamic of Condensed Systems Group at the University of Vienna) for his support with SEM measurements.

Tables

Table 1

Binary invariant phase equilibria relevant to the present study.

Phase reaction	Composition of the involved Phases / at. %			T / °C	Ref.
L=Al+Si	12.2 ±0.1 Si	1.5 ± 0.1 Si	100 Si	577±1	[28]
L+(Mo)=Mo ₃ Si	25.72 Si	4 Si	25 Si	2025	[3]
L =Mo ₃ Si+Mo ₅ Si ₃	26.4 Si	25 Si	37 Si	2020	[3]
L= Mo ₅ Si ₃		37.5 Si		2180	[3]
L = Mo ₅ Si ₃ +MoSi ₂	54 Si	40 Si	66.7 Si	1900	[3]
L = β-MoSi ₂		66.7 Si		2020	[3]
L= MoSi ₂ +(Si)	98.3 Si	66.7 Si	100 Si	1400	[3]
L+(Mo)=AlMo ₃	~65 Mo	20.5 Mo	25 Mo	~2150	[11]
L+Al ₃ Mo=AlMo	~45 Mo	73 Mo	54 Mo	~1720	[11]
L+AlMo=Al ₆₃ Mo ₃₇	~35 Mo	48 Mo	37 Mo	1570	[11]
L=Al ₈ Mo ₃		27.3 Mo		1577	[11]

				1555±10	[14]
				1546±3	[15]
			37 Mo	1535	[11]
		28.5 Mo	~27.8 Mo		
	$L = Al_8Mo_3 + Al_{63}Mo_{37}$				
		37 Mo	~28.6 Mo	1490	[11]
	$Al_{63}Mo_{37} = Al_8Mo_3 + AlMo$				
		50 Mo	~28.7 Mo	1470	[11]
	$AlMo = Al_8Mo_3 + AlMo_3$				
		~5 Mo	~29 Mo	1260	[14]
	$L + Al_8Mo_3 = Al_{3+x}Mo_{1-x}(h)$				
		~29 Mo	~23.8 Mo	1222	[14]
	$Al_8Mo_3 + Al_{3+x}Mo_{1-x}(h) = Al_3Mo(h)$				
		~4 Mo	~21 Mo	1177	[14]
	$L + Al_{3+x}Mo_{1-x}(h) = Al_4Mo(h)$				
		~22 Mo	25 Mo	1154	[14]
	$Al_{3+x}Mo_{1-x}(h) = Al_3Mo(h) + Al_4Mo(h)$				
		~1.7 Mo	20 Mo	1034	[14]
	$L + Al_4Mo(h) = Al_{17}Mo_4$				
				<1000	[15]
		~3 Mo	25.5 Mo	1130	[11]
	$L + Al_8Mo_3 = Al_4Mo$				
		20 Mo	25 Mo	942	[14]
	$Al_4Mo(h) = Al_3Mo(h) + Al_{17}Mo_4$				
		~1 Mo	~19 Mo	964	[14]
	$L + Al_{17}Mo_4 = Al_{22}Mo_5(h)$				
				<950	[15]
		~0.5 Mo	~18.4 Mo	846	[14]
	$L + Al_{22}Mo_5 = Al_5Mo(h)$				

$\text{Al}_{22}\text{Mo}_5(\text{h}) = \text{Al}_{17}\text{Mo}_4 + \text{Al}_5\text{Mo}(\text{h})$	~18.4 Mo	~19 Mo	16.7 Mo	831	[14]
$\text{Al}_5\text{Mo}(\text{h}) = \text{Al}_5\text{Mo}(\text{h}')$				750 < T < 800	[14]
$\text{Al}_5\text{Mo}(\text{h}') = \text{Al}_5\text{Mo}(\text{r})$				600 < T < 700	[14]
$\text{L} + \text{Al}_5\text{Mo}(\text{h}') = \text{Al}_{12}\text{Mo}$	0.03 Mo	16.7 Mo	7.7 Mo	712	[14]
				700	[11]
$\text{L} + \text{Al}_{12}\text{Mo} = (\text{Al})$	0.03 Mo	7.7 Mo	0.064 Mo	661	[11]
				660	[14]

Table 2

Invariant reactions predicted by Liu et. al [8]

Type	Reaction
U	$L + C11_b = C40 + Mo_5Si_3$
P	$L + C40 + Mo_5Si_3 = C54$
U	$L + C54 = C40 + Al_8Mo_3$
E	$L = Mo_5Si_3 + C54 + Al_8Mo_3$
E	$L = Mo_5Si_3 + Mo_3(Al,Si) + Al_8Mo_3$
U	$L + Al_{63}Mo_{37} = Mo_3(Al,Si) + Al_8Mo_3$
U	$L + (Mo) = Al_{63}Mo_{37} + Mo_3(Al,Si)$
U	$L + Al_8Mo_3 = C40 + Al_4Mo$

Table 3
Phase composition in various samples determined by EPMA.

sample	Phase composition by EPMA /at. %				
composition	T / °C	Phase field			
nominal / (calculated ^a)	of annealing	determined by XRD	Al	Mo	Si
Al ₂₀ Mo ₂₃ Si ₅₇	550	[(Al)+(Si)+C40]	(Al) 98.9 (1)	0.1 (1)	1.1(1)
(Al _{14.7} Mo _{24.5} Si _{60.8})			(Si) 0.3	0	99.7
			C40 8.4(1)	34.3(1)	57.3(1)
Al ₉₀ Mo ₅ Si ₅	600	[(Al)+Al ₁₂ Mo+C40]	(Al) –	–	– ^b
(Al _{89.9} Mo _{5.0} Si _{5.1})			Al ₁₂ Mo 84.7(2)	7.7(1)	7.2(1)
			C40 16.5(5)	33.4(1)	49.7(3)
Al ₈₃ Mo ₁₂ Si ₅	600	[Al ₁₂ Mo+Al ₅ Mo+C40]	Al ₁₂ Mo 88.1(1)	7.8(1)	3.9(1)
(Al _{82.9} Mo _{12.1} Si _{5.0})			Al ₅ Mo 82.2(1)	16.8(2)	0.9(1)
			C40 16.6(1)	34.5(1)	48.8(1)

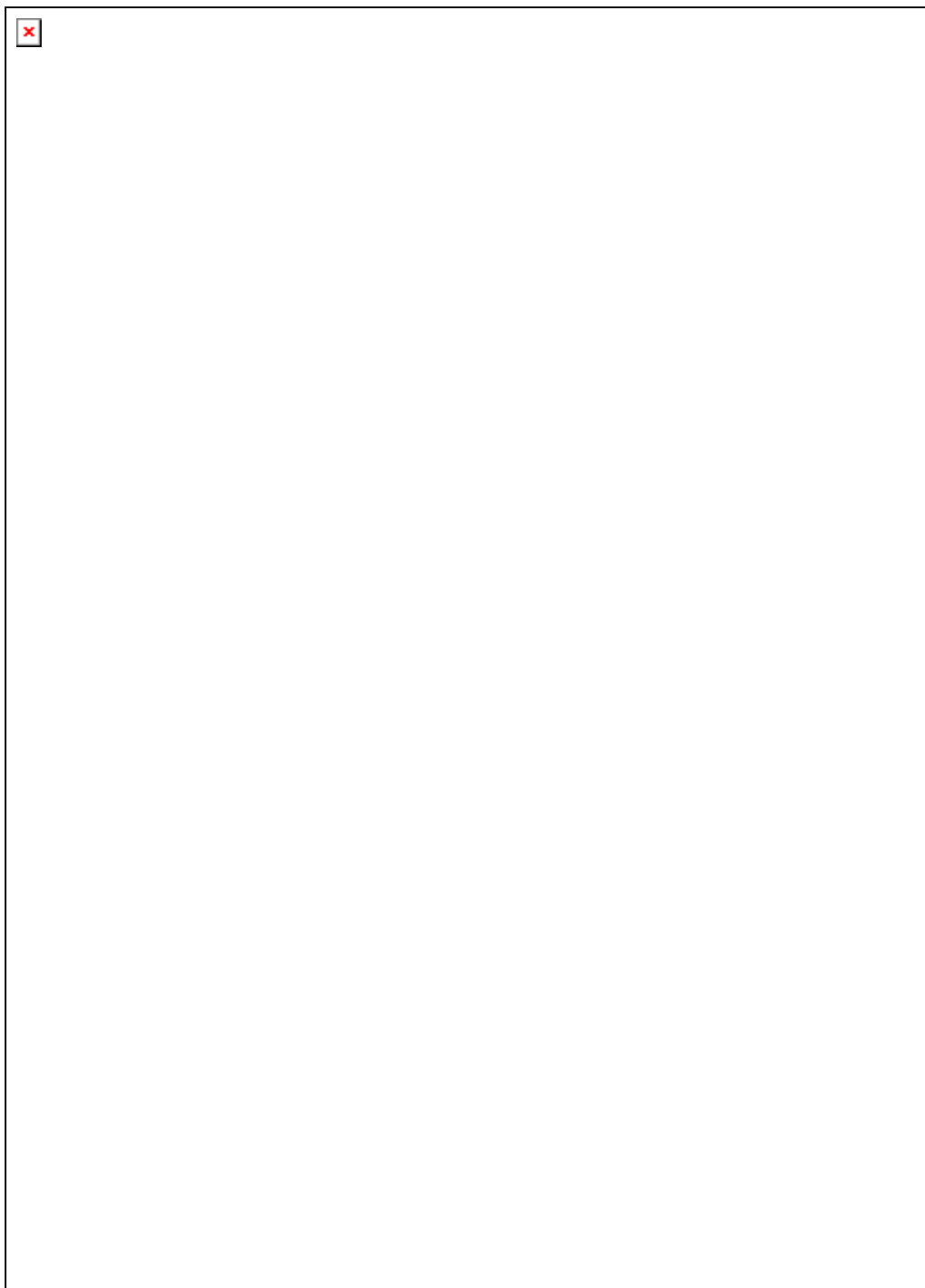
$\text{Al}_{79.5}\text{Mo}_{18}\text{Si}_{2.5}$ ($\text{Al}_{78.5}\text{Mo}_{18.9}\text{Si}_{2.6}$)	600	$[\text{Al}_5\text{Mo} + \text{Al}_{17}\text{Mo}_4 + \text{Al}_4\text{Mo}]$	Al_5Mo	82.8(4)	16.8(3)	0.2(1)
			$\text{Al}_{17}\text{Mo}_4$	80.9(2)	18.7(2)	0.4(1)
			Al_4Mo	75.5(3)	20.3(1)	4.1(4)
$\text{Al}_{77}\text{Mo}_{18}\text{Si}_5$ ($\text{Al}_{76.6}\text{Mo}_{18.3}\text{Si}_{5.1}$)	600	$[\text{Al}_5\text{Mo} + \text{Al}_4\text{Mo} + \text{C40}]$	Al_5Mo	82.3(3)	16.9(3)	0.7(2)
			Al_4Mo	73.8(3)	20.1(2)	6.0(1)
			C40	17.0(5)	33.6(1)	48.3(5)
$\text{Al}_{78}\text{Mo}_{21}\text{Si}_1$ ($\text{Al}_{77.0}\text{Mo}_{21.9}\text{Si}_{1.1}$)	600	$[\text{Al}_{17}\text{Mo}_4 + \text{Al}_4\text{Mo} + \text{Al}_8\text{Mo}_3]$	$\text{Al}_{17}\text{Mo}_4$	81.0(1)	18.8(1)	0.2(1)
			Al_4Mo	77.2(4)	20.3(3)	2.4(3)
			Al_8Mo_3	71.5(1)	27.9(1)	0.5 (1)
$\text{Al}_{72}\text{Mo}_{23}\text{Si}_5$ ($\text{Al}_{70.9}\text{Mo}_{23.9}\text{Si}_{5.2}$)	600	$[\text{Al}_4\text{Mo} + \text{Al}_8\text{Mo}_3 + \text{C40}]$	Al_4Mo	75.9(3)	20.5(1)	3.4(1)
			Al_8Mo_3	69.5(1)	28.0(3)	2.3(1)
			C40	30.7(2)	33.5(3)	35.8(1)
$\text{Al}_{53}\text{Mo}_{40}\text{Si}_7$ ($\text{Al}_{54.1}\text{Mo}_{39.6}\text{Si}_{6.9}$)	1400	$[\text{Al}_8\text{Mo}_3 + \text{Mo}_5\text{Si}_3 + \text{Mo}_3(\text{Al}, \text{Si})]$	Al_8Mo_3	70.8(2)	27.8(3)	1.3 (2)
			Mo_5Si_3	12.8(2)	61.1(4)	26.0(2)
			$\text{Mo}_3(\text{Al}, \text{Si})$	17.4(2)	74.3(2)	8.2(1)
$\text{Al}_{43}\text{Mo}_{40}\text{Si}_{17}$	1400	$[\text{Al}_8\text{Mo}_3 + \text{C54} + \text{Mo}_5\text{Si}_3]$	Al_8Mo_3	70.1 (1)	27.9(1)	1.9(1)

$(\text{Al}_{44.0}\text{Mo}_{39.3}\text{Si}_{16.7})$		C54	43.2(2)	34.1(1)	22.6(4)
		Mo_5Si_3	10.3(1)	61.1(1)	28.6(1)
$\text{Al}_{37}\text{Mo}_{35}\text{Si}_{28}$ 1400 $(\text{Al}_{31.5}\text{Mo}_{38.0}\text{Si}_{30.5})$		C54	37.7(1)	33.9(2)	28.3(1)
		C40	32.8(2)	34.2(3)	32.9(1)
		[C54+C40+ Mo_5Si_3]			
		Mo_5Si_3	6.5(1)	61.3 (2)	32.3(3)
$\text{Al}_5\text{Mo}_{40}\text{Si}_{55}$ 1400 $(\text{Al}_{1.7}\text{Mo}_{41.4}\text{Si}_{56.9})$		C40	7.9(1)	34.0(4)	58.0(5)
		C11 _b	3.0(1)	34.2(2)	62.8(1)
		[C40+C11 _b + Mo_5Si_3]			
		Mo_5Si_3	0.3(1)	62.0(1)	37.6(1)

^a sample composition calculated under the assumption that the weight loss during sample preparation

is due to evaporated aluminum

^b not measured due to fine microstructure



Al ₅ Mo	81.5	18	0.5		
P2: L+Al ₈ Mo ₃ +C40=Al ₄ Mo	1218±1	L	79.5	18	2.5
		Al ₈ Mo ₃	69.5	28.0	2.5
		C40	30.5	33	46.5
		Al ₄ Mo	78	20	2
U5: L+C54=Al ₈ Mo ₃ +C40	1218 < T < 1507	L	65.5	27.5	7
		C54	38.5	33	28.5
		Al ₈ Mo ₃	69.5	28	2.5
		C40	33.5	33	35.5
U6: L+C11 _b =C40+Si	T < 1400	L	3	3	94
		C11 _b	3.5	33	63.5
		C40	8.5	33	58.5
		Si	0	0	100

U7: L+Mo ₅ Si ₃ =Al ₈ Mo ₃ +C54	1507±3	L	63.5	29	7.5
		Mo ₅ Si ₃	10	62	28
		Al ₈ Mo ₃	69.5	28	2.5
		C54	43.5	33	23.5
U8: L+Mo ₃ (Al,Si)=Al ₈ Mo ₃ +Mo ₅ Si ₃	1507±3	L	63	29.5	7.5
		Mo ₃ (Al,Si)	17.5	74	8.5
		Al ₈ Mo ₃	70	28	2
		Mo ₅ Si ₃	10	62	28
P3: L+Mo ₅ Si ₃ +C40=C54	1619±3	L	48	32	20
		Mo ₅ Si ₃	7	62	31
		C40	33.5	33	33.5
		C54	38.5	33	28.5

U9: L+C40 =Mo ₅ Si ₃ +C11 _b	1917±3	L	1	44	55
		C40	8.5	33	58.5
		Mo ₅ Si ₃	0.5	62	37.5
		C11 _b	3.5	33	63.4

Table 5

Primary crystallization observed in different as-cast alloys

Nominal sample composition	Primary crystallizing phase
$\text{Al}_{25}\text{Mo}_{70}\text{Si}_5$	(Mo)
$\text{Al}_{45}\text{Mo}_{50}\text{Si}_5$	$\text{Mo}_3(\text{Al}, \text{Si})$
$\text{Al}_{40}\text{Mo}_{50}\text{Si}_{10}$	$\text{Mo}_3(\text{Al}, \text{Si})$
$\text{Al}_{30}\text{Mo}_{50}\text{Si}_{20}$	Mo_5Si_3
$\text{Al}_{20}\text{Mo}_{50}\text{Si}_{30}$	Mo_5Si_3
$\text{Al}_{50}\text{Mo}_{40}\text{Si}_{10}$	Mo_5Si_3
$\text{Al}_{45}\text{Mo}_{40}\text{Si}_{15}$	Mo_5Si_3
$\text{Al}_{40}\text{Mo}_{40}\text{Si}_{20}$	Mo_5Si_3
$\text{Al}_{30}\text{Mo}_{40}\text{Si}_{30}$	Mo_5Si_3
$\text{Al}_{20}\text{Mo}_{40}\text{Si}_{40}$	Mo_5Si_3
$\text{Al}_{15}\text{Mo}_{40}\text{Si}_{45}$	Mo_5Si_3
$\text{Al}_{10}\text{Mo}_{40}\text{Si}_{50}$	C40

$\text{Al}_{56}\text{Mo}_{34}\text{Si}_{10}$	Mo_5Si_3
$\text{Al}_{51}\text{Mo}_{34}\text{Si}_{15}$	Mo_5Si_3
$\text{Al}_{46}\text{Mo}_{34}\text{Si}_{20}$	Mo_5Si_3
$\text{Al}_{37}\text{Mo}_{34}\text{Si}_{29}$	Mo_5Si_3
$\text{Al}_{65}\text{Mo}_{30}\text{Si}_5$	Al_8Mo_3
$\text{Al}_{60}\text{Mo}_{30}\text{Si}_{10}$	C54
$\text{Al}_{55}\text{Mo}_{30}\text{Si}_{15}$	C54
$\text{Al}_{50}\text{Mo}_{30}\text{Si}_{20}$	C40
$\text{Al}_{40}\text{Mo}_{30}\text{Si}_{30}$	C40
$\text{Al}_{35}\text{Mo}_{30}\text{Si}_{35}$	C40
$\text{Al}_{20}\text{Mo}_{30}\text{Si}_{50}$	C40
$\text{Al}_{70}\text{Mo}_{25}\text{Si}_5$	Al_8Mo_3
$\text{Al}_{60}\text{Mo}_{20}\text{Si}_{20}$	C40
$\text{Al}_{50}\text{Mo}_{20}\text{Si}_{30}$	C40
$\text{Al}_{20}\text{Mo}_{20}\text{Si}_{60}$	C40

Figures

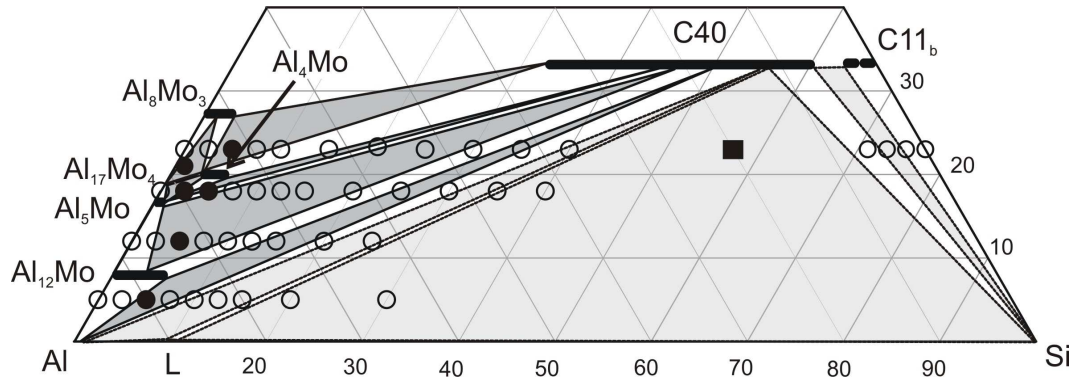


Fig. 1: Partial isothermal section of the Al-Mo-Si system at 600 °C.

Open circles: nominal composition of the samples; black circles: samples used for determination of the three phase fields; black square: additional sample annealed at 550 °C to avoid equilibrium with liquid.

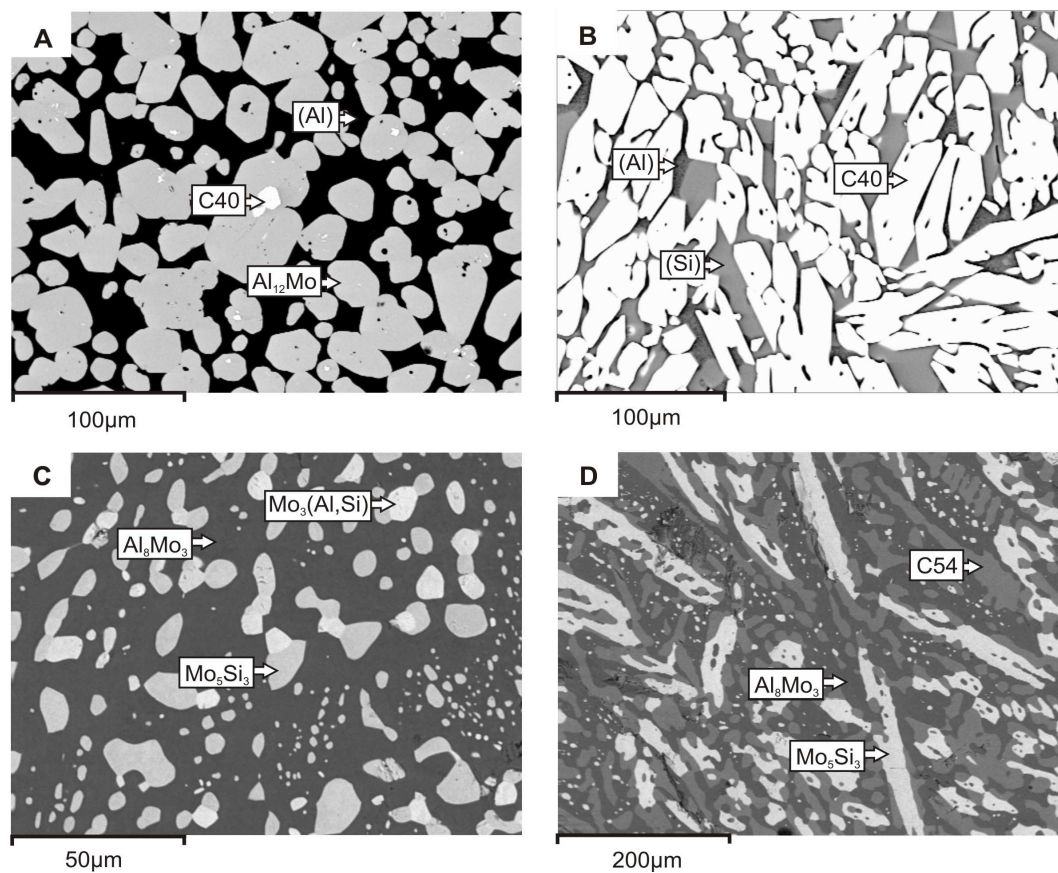


Fig. 2: BSE images of samples with the nominal composition A) $\text{Al}_{90}\text{Mo}_5\text{Si}_5$ (annealed at 600 °C), B) $\text{Al}_{20}\text{Mo}_{23}\text{Si}_{57}$ (annealed at 550°C), C) $\text{Al}_{60}\text{Mo}_{30}\text{Si}_{10}$ and D) $\text{Al}_{20}\text{Mo}_{20}\text{Si}_{60}$ (both annealed at 1400 °C).

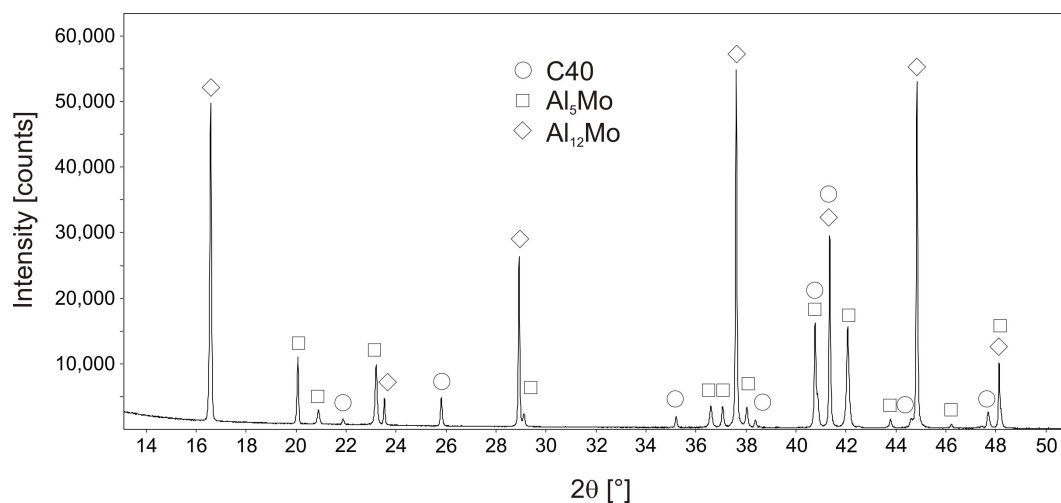


Fig. 3: X-ray powder pattern of a sample with the nominal composition $\text{Al}_{83}\text{Mo}_{12}\text{Si}_5$

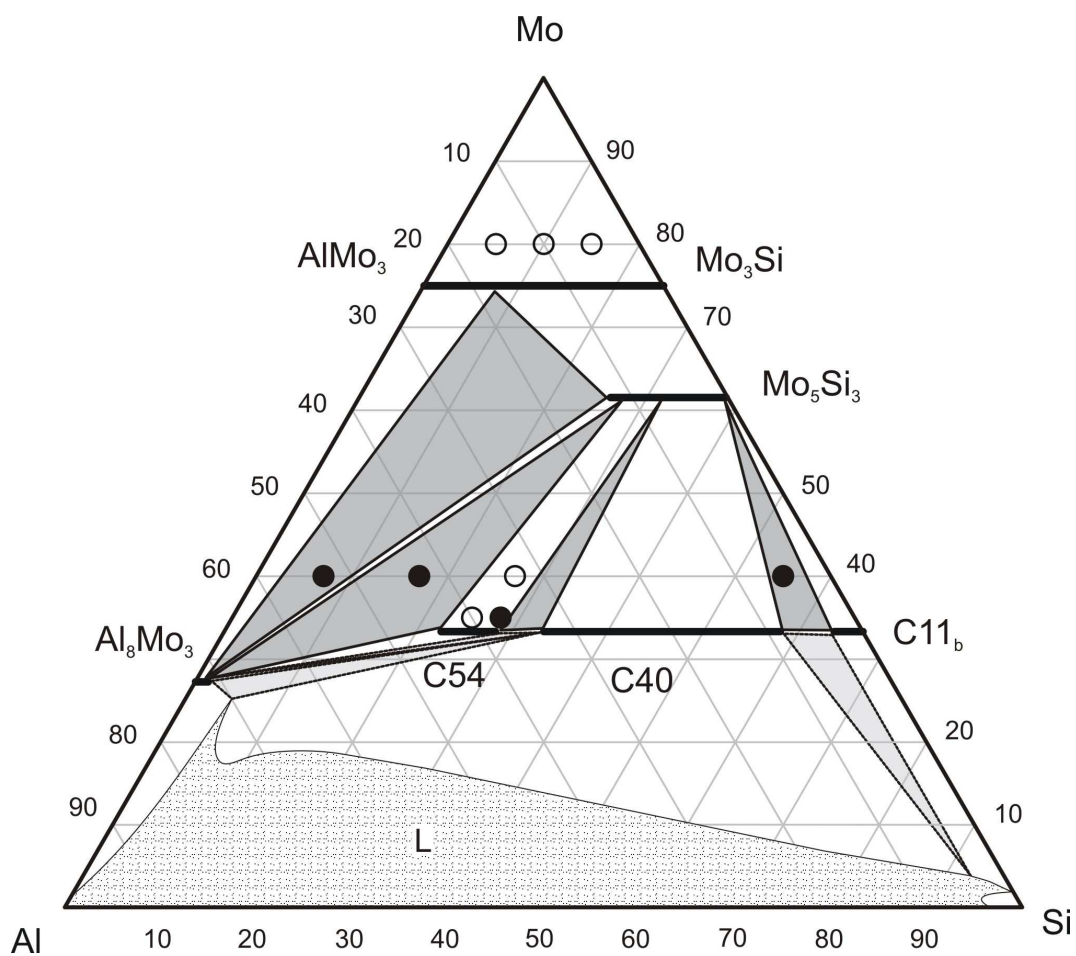


Fig. 4: Partial isothermal section of the Al-Mo-Si system at 1400 °C.

circles: nominal composition of the samples; black circles: samples investigated by EPMA

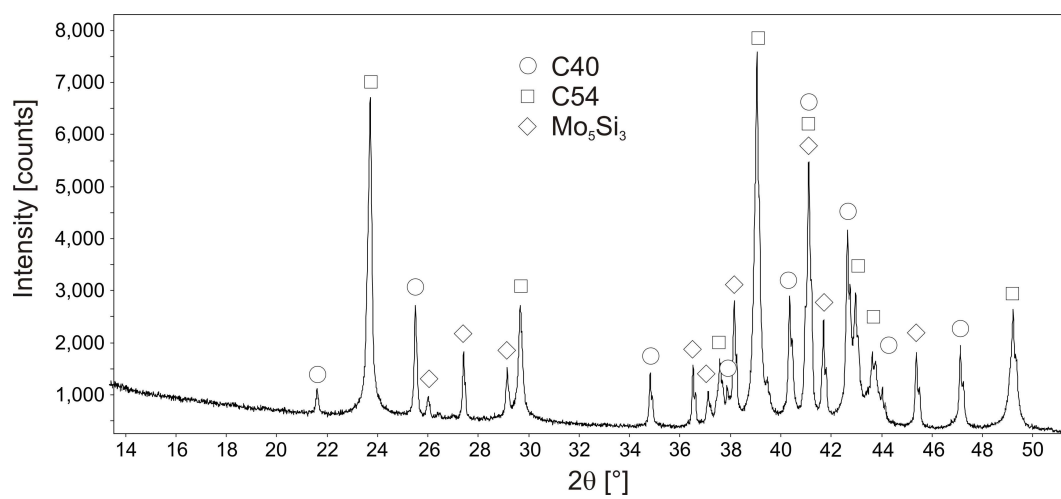


Fig. 5: X-ray powder pattern of a sample with the nominal composition $\text{Al}_{37}\text{Mo}_{35}\text{Si}_{28}$

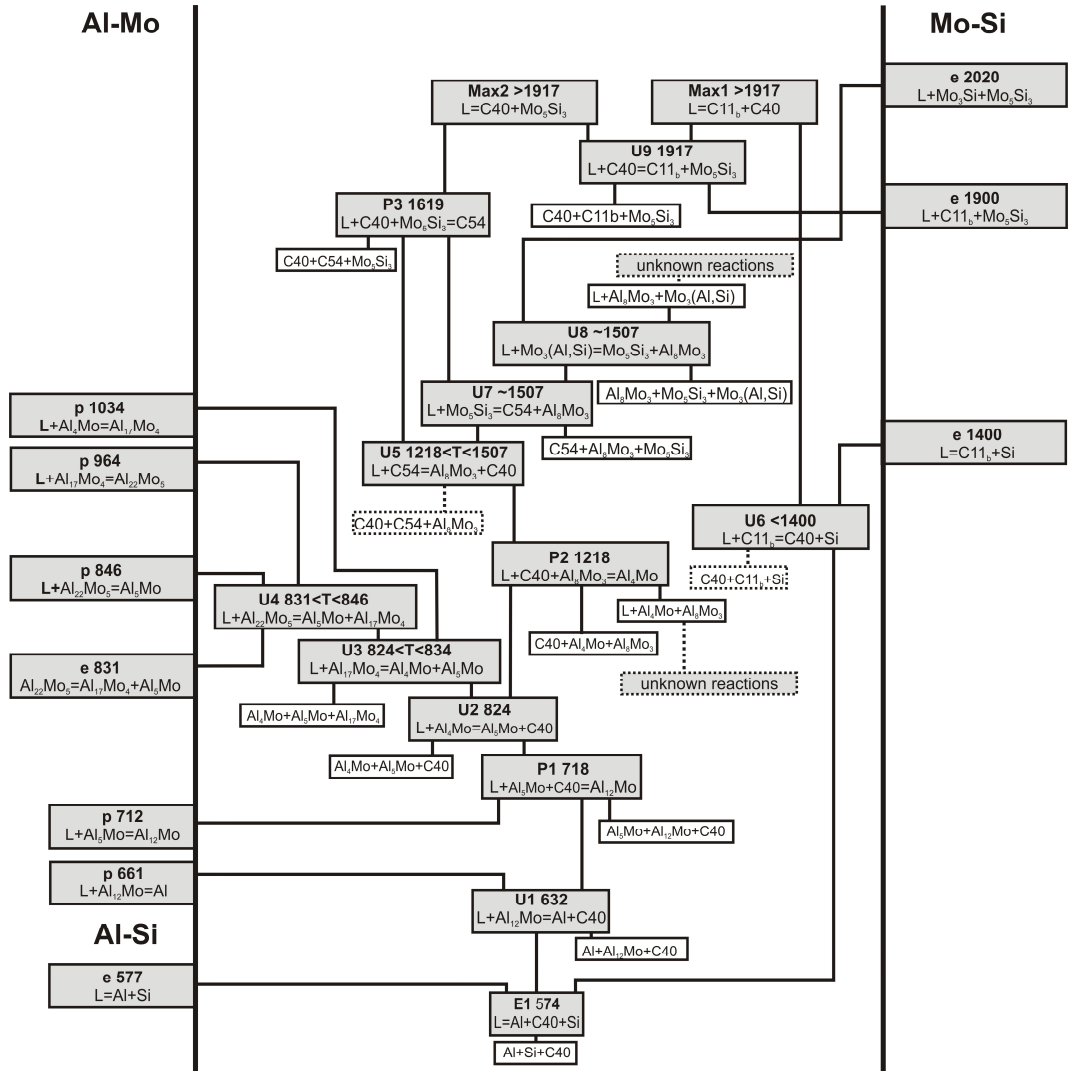


Fig. 6: Ternary reaction scheme (Scheil Diagram) for Al-Mo-Si.

Dashed three phase field: not determined experimentally

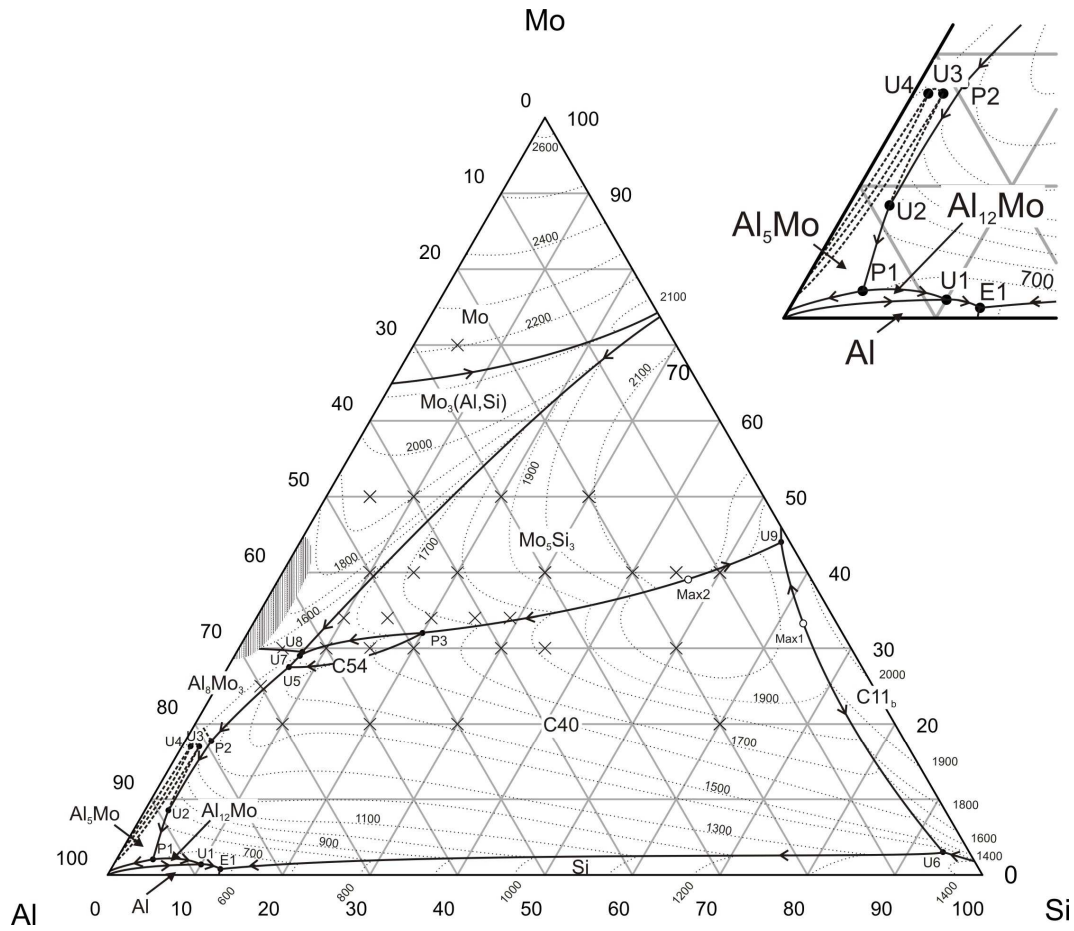


Fig. 7: Liquidus surface projection of Al-Mo-Si including fields of primary crystallisation. Solid lines: liquidus valleys; dotted thick lines in the Al-rich corner: liquidus valleys not confirmed experimentally; dotted thin lines: isotherms; full circles: invariant points, open circles: maxima, crosses: nominal composition of samples used to determine the liquidus surface

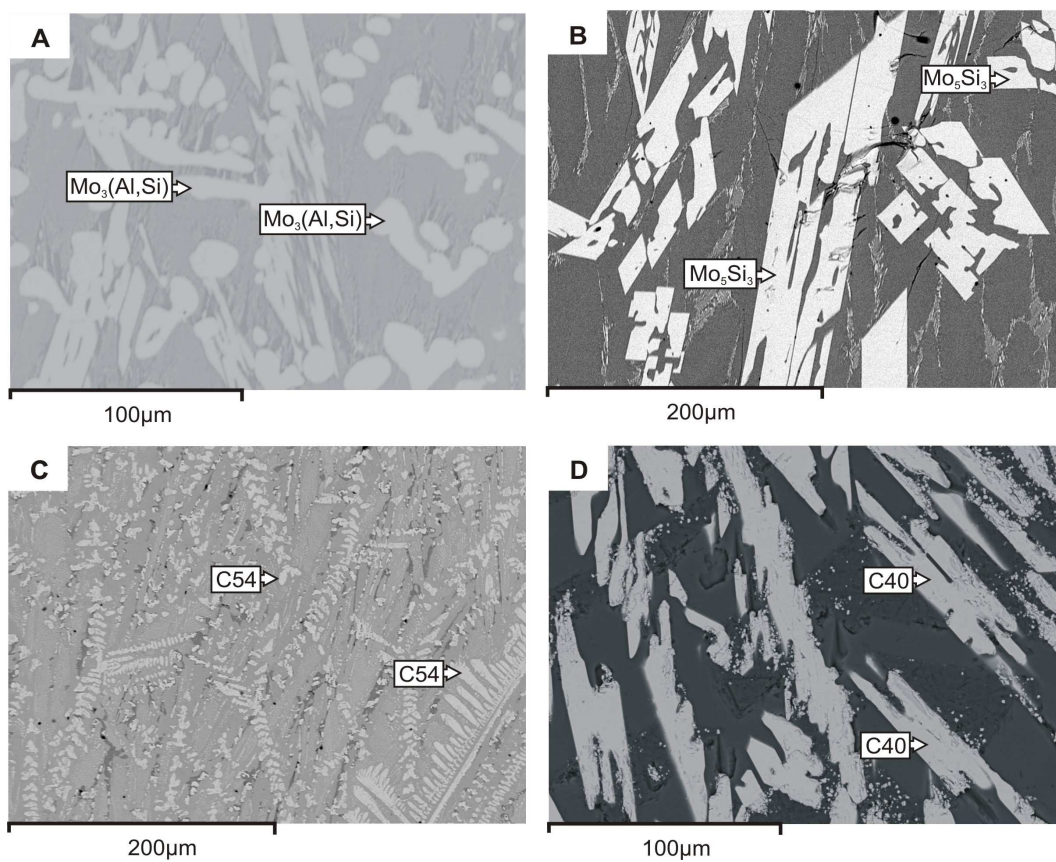


Fig. 8: BSE images of samples with the nominal composition A) $\text{Al}_{40}\text{Mo}_{50}\text{Si}_{10}$, B) $\text{Al}_{45}\text{Mo}_{40}\text{Si}_{15}$, C) $\text{Al}_{60}\text{Mo}_{30}\text{Si}_{10}$ and D) $\text{Al}_{20}\text{Mo}_{20}\text{Si}_{60}$. The marked phases indicate the primary crystals.

References

- [1] A.K. Vasudevan, J.J. Petrovic, A comparative overview of molybdenum disilicide composites, *Mater. Sci. Eng., A*, A155 (1992) 1-17.
- [2] Z. Yao, J. Stiglich, T.S. Sudarshan, Molybdenum silicide based materials and their properties, *J. Mater. Eng. Perform.*, 8 (1999) 291-304.
- [3] A.B. Gokhale, G.J. Abbaschian, The Mo-Si (molybdenum-silicon) system, *J. Phase Equilib.*, 12 (1991) 493-498.
- [4] R. Kieffer, E. Cerwenka, The system molybdenum-silicon, *Z. Metallk.*, 43 (1952) 101-105.
- [5] V.N. Svechnikov, Y.A. Kocherzhinskii, L.M. Yupko, Phase diagram of the molybdenum-silicon system, *Diagrammy Sostoyaniya Metal. Sist., Mater. Vses. Soveshch.*, 4th, (1971) 116-119.
- [6] W.J. Boettinger, J.H. Perepezko, P.S. Frankwicz, Application of ternary phase diagrams to the development of MoSi₂-based materials, *Mater. Sci. Eng., A*, 155 (1992) 12.
- [7] P.S. Frankwicz, J.H. Perepezko, Phase stability of MoSi₂ in the C11b and C40 structures at high temperatures, *Mater. Sci. Eng., A*, 246 (1998) 199-206.
- [8] Y. Liu, G. Shao, P. Tsakiroopoulos, Thermodynamic reassessment of the Mo-Si and Al-Mo-Si systems, *Intermetallics*, 8 (2000) 953-962.
- [9] D.L. Anton, D.M. Shah, High-temperature properties of refractory intermetallics, *Mater. Res. Soc. Symp. Proc.*, 213 (1991) 733-738.
- [10] M.K. Meyer, M. Akinc, Oxidation behavior of boron modified Mo₅Si₃ at 800-1300°C, *J. Am. Ceram. Soc.*, 79 (1996) 7.
- [11] N. Saunders, The Al-Mo system (aluminum-molybdenum), *J. Phase Equilib.*, 18 (1997) 370-378.
- [12] J. Rexer, Phase Equilibria in Aluminium-Molybdenum System at Temperatures above 1400 Degrees C, *Z. Metallkd.*, 62 (1971) 844-&.
- [13] D.M. Cupid, O. Fabrichnaya, F. Ebrahimi, S.H. J., Thermodynamic assessment of the Al-Mo system and of the Ti-Al-Mo System from 0 to 20 at.% Ti, *Intermetallics*, 18 (2010) 17.

- [14] J.C. Schuster, H. Ipser, The Al-Al₈Mo₃ section of the binary system aluminum-molybdenum, *Metall. Trans. A*, 22A (1991) 1729-1736.
- [15] M. Eumann, G. Sauthoff, M. Palm, Re-evaluation of phase equilibria in the Al-Mo system, *International Journal of Materials Research*, 97 (2006) 1502-1511.
- [16] H. Okamoto, Al-Mo (Aluminum-Molybdenum), *J. Phase Equilib. Diffus.*, Online FirstTM (2010).
- [17] T.B. Massalski, H. Okamoto, P.R. Subramanian, L. Kacprzak, *Binary alloy phase diagrams*, ASM, (1990).
- [18] H. Nowotny, C. Brukl, Ternary system-Mo-Al-Si, *Monatsh. Chem.*, 91 (1960) 313-318.
- [19] C. Brukl, H. Nowotny, O. Schob, F. Benesovsky, Crystal structures of TiSi, Ti(Al,Si)₂, and Mo(Al,Si)₂, *Monatsh. Chem.*, 92 (1961) 781-788.
- [20] T. Tabaru, K. Shobu, M. Sakamoto, S. Hanada, Effects of substitution of Al for Si on the lattice variations and thermal expansion of Mo(Si,Al)₂, *Intermetallics*, 12 (2004) 33-41.
- [21] K. Yanagihara, T. Maruyama, K. Nagata, Isothermal and cyclic oxidation of Mo(Si_{1-x}, Al_x) up to 2048 K, *Mater. Trans., JIM*, 34 (1993) 1200-1206.
- [22] P.D. Eason, K.L. Jolly, M.J. Kaufman, Reassessment of the Mo-Si-Al ternary isotherm at 1400 °C, *Ceram. Eng. Sci. Proc.*, 19 (1998) 437-444.
- [23] J. Emsley, *The Elements*, in, Clarendon Press, Oxford, 1989.
- [24] TOPAS, Version 3.0, Bruker AXS Inc., Karlsruhe, Germany, (1999).
- [25] L.K. Walford, The structures of the intermetallic phases MoAl₁₂, ReAl₁₂, and TcAl₁₂, *Acta Crystallogr.*, 17 (1964) 57-59.
- [26] J.A. Leake, The refinement of the crystal structure of the intermetallic phase Al₄Mo, *Acta Crystallogr.*, 17 (1964) 918-924.
- [27] Y. Harada, M. Morinaga, D. Saso, M. Takata, M. Sakata, Refinement in crystal structure of MoSi₂, *Intermetallics*, 6 (1998) 523-527.
- [28] J.L. Murray, A.J. McAlister, The Al-Si (aluminum-silicon) system, *Bull. Alloy Phase Diagr.*, 5 (1984) 74-84, 89-90.

4 Summary

Fundamental understanding of phase equilibria and structures in alloy systems is crucial for proper materials design. Therefore, detailed research in alloy systems is necessary to clarify discrepancies in literature data and obtain information on so far unexplored fields.

The current work provides a detailed investigation of the alloy systems Al-Cu, CuSi, Al-Cu-Si and Al-Mo-Si, both in phase equilibria and structural analysis. The systems were investigated using light optical microscopy (LOM), scanning electron microscopy (SEM) in combination with EDS and electron probe microanalysis (EPMA), powder X-Ray diffraction (XRD) at ambient and at elevated temperature and differential thermal analysis (DTA).

The currently accepted phase diagram of Al-Cu does not represent the actual state of knowledge in the system. In the present work, detailed experimental analysis lead to an improved phase diagram exhibiting new phase equilibria. The existence of the high temperature phase β_0 was not confirmed and the transition of the high temperature phase γ_0 to the low temperature phase γ_1 was found to be a higher order transition. Additionally, it was possible to determine the structure of the high temperature phase η_1 -Al₁₋₈Cu (*Cmmm*, Al₁₋₈Cu-type) using high temperature XRD in combination with Simulated Annealing. Comparing the structure of the high temperature phase η_1 and the low temperature phase η_2 and considering the high heat exchange during the transition $\eta_2 = \eta_1$ measured by DTA, the present study states, that this transition reaction is a first order reaction.

In the system Cu-Si, the phase ε -Cu₁₅Si₄ in the binary was confirmed to be an equilibrium phase. An extensive number of experiments suggest though, that the formation of the phase could be inhibited kinetically due to nucleation difficulties. Additionally, the phase equilibria in the Cu-rich part of the phase diagram were investigated. Phase equilibria and stable phases were confirmed in the main. Selected compositions and a few invariant reactions have been modified, e.g. the

stability ranges of β -(Cu,Si), δ -(Cu,Si) and η -(Cu,Si) and the nature of the $\gamma = \delta$ transition. The structure of the high-temperature phase β -(Cu,Si) (*cI2*, W-type) was confirmed by high-temperature powder XRD; some uncertainties concerning the structure of the high-temperature phase δ -(Cu,Si) are still remaining.

The system Al-Cu-Si was re-evaluated. An isothermal section at 500 °C over the whole composition range as well as an isothermal section at 700 °C covering the Cu-rich part of the phase diagram was investigated. At 700 °C, a new ternary compound τ , which decomposes to ε -(Cu,Si), $\gamma_{0,1}$ -(Al,Cu) and κ -(Cu,Si) between 700 and 500 °C, was discovered. Although two isopleths at 40 at.% and 10 at.% Si were investigated, solid state reactions in the Cu-rich part of the phase diagram remain still unclear. However, a partial reaction scheme (Scheil Diagram) including invariant reactions in the Cu-poor part was established.

Due to complicated phase equilibria in the Al-rich part of the phase diagram, previous investigations in the Al-Mo-Si system were not dealing with this area. In the present work, an isotherm at 600 °C in the Mo-poor part of the phase diagram and an isotherm at 1400 °C in the Mo-rich part were investigated. At 600 °C, the three phase fields in the Mo-poor region were determined for the first time. The phase Al_{12}Mo shows the highest solubility of Si (7.2(1) at.%) and the binary high temperature phase Al_4Mo is stabilized at 600 °C by addition of Si. At 1400 °C the three phase fields determined do confirm previous findings, although the solubility ranges differ significantly. It was possible to determine the ternary reaction scheme containing 9 invariant reactions. Additionally, the liquidus surface projection, showing some uncertainties in the Al-rich corner and near AlMo , was determined. It shows the primary crystallization fields of (Al), (Si), Al_{12}Mo , C11_b, C40, C54, Al_8Mo_3 , Mo_5Si_3 , $\text{Mo}_3(\text{Al,Si})$ and (Mo).

5 Zusammenfassung

Fundamentales Verständnis von Phasengleichgewichten und Strukturen in Legierungen ist für die Materialentwicklung von großer Bedeutung. Die detaillierte Erforschung von Legierungssystemen ist hier notwendig um Diskrepanzen in Literaturdaten zu beseitigen und Informationen über bislang unerforschte Gebiete zu erhalten.

In der vorliegenden Arbeit werden die Legierungssysteme Al-Cu, Cu-Si, Al-Cu-Si und Al-Mo-Si bezüglich ihrer Phasengleichgewichte und Strukturen untersucht. Die Systeme wurden mit Hilfe von optischer Mikroskopie (LOM), Elektronenstrahlmikroskopie (SEM) in Kombination mit EDS und Elektronenstrahlmikroanalyse (EPMA), Pulverröntgendiffraktometrie (XRD) bei niedriger und hoher Temperatur und Differentialthermoanalyse (DTA) untersucht.

Das gegenwärtig akzeptierte Phasendiagramm von Al-Cu entspricht nicht dem aktuellen Wissensstand. In der vorliegenden Arbeit führten detaillierte experimentelle Untersuchungen zu einem verbesserten Phasendiagramm das neue Phasengleichgewichte zeigt. Die Existenz der Hochtemperaturphase β_0 wurde nicht bestätigt und der Übergang zwischen der Hochtemperaturphase γ_0 zur Tieftemperaturphase γ_1 wurde als Übergang höherer Ordnung identifiziert. Weiters wurde die Struktur der Hochtemperaturphase η_1 -Al_{1- δ} Cu (*Cmmm*, η_1 -Al_{1- δ} Cu-Typ) mit Hochtemperatur-XRD in Kombination mit Simulated Annealing aufgeklärt. Vergleich der Strukturen der Hoch- und Tieftemperaturphasen η_1 und η_2 unter Berücksichtigung des Wärmeumsatzes bei der Umwandlung $\eta_2 = \eta_1$ bei der DTA-Messung zeigt, dass ein Übergang erster Ordnung erfolgt.

Im System Cu-Si konnte nach umfangreichen Experimenten dargelegt werden, dass die Phase ε -Cu₁₅Si₄ eine Gleichgewichtsphase ist. Ihre Bildung kann jedoch aufgrund von Problemen bei der Keimbildung kinetisch gehemmt sein. Zusätzlich wurden die Phasengleichgewichte im Cu-reichen Teil des Phasendiagramms untersucht. Im Großen und Ganzen wurden die Phasengleichgewichte bestätigt.

Bestimmte Zusammensetzungen und einige invariante Reaktionen wurden modifiziert, z.B. die Stabilitätsbereiche von β -(Cu,Si), δ -(Cu,Si) und η -(Cu,Si) und die Umwandlung $\gamma = \delta$. Die Struktur der Hochtemperaturphase β -(Cu,Si) (*cI2*, W-Typ) wurde bestätigt; Unsicherheiten bleiben bzgl. der Struktur von δ -(Cu,Si).

Weiters wurde das System Al-Cu-Si neu erforscht. Eine Isotherme bei 500 °C über den gesamten Zusammensetzungsbereich und eine Isotherme bei 700 °C im Cu-reichen Teil des Phasendiagramms wurden untersucht. Bei 700 °C wurde eine neue ternäre Verbindung τ gefunden, die sich zwischen 700 und 500 °C in ε -(Cu,Si), $\gamma_{0,1}$ -(Al,Cu) and κ -(Cu,Si) zersetzt. Obwohl zwei Isoplethen bei 40 at.% und 10 at.% Si untersucht wurden, bleiben die Festphasenumwandlungsreaktionen im Cu-reichen Teil des Phasendiagramms unklar. Jedoch war es möglich, ein partielles Reaktionsschema (Scheil Diagramm) der invarianten Reaktionen im Cu-armen Teil aufzustellen.

Aufgrund der komplexen Phasengleichgewichte im Al-reichen Teil des Phasendiagramms Al-Mo-Si haben frühere Untersuchungen diesen kaum berücksichtigt. In der vorliegenden Arbeit wurden Isothermen im Mo-armen Bereich bei 600 °C und im Mo-reichen Teil bei 1400 °C untersucht. Bei 600 °C wurden die Phasengleichgewichte erstmals bestimmt. Die Phase Al_{12}Mo zeigt mit 7.2 at.% die höchste Löslichkeit von Si. Die binäre Hochtemperaturphase Al_4Mo wird durch Zugabe von Si bei 600 °C stabilisiert. Bei 1400 °C werden die Dreiphasenfelder aus früheren Untersuchungen bestätigt, jedoch unterscheiden sich die Löslichkeiten signifikant. Es war möglich, das ternäre Reaktionsschema mit 9 invarianten Reaktionen aufzustellen. Zusätzlich wurde die Liquidusprojektion bestimmt. Diese zeigt einige Unsicherheiten im Al-reichen Bereich und in der Nähe von AlMo , jedoch konnten die primären Kristallisationsfelder von (Al), (Si), Al_{12}Mo , C11_b , C40, C54, Al_8Mo_3 , Mo_5Si_3 , $\text{Mo}_3(\text{Al,Si})$ and (Mo) bestimmt werden.

Appendix A: Supplementary material

Re-investigation of phase equilibria in the system Al-Cu and structural analysis of the high-temperature phase η_1 -Al₁₋₈Cu

sample composition	phases observed by		SEM analysis			thermal analysis (DTA)		
	XRD analysis	phase	Al	Cu	invariant effects	other effects	liquidus on heating	liquidus on cooling
Al ₉₀ Cu ₁₀	---	(Al) θ	97.8(5) 68(5)	2.2(5) 32(5)	551(1)		598(1)	583(3)
Al ₈₀ Cu ₂₀	---				551(1)		564(2)	539(1)
Al ₇₀ Cu ₃₀	---				549(1)		597(1)	575(2)
Al ₆₅ Cu ₃₅	---				571(2) 594(1)		602(2)	595(1)
Al ₆₀ Cu ₄₀	---				571(1) 590(1) 624(1)		664(3)	627(1)
Al _{52.5} Cu _{47.5}	θ	θ	66.4(5)	33.6(5)	576(1)			
	η_2	η_2	48.1(5)	51.9(5)	589(1) 624(1)		771(2)	772(1)
Al ₅₀ Cu ₅₀	θ				577(1) 590(1) 625(1)		804(2)	794(2)
	η_2				573(1)			
Al ₄₉ Cu ₅₁	θ				590(1)	574(1)	825(1)	819(1)
	η_2				625(1)			
Al _{47.5} Cu _{52.5}					574(1) 626(1)	576(1)	852(1)	851(1)
	η_2							

$\text{Al}_{46.5}\text{Cu}_{53.5}$	η_2	580(1) 597(1) 623(1)	866(1)	864(1)
$\text{Al}_{45}\text{Cu}_{55}$	η_2 traces of ζ_1	596(1)	892(1)	889(1)
$\text{Al}_{42.5}\text{Cu}_{57.5}$	ζ_1 small unidentified peaks	561(2) 578(2)	530(2) 760(3) 847(1)	929(1) 926(1)
$\text{Al}_{40}\text{Cu}_{60}$	δ	683(1)	847(1) 942(1)	960(1) 957(1)
$\text{Al}_{39}\text{Cu}_{61}$	δ	684(1) 961(2)	655(3) 814(3) 847(1) 893(1)	973(2) 969(1)
$\text{Al}_{38}\text{Cu}_{62}$	δ	959(1)	846(1) 920(1)	985(1) 980(1)
$\text{Al}_{37}\text{Cu}_{63}$	δ	959(1)	837(3) 875(3) 951(1)	997(2) 993(1)
$\text{Al}_{36}\text{Cu}_{64}$	δ small unidentified peaks	958(1)	873(1)	1009(1) 992(1)
$\text{Al}_{35}\text{Cu}_{65}$	γ_1	994(1)	872(2) 936(3)	1022(1) 1013(2)
$\text{Al}_{34}\text{Cu}_{66}$	γ_1	992(1)	872(2)	1023(2) 1008(2)
$\text{Al}_{33}\text{Cu}_{67}$	γ_1		858(1)	1027(1) 1017(1)

Al ₃₂ Cu ₆₈	γ ₁	839(1) 1018(1)	1036(1)	1029(1)
Al ₃₁ Cu ₆₉	γ ₁	801(3) 1008(3)	1040(1)	1030(1)
Al ₃₀ Cu ₇₀	γ ₁ (Cu)	568(1)	1054(2)	1042(2)
Al ₂₉ Cu ₇₁	γ ₁ (Cu)	567(2)	1057(1)	1040(4)
Al _{27.5} Cu _{72.5}	γ ₁ (Cu)	567(1)	843(3)	1043(1)
Al ₂₅ Cu ₇₅	γ ₁ (Cu)	γ ₁ (Cu) 29.5(5) 18(1) 70.5(1) 82(1)	568(1)	1046(1)
Al _{22.5} Cu _{77.5}	γ ₁ (Cu)	567(1)	1056(1)	1041(1)
Al ₂₁ Cu ₇₉	γ ₁ (Cu)	567(1)	810(3)	1041(1)
Al ₂₀ Cu ₈₀	γ ₁ (Cu)	566(1)	905(3)	1038(1)
Al ₁₉ Cu ₈₁	(Cu)	567(1)	1042(3) 1046(3)	1033(3)
Al ₁₇ Cu ₈₃	(Cu)	921(3) 944(3) 1032(3)	1045(1)	1030(1)

New investigation of phase equilibria in the system Al-Cu-Si

sample composition	thermal analysis (DTA)			
	invariant effects	other effects	liquidus on heating	liquidus on cooling
Cu ₆₀ Si ₄₀	547(1)			
	555(1)		987(1)	978(1)
	804(1)			
Al ₄ Cu ₅₆ Si ₄₀		512(2)		
	579(1)	549(1)	not determined	not determined
	728(1)	777(1)		
Al ₅ Cu ₅₅ Si ₄₀	581(1)	770(1)	1020(1)	1014(1)
	732(1)			
Al ₆ Cu ₅₄ Si ₄₀		512(1)		
	580(1)	550(1)	1019(1)	1009(1)
	729(1)	751(3)		
Al _{7.5} Cu _{52.5} Si ₄₀	580(1)		not determined	not determined
	730(1)			
Al ₈ Cu ₅₂ Si ₄₀	580(1)	512(2)	1028(1)	1019(1)
	728(1)	550(1)		
Al _{8.5} Cu _{51.5} Si ₄₀	580(1)	513(2)	not determined	not determined
	729(1)	550(2)		
Al ₁₀ Cu ₅₀ Si ₄₀		512(1)		
		550(1)		
	579(1)	727(2)	1035(1)	1028(2)
		744(2)		
Al ₁₁ Cu ₄₉ Si ₄₀		551(1)		
	579(1)	731(1)	1042(1)	1038(1)
		746(1)		
Al ₁₂ Cu ₄₈ Si ₄₀	579(1)	551(1)	1043(1)	1035(1)

Appendix A

	735(1)	753(3)		
Al ₁₃ Cu ₄₇ Si ₄₀	741(1)	760(2)	1046(2)	1043(1)
		550(1)		
Al ₁₄ Cu ₄₆ Si ₄₀		745(1)	1048(1)	1042(1)
		765(1)		
Al ₁₅ Cu ₄₅ Si ₄₀		754(1)	1046(1)	1046(1)
		774(1)		
Al ₁₆ Cu ₄₄ Si ₄₀		757(1)	1073(4)	1084(3)
Al ₁₇ Cu ₄₃ Si ₄₀		764(1)	1053(1)	1047(1)
Al ₂₀ Cu ₄₀ Si ₄₀		776(1)	1054(2)	1058(2)
Al ₂₁ Cu ₃₉ Si ₄₀		768(1)	1056(1)	1050(1)
Al ₂₃ Cu ₃₇ Si ₄₀	746(1)	770(2)	1063(2)	1050(2)
Al ₂₆ Cu ₃₄ Si ₄₀	570(3)	749(1)	1064(4)	1051(1)
Al ₂₇ Cu ₃₃ Si ₄₀	597(2) 604(2)	745(1)	1056(1)	1053(1)
Al ₃₀ Cu ₃₀ Si ₄₀	572(1) 605(1)	724(1)	1045(5)	1045(1)
Al ₃₅ Cu ₂₅ Si ₄₀	574(1) 605(1)	663(1)	1051(5)	1059(1)
Al ₄₀ Cu ₂₀ Si ₄₀	575(2)	521(1)	1018(2)	1014(2)
Al ₄₅ Cu ₁₅ Si ₄₀	522(1)	568(2)	1009(3)	1012(1)
Al ₅₀ Cu ₁₀ Si ₄₀	522(1)		961(4)	957(1)
Al ₅₅ Cu ₅ Si ₄₀	523(1)	552(1)	978(2)	977(1)
Al ₆₀ Si ₄₀	578(2)		947(4)	937(1)
Cu ₉₀ Si ₁₀		885(1)	983(1)	979(2)
Al _{2.5} Cu _{87.5} Si		824(1)		
10		868(2)	963(1)	956(1)
Al ₅ Cu ₈₅ Si ₁₀		799(1)	948(2)	947(1)
		895(1)		
Al _{6.5} Cu _{83.5} Si		758(3)	931(1)	928(1)

[illegible]

$\text{Al}_{50}\text{Cu}_{400}\text{Si}_1$	573(2)			
0	601(1)	682(2)	744(4)	705(1)
$\text{Al}_{55}\text{Cu}_{35}\text{Si}_{10}$	574(1)			
	603(1)	633(1)	720(5)	690(3)
$\text{Al}_{60}\text{Cu}_{20}\text{Si}_{10}$	577(4)		706(2)	662(19)
$\text{Al}_{65}\text{Cu}_{25}\text{Si}_{10}$	521(2)	574(2)	688(4)	639(1)
$\text{Al}_{80}\text{Cu}_{10}\text{Si}_{10}$	521(2)		532(2)	528(3)
$\text{Al}_{85}\text{Cu}_5\text{Si}_{10}$	520(1)		573(1)	547(3)
$\text{Al}_{90}\text{Si}_{10}$	577(1)			
	583(2)		591(1)	583(1)

Appendix B: Permissions for prints

Am 19.07.2011, 14:04 Uhr, schrieb Parker, Kerry (ELS-OXF) <Kerry.Parker@elsevier.com>:

Dear Norbert,

Thermal Analysis, 9780127656052, 1990, Wunderlich, 1 figure only

As per your email dated 18th July 2011, Elsevier has no objection to granting its permission for you to use the aforementioned material subject to suitable acknowledgement to the source as follows:

Reprinted from Publication title, Vol number, Author(s), Title of article, Pages No., Copyright (Year).

However we haven't been able to locate the contract for this title in our archives so we are unable to confirm that we are the legal copyright holders of this material. Therefore it is important that you also obtain permission from the author(s) prior to use. If any part of the material to be used (for example, figures) has appeared in the original publication with credit or acknowledgement to another source, permission must also be sought from that source.

Kind regards
Kerry

Kerry Parker :: Rights Associate
Global Rights Dpt :: Elsevier Ltd

Tel: +44 1865 843280
Fax: +44 1865 853333
Email: kerry.parker@elsevier.com

-----Original Message-----

From: norbert.ponweiser@univie.ac.at [mailto:norbert.ponweiser@univie.ac.at]
Sent: 18 July 2011 20:49
To: Rights and Permissions (ELS)
Subject: Obtain Permission

This Email was sent from the Elsevier Corporate Web Site
and is related to Obtain Permission form:

Product: Customer Support
Component: Obtain Permission
Web server: <http://www.elsevier.com>
IP address: 131.130.27.5
Client: Opera/9.80 (Windows NT 5.1; U; de) Presto/2.9.168 Version/11.50
Invoked from:
http://www.elsevier.com/wps/find/obtainpermissionform.cws_home?isSubmitted=yes&navigateXmlFileName=/store/p65idstarget/act/framework_support/obtainpermission.xml

Request From:
Mag. Norbert Ponweiser
University of Vienna
Wahringer Strasse 42
1090 Vienna

Vienna, Austria

Contact Details:

Telephone: +43-660-7635146

Fax: +43-1-4277-9529

Email Address: norbert.ponweiser@univie.ac.at

To use the following material:

ISSN/ISBN: 0-12-765605-7

Title: Thermal Analysis

Author(s): Bernhard Wunderlich

Volume: 1

Issue: 1

Year: 1990

Pages: 174 - 174

Article title: Thermal Analysis

How much of the requested material is to be used:

I only need this one figure for my thesis.

Are you the author: No

Author at institute: No

How/where will the requested material be used: [how_used]

Details: The figure used in the introduction of my thesis. Proper citation of the book mentioned above is self-evident. Since it is for academic use, I hope you can grant me permission to use the figure without charges.

Additional Info:

[acronym]

- end -

Elsevier Limited. Registered Office: The Boulevard, Langford Lane, Kidlington, Oxford, OX5 1GB, United Kingdom, Registration No. 1982084 (England and Wales).

Am 19.07.2011, 20:30 Uhr, schrieb Bernhard Wunderlich <Wunderlich@chartertn.net>:

Dear Mr. Ponweiser:

The figure you requested to use in your thesis:

Bernhard Wunderlich – Thermal Analysis

ISBN 0-12-765605-7

Copyright © 1990 by Academic Press, Inc.

Page 174, Fig 4.23 PHASE DIAGRAMS 1. General description

is also part of the illustrations which I use when teaching my course "Thermal Analysis of Materials" and I gladly give you permission to use it.

In the last version of the course, the figure has changed slightly, so I include the last figures, to give you an easily copyable file. In case you are interested in the text to the figures, see: B. Wunderlich, Thermal Analysis of Materials. A computer-assisted lecture course of 36 lectures.

Updated and changed to newly developed presentation software, published via the Internet (2005–2007). Available by downloading through the internet sites: <http://www.scite.eu> (under ‘Books and more’), <http://athas.prz.rzeszow.pl> (under ‘Teaching’), and <http://www.evitherm.org/index.asp> (from their home page, go to ‘Thermal analysis & calorimetry’).

Good luck with your thesis,

Bernhard Wunderlich
Professor emeritus, from the
University of Tennessee, Knoxville (UTK)
and Rensselaer Polytechnic Institute (RPI)

Appendix C: *Curriculum vitae*

First name: Norbert
Last name: Ponweiser
Degree: Mag. rer. nat.
Date of birth: Jan. 14th, 1981
E-Mail: norbert.ponweiser@univie.ac.at

Education (school)

09/1991 - 06/1999 Matura, BRG Groehrmuehlgasse, Wiener Neustadt

Military service

09/1999 - 04/2000 Oesterreichisches Bundesheer, PzGrenB 35

Education (university)

10/2000–05/2006 Diploma-study Chemistry, University of Vienna

Focus: Materials Chemistry, Physical Chemistry, Analytical Chemistry

Title of the diploma thesis: *Substitution in Ternary Germanides in the System Hf-Zr-Ge*

10/2004 – 01/2005 research stay at the *Laboratoire de Cristallochimie et de Physico-Chimie du solide*, Université des Sciences et Technologie de Lille, France (Erasmus scholarship holder)

06 – 07/2006 Participant in the 9th *Intensive Program: Physics and Chemistry of Multifunctional Materials*, Genova, Italy

06/2006 – 12/2007 project collaborator / Universitaet Wien

since 06/2006 Doctoral study: Materials Chemistry/ University of Vienna

since 01/2008 Employment as Assistent in Ausbildung / University of Vienna

Additional qualifications:

Languages:

German first language

English very experienced

French medium

Teaching activity at the University of Vienna:

Tutor:

Basic Chemistry Laboratory Course I - Introductory Lab Course

Chemical Laboratory Course for Biology

Assistant:

Basic Chemistry Laboratory Course I - Introductory Lab Course

Basic Chemistry Laboratory Course I - Introductory Seminar

Chemical Laboratory Course for Biology

Solid State Chemistry - Syntheses and Structure of Materials

Laboratory course on the characterization of inorganic materials - thermal and thermodynamic methods

List of publications:

Ponweiser, N.; Ipser, H.; Richter, K.W. Phase equilibria in the system Hf-Zr-Ge at 1350 °C. *Journal of Alloys and Compounds* (2008), 452(1), 80-84

Ponweiser, N.; Warczok, P.; Lengauer, C.L.; Richter, K.W. Partial ordering in the section $\text{Hf}_5\text{Ge}_4\text{-Zr}_5\text{Ge}_4$: Crystallographic investigation and modeling based on ab initio calculations. *Solid State Sci.* (2009), 11(2), 395-401

Ponweiser, N.; Paschinger, W.; Ritscher, A.; Schuster, J.C.; Richter, K.W. Phase equilibria in the Al-Mo-Si system. *Intermetallics* (2011), 19(3), 409-418

Sufryd, K.; Ponweiser, N.; Riani, P.; Richter, K.W.; Cacciamani, G. Experimental investigation of the Cu-Si phase diagram at $(\text{Cu}) > 0.72$, *Intermetallics* (2011), 19(10), 1479-1488

Ponweiser, N.; Lengauer, C.L.; Richter, K.W. Re-investigation of phase equilibria in the system Al-Cu and structural analysis of the high-temperature phase $\eta_1\text{-Al}_{1-\delta}\text{Cu}$, *Intermetallics* (2011), 19, 1737-1746

Ponweiser, N.; Richter, K.W. Investigation of phase equilibria in the system Al-Cu-Si, *J. Alloys Compd.*, submitted September 2011

Participations in conferences:

09/2010	TOFA 2010 – Discussion Meeting on Thermodynamics of Alloys, Porto, Portugal: Talk
08/2009	13 th Austrian Chemistry Days, Vienna, Austria: Talk
06/2008	TOFA 2008 – Discussion Meeting on Thermodynamics of Alloys, Krakow, Poland: Talk
03/2008	5. Workshop Inorganic Chemistry in Austria, Graz, Austria: Talk
09/2007	12 th Austrian Chemistry Days, Klagenfurt, Austria: Poster
07/2007	9 th FIGIPAS Meeting in Inorganic Chemistry, Vienna, Austria: Poster
09/2006	IUPAC-Conference on High Temperature Materials Science, Vienna, Austria: Poster
03/2005	2 ^{me} Journées Nord-Européennes des Jeunes Chercheurs, Lille, France: Poster